Functional renormalization group approach to correlated fermion systems

Walter Metzner

Max-Planck-Institute for Solid State Research, Heisenbergstraße 1, D-70569 Stuttgart, Germany

Manfred Salmhofer

Institut für Theoretische Physik, Universität Heidelberg, Philosophenweg 19, D-69120 Heidelberg, Germany

Carsten Honerkamp

Institut für Theoretische Festkörperphysik and JARA-Fundamentals of Future Information Technology, RWTH Aachen University, D-52056 Aachen, Germany

Volker Meden

Institut für Theorie der Statistischen Physik and JARA-Fundamentals of Future Information Technology, RWTH Aachen University, D-52056 Aachen, Germany

Kurt Schönhammer

Institut für Theoretische Physik, Universität Göttingen, Friedrich-Hund-Platz 1, D-37077 Göttingen, Germany

(published 12 March 2012)

Numerous correlated electron systems exhibit a strongly scale-dependent behavior. Upon lowering the energy scale, collective phenomena, bound states, and new effective degrees of freedom emerge. Typical examples include (i) competing magnetic, charge, and pairing instabilities in two-dimensional electron systems; (ii) the interplay of electronic excitations and order parameter fluctuations near thermal and quantum phase transitions in metals; and (iii) correlation effects such as Luttinger liquid behavior and the Kondo effect showing up in linear and nonequilibrium transport through quantum wires and quantum dots. The functional renormalization group is a flexible and unbiased tool for dealing with such scale-dependent behavior. Its starting point is an exact functional flow equation, which yields the gradual evolution from a microscopic model action to the final effective action as a function of a continuously decreasing energy scale. Expanding in powers of the fields one obtains an exact hierarchy of flow equations for vertex functions. Truncations of this hierarchy have led to powerful new approximation schemes. This review is a comprehensive introduction to the functional renormalization group method for interacting Fermi systems. A self-contained derivation of the exact flow equations is presented and frequently used truncation schemes are described. Reviewing selected applications it is shown how approximations based on the functional renormalization group can be fruitfully used to improve our understanding of correlated fermion systems.

DOI: 10.1103/RevModPhys.84.299 PACS numbers: 71.10.−w

CONTENTS

I. INTRODUCTION

A. Motivation

The Coulomb interaction between electrons in solids leads to a virtually unlimited variety of phenomena, such as magnetic correlations and magnetic order, high-temperature superconductivity, metal-insulator transitions, phase separation and stripes, and the formation of exotic quantum liquid phases. The latter include Luttinger liquids, quantum critical points, and fractional quantum Hall states.

Interacting electron systems usually exhibit very distinct behavior on different energy scales. Composite objects and collective phenomena emerge at scales far below the bare energy scales of the microscopic Hamiltonian. For example, in cuprate high-temperature superconductors one bridges 3 orders of magnitude from the highest scale, the bare Coulomb interaction, via the intermediate scale of short-range magnetic correlations, down to the lowest scale of d-wave superconductivity (SC) and other ordering phenomena (see Fig. 1).

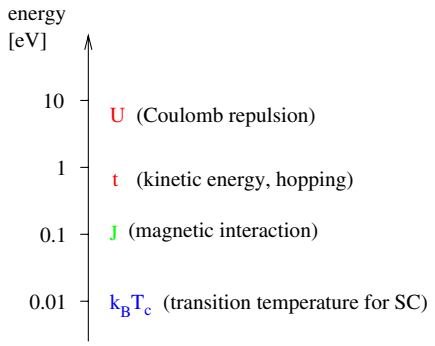

FIG. 1 (color online). Important energy scales in high-temperature superconductors of the cuprate family. Magnetic interactions and superconductivity are generated from the kinetic energy (hopping) and the Coulomb repulsion.

This diversity of scales is a major obstacle to a straightforward numerical solution of microscopic models, since the most interesting phenomena emerge only at low temperatures and in systems with a large size. It is also hard to deal with by conventional many-body methods, if one tries to treat all scales at once and within the same approximation, for example, by summing a subclass of Feynman diagrams. Perturbative approaches which do not separate different scales are plagued by infrared divergences and are therefore often inapplicable even at weak coupling, especially in low dimensions.

It is thus natural to treat degrees of freedom with different energy scales successively, descending step by step from higher to lower scales. This is the main idea behind the renormalization group (RG).

B. RG for interacting Fermi systems

Renormalization group methods have a long tradition in the theory of interacting Fermi systems. Already in the 1970s, various versions of the RG have been used to deal with infrared singularities arising in one-dimensional Fermi systems (Sólyom, 1979). Naturally, the RG was also applied to (mostly bosonic) effective field theories describing critical phenomena at continuous classical or quantum phase transitions in interacting Fermi systems (Fradkin, 1991; Sachdev, 1999).

Renormalization group approaches dealing with interacting fermions in arbitrary dimensions d were developed much later. Because of the extended (not pointlike) geometry of the Fermi surface singularity in dimensions $d > 1$, the renormalization group flow cannot be reduced to a finite number of running couplings. However, the main reason for the delayed development of a comprehensive RG approach for interacting Fermi systems in higher dimensions was probably not this difficulty, but rather a lack of motivation. The few infrared singularities appearing in three-dimensional Fermi systems

could usually be handled by simple resummations of perturbation theory (Abrikosov, Gorkov, and Dzyaloshinski, 1963; Nozières, 1964). Triggered by the issue of non-Fermi-liquid behavior in two-dimensional systems, and the related discussion on the validity of perturbation theory, systematic RG approaches to interacting Fermi systems in arbitrary dimensions were developed by various groups in the early 1990s.

Aiming at mathematical control of interacting Fermi systems, Feldman and Trubowitz (1990, 1991), and independently Benfatto and Gallavotti (1990a, 1990b) formulated a rigorous fermionic version of Wilson's momentum-shell RG (Wilson and Kogut, 1974). Important rigorous results have indeed been obtained in one-dimensional (Benfatto *et al.*, 1994) and two-dimensional (Feldman *et al.*, 1992, Feldman, Salmhofer, and Trubowitz, 1996; Disertori and Rivasseau, 2000; Feldman, Knörrer, and Trubowitz, 2003, 2004; Benfatto, Giuliani, and Mastropietro, 2006) systems. The essential message from these results is that no hitherto unknown instabilities or nonperturbative effects occur in Fermi systems with sufficiently weak short-range interactions, at least in the absence of special features such as van Hove singularities at the Fermi level.

The Wilsonian RG for interacting Fermi systems was popularized among (nonmathematical) physicists by Shankar (1991, 1994) and Polchinski (1993), who presented some of the main ideas in a pedagogical style. In particular, they provided an intuitive RG perspective of Fermi-liquid theory. Subtleties associated with the singularities of the interaction vertex for forward scattering were clarified a bit later (Chitov and Sénéchal, 1995; Metzner, Castellani, and Di Castro, 1998). A Hamiltonian-based RG interpretation of Fermi-liquid theory was presented by Hewson (1994), who discussed not only translation-invariant systems but also models for magnetic impurities in metals.

As an alternative to the Wilsonian RG one can also use flow equations for Hamiltonians based on infinitesimal unitary transformations, which make the Hamiltonian successively more diagonal (Wegner, 1994). This approach has been used successfully for quantum impurity models and other systems (Kehrein, 2006). A weak-coupling truncation of the flow equations has been applied to identify instabilities of the two-dimensional Hubbard model (Grote, Körding, and Wegner, 2002).

There is much current interest in RG methods for correlated fermions in nonequilibrium. The perturbative RG (Rosch, Kroha, and Wölfle, 2001; Mitra *et al.*, 2006), Wilson's numerical RG (Anders and Schiller, 2005), as well as Wegner's flow-equation approach (Kehrein, 2006) were extended to nonequilibrium, and real-time RG methods were developed (Schoeller, 2000, 2009; Schoeller and König, 2000).

C. Functional renormalization group

The Wilsonian RG is not only useful for a deeper and partially even rigorous understanding of interacting fermion systems. A specific version of Wilson's RG known as *exact* or *functional* RG turned out to provide a valuable framework for computational purposes. Approximations derived from exact functional flow equations have played an increasingly important role in the last decade. These developments are the central topic of this review.

Exact flow equations describe the evolution of a generating functional for all many-particle Green or vertex functions as a function of a flow parameter Λ, usually an infrared cutoff. They can be derived relatively easily from a functional integral representation of the generating functional. Exact flow equations have been known since the early years of the RG, starting with the work of Wegner and Houghton (1973). Polchinski (1984) employed an exact flow equation to formulate a relatively simple proof of renormalizability of the Φ^4 theory in four dimensions. Renormalizability proofs can be further simplified by using a Wick-ordered variant of Polchinski's equation (Wieczerkowski, 1988).

For computational purposes the exact flow equation for the effective action, first derived in the context of bosonic field theories by Wetterich (1993), turned out to be most convenient. The effective action $\Gamma^\Lambda[\phi]$ is the generating functional for one-particle irreducible vertex functions. The latter are obtained by taking derivatives with respect to the source field ϕ. The flow parameter Λ describes a regularization of the underlying bare action, which regularizes infrared divergencies in perturbation theory. The regularization is removed at the end of the flow, say for $\Lambda \to 0$. The initial regulator (for $\Lambda = \Lambda_0$) can be chosen such that $\Gamma^{\Lambda_0}[\phi]$ is given by the bare action. The flow of $\Gamma^\Lambda[\phi]$ then provides a smooth interpolation between the bare action of the system and the final effective action $\Gamma[\phi]$, from which any desired information can be extracted. This flow is determined by an exact functional differential equation (Wetterich, 1993; Ellwanger and Wetterich, 1994; Morris, 1994). Expanding in the fields one obtains a hierarchy of flow equations for the one-particle irreducible vertex functions. The advantage of that hierarchy compared to others, obtained, for example, from Polchinski's equation, is that self-energy feedback is included automatically and no one-particle reducible terms appear.

The expression *functional* RG stems from the feature in which the exact flow equations describe the flow of a functional or (equivalently) of a hierarchy of functions. An important difference compared to Wilson's original formulation is that a complete set of source fields is kept in the flowing generating functionals, not only those corresponding to scales below Λ. Hence, the full information on the properties of the system remains accessible, not only the low energy or long wavelength behavior.

Exact flow equations can be solved exactly only in special cases, where the underlying model can also be solved exactly, and more easily, by other means.[1] However, the functional RG is a valuable source for devising powerful new approximation schemes, which can be obtained by truncating the hierarchy and/or by a simplified parametrization of the Green or vertex functions. These approximations have several distinctive advantages: (i) they have a renormalization group structure built in, that is, scales are handled successively and infrared singularities are thus treated properly; (ii) they can be applied directly to microscopic models, not only to effective

[1]An instructive example is provided by the exact solution of the Tomonaga-Luttinger model via functional RG flow equations (Schütz, Bartosch, and Kopietz, 2005).

field theories which capture only some asymptotic behavior; (iii) they are physically transparent, for example, one can see directly how and why new correlations form upon lowering the scale; and (iv) one can use different approximations at different scales. Small steps from a scale Λ to a slightly smaller scale Λ' are much easier to control than an integration over all degrees of freedom in one shot, and one can take advantage of the flexibility provided by the choice of a suitable flow parameter.

Approximations derived from exact flow equations have been applied in many areas of quantum field theory and statistical physics (Berges, Tetradis, and Wetterich, 2002). In the context of interacting Fermi systems, functional RG methods were first used for an unbiased stability analysis of the two-dimensional Hubbard model (Zanchi and Schulz, 1998, 2000; Halboth and Metzner, 2000a; Honerkamp *et al.*, 2001). Since then, approximations derived within the functional RG framework have been applied to numerous interacting fermion systems.

D. Scope of the review

This review provides a thorough introduction to the functional RG in the context of interacting Fermi systems. It serves as a manual and reference for many-body theorists who want to apply approximations based on the functional RG to their own problem of interest. We first describe the functional RG framework and derive, in particular, the exact flow equations, which are the starting point for approximations. We discuss general aspects related to the flow equations such as the choice of cutoffs, power counting, and truncations. Links to the use of flow equations in the mathematical literature are pointed out along the way. We then review some of the most interesting applications of truncated functional RG equations. Our aim is not to deliver an exhaustive overview of all applications, but rather to show via selected applications how the functional RG method can be fruitfully used.

The functional RG was recently extended to Fermi systems out of equilibrium (Jakobs, 2003; Gezzi, Pruschke, and Meden, 2007; Jakobs, Meden, and Schoeller, 2007; Jakobs, Pletyukhov, and Schoeller, 2010a, 2010b; Karrasch *et al.*, 2010; Karrasch, Pletyukhov *et al.*, 2010). In the derivation of the flow equations in Sec. II we restrict ourselves to the equilibrium formalism. Functional RG flow equations for nonequilibrium Keldysh Green and vertex functions can be derived in close analogy (Jakobs, 2003, 2010; Gezzi, Pruschke, and Meden, 2007; Karrasch, 2010). The necessary extensions are briefly mentioned when discussing the application of this method to finite bias steady-state transport through correlated quantum wires and quantum dots in Sec. VI.

A number of reviews with a focus on the functional RG are already available. Mathematically rigorous developments until the end of the last millenium were summarized by Salmhofer (1999), who dedicated a large portion to interacting Fermi systems. Examples of approximations derived from the exact flow equation for the effective action with many applications in quantum field theory and statistical physics were presented by Berges, Tetradis, and Wetterich (2002). A detailed introduction to the functional RG in a textbook style supplemented by selected applications (including Fermi systems) can be found in Kopietz, Bartosch, and Schütz (2010).

II. FUNCTIONAL FLOW EQUATIONS

In this section we present the general functional RG framework. The reader should be familiar with the functional integral formalism for quantum many-body systems, as described by Negele and Orland (1987). After introducing the generating functionals for Green and vertex functions in Sec. II.A, we derive the exact functional flow equations in Sec. II.B. The flow equation (35) for the effective action Γ^Λ is the central equation of this review. Expanding in the fields we derive the hierarchy of flow equations for vertex functions in Sec. II.C, which is the starting point for approximations. Possible choices of flow parameters are reviewed in Sec. II.D. The general structure of the RG hierarchy and power counting are discussed in Sec. II.E, with various references to the closely related mathematical literature. Section II.F is dedicated to flow equations for observables and correlation functions. Coupled flow equations for fermions and bosons, which are useful for studies of spontaneous symmetry breaking and quantum criticality, are derived in Sec. II.G.

A. Generating functionals

We consider a system of interacting fermions which can be described by Grassmann fields ψ, $\bar{\psi}$, and an action of the form

$$\mathcal{S}[\psi,\bar{\psi}] = -(\bar{\psi}, G_0^{-1}\psi) + V[\psi,\bar{\psi}], \tag{1}$$

where $V[\psi,\bar{\psi}]$ is an arbitrary many-body interaction, and G_0 is the propagator of the noninteracting system. The bracket $(.,.)$ is a shorthand notation for the sum $\sum_x \bar{\psi}(x)(G_0^{-1}\psi)(x)$, where $(G_0^{-1}\psi)(x) = \sum_{x'} G_0^{-1}(x,x')\psi(x')$. The Grassmann field index x collects the quantum numbers of a suitable single-particle basis set and imaginary time or frequency. In case of continuous variables, the sum over x includes the appropriate integrals. Prefactors such as temperature or volume factors depend on the representation (e.g., real or momentum space) and are therefore not written in this general part. A two-particle interaction has the general form

$$V[\psi,\bar{\psi}] = \frac{1}{4}\sum_{\substack{x_1,x_2\\ x_1',x_2'}} V(x_1',x_2';x_1,x_2)\bar{\psi}(x_1')\bar{\psi}(x_2')\psi(x_2)\psi(x_1). \tag{2}$$

In particular, for spin-$\frac{1}{2}$ fermions with a single-particle basis labeled by momentum $\mathbf{k}$ and spin orientation σ, one has $x = (k_0, \mathbf{k}, \sigma)$, where k_0 is the fermionic Matsubara frequency. If the bare part of the action is translation and spin-rotation invariant, the bare propagator has the diagonal and spin-independent form $G_0(x,x') = \delta_{k_0 k_0'}\delta_{\mathbf{k}\mathbf{k}'}\delta_{\sigma\sigma'}G_0(k_0,\mathbf{k})$ with

$$G_0(k_0,\mathbf{k}) = \frac{1}{ik_0 - \xi_{\mathbf{k}}}, \tag{3}$$

where $\xi_{\mathbf{k}} = \epsilon_{\mathbf{k}} - \mu$ is the single-particle energy relative to the chemical potential.

Connected Green functions can be obtained from the generating functional (Negele and Orland, 1987)

$$\mathcal{G}[\eta, \bar{\eta}] = -\ln \int \mathcal{D}\psi \mathcal{D}\bar{\psi} e^{-\mathcal{S}[\psi,\bar{\psi}]} e^{(\bar{\eta},\psi)+(\bar{\psi},\eta)}, \tag{4}$$

where $\int \mathcal{D}\psi \mathcal{D}\bar{\psi} \cdots = \int \prod_x d\psi(x) d\bar{\psi}(x) \cdots$. Completing squares yields the identity

$$\int \mathcal{D}\psi \mathcal{D}\bar{\psi} e^{(\bar{\psi}, G_0^{-1}\psi)} e^{(\bar{\eta},\psi)+(\bar{\psi},\eta)} = \mathcal{Z}_0 e^{(-\bar{\eta}, G_0 \eta)}, \tag{5}$$

where $\mathcal{Z}_0 = \int \mathcal{D}\psi \mathcal{D}\bar{\psi} e^{(\bar{\psi}, G_0^{-1}\psi)}$ is the partition function of the noninteracting system. Hence $\mathcal{G}[\eta, \bar{\eta}] = -\ln \mathcal{Z}_0 + (\bar{\eta}, G_0 \eta)$ in the noninteracting case $V[\psi, \bar{\psi}] = 0$. For vanishing source fields, $\mathcal{G}[0, 0] = -\ln \mathcal{Z}$, where

$$\mathcal{Z} = \int \mathcal{D}\psi \mathcal{D}\bar{\psi} e^{-\mathcal{S}[\psi,\bar{\psi}]} \tag{6}$$

is the partition function of the interacting system. The connected m-particle Green functions are given by

$$\begin{aligned} G^{(2m)}(x_1, \ldots, x_m; x_1', \ldots, x_m') &= -\langle \psi(x_1) \cdots \psi(x_m) \bar{\psi}(x_m') \cdots \bar{\psi}(x_1') \rangle_c \\ &= (-1)^m \frac{\partial^{2m} \mathcal{G}[\eta, \bar{\eta}]}{\partial \bar{\eta}(x_1) \cdots \partial \bar{\eta}(x_m) \partial \eta(x_m') \cdots \partial \eta(x_1')} \Bigg|_{\eta, \bar{\eta}=0}, \end{aligned} \tag{7}$$

where $\langle \cdots \rangle_c$ is the connected average of the product of Grassmann variables between the brackets. The one-particle Green function $G^{(2)}$ is the propagator of the interacting system, which we usually denote without the superscript by G. Expanding $\mathcal{G}[\eta, \bar{\eta}]$ in the fields yields a formal power series with the connected Green functions as coefficients,

$$\begin{aligned} \mathcal{G}[\eta, \bar{\eta}] &= -\ln \mathcal{Z} + (\bar{\eta}, G\eta) + \frac{1}{(2!)^2} \sum_{x_1, x_2, x_1', x_2'} G^{(4)}(x_1, x_2; x_1', x_2') \\ &\quad \times \bar{\eta}(x_1) \bar{\eta}(x_2) \eta(x_2') \eta(x_1') + \cdots. \end{aligned} \tag{8}$$

Renormalization group equations are most conveniently formulated for the Legendre transform of $\mathcal{G}[\eta, \bar{\eta}]$, the so-called effective action

$$\Gamma[\psi, \bar{\psi}] = (\bar{\eta}, \psi) + (\bar{\psi}, \eta) + \mathcal{G}[\eta, \bar{\eta}], \tag{9}$$

with $\psi = -\partial \mathcal{G}/\partial \bar{\eta}$ and $\bar{\psi} = \partial \mathcal{G}/\partial \eta$, which generates one-particle irreducible vertex functions (Negele and Orland, 1987)

$$\begin{aligned} \Gamma^{(2m)}(x_1', \ldots, x_m'; x_1, \ldots, x_m) &= \frac{\partial^{2m} \Gamma[\psi, \bar{\psi}]}{\partial \bar{\psi}(x_1') \cdots \partial \bar{\psi}(x_m') \partial \psi(x_m) \cdots \partial \psi(x_1)} \Bigg|_{\psi, \bar{\psi}=0}. \end{aligned} \tag{10}$$

In the noninteracting case one obtains $\Gamma[\psi, \bar{\psi}] = -\ln \mathcal{Z}_0 - (\bar{\psi}, G_0^{-1}\psi)$. The Legendre correspondence between the functionals $\mathcal{G}$ and Γ yields relations between the connected Green functions $G^{(2m)}$ and the vertex functions $\Gamma^{(2m)}$. In particular,

$$\Gamma^{(2)} = G^{-1} = G_0^{-1} - \Sigma, \tag{11}$$

where Σ is the self-energy. The connected two-particle Green function is related to the two-particle vertex by

$$\begin{aligned} G^{(4)}(x_1, x_2; x_1', x_2') &= \sum_{y_1, y_2, y_1', y_2'} G(x_1, y_1') G(x_2, y_2') \Gamma^{(4)}(y_1', y_2'; y_1, y_2) \\ &\quad \times G(y_1, x_1') G(y_2, x_2'), \end{aligned} \tag{12}$$

while the three-particle Green function $G^{(6)} = G^3 \Gamma^{(6)} G^3 + G^3 \Gamma^{(4)} G \Gamma^{(4)} G^3$ involves $\Gamma^{(4)}$ and $\Gamma^{(6)}$. More generally, the connected m-particle Green functions are obtained by adding all possible trees that can be formed with vertex functions of equal or lower order and G lines (Negele and Orland, 1987).

The effective action obeys the reciprocity relations

$$\frac{\partial \Gamma}{\partial \psi} = -\bar{\eta}, \qquad \frac{\partial \Gamma}{\partial \bar{\psi}} = \eta. \tag{13}$$

The second functional derivatives of $\mathcal{G}$ and Γ with respect to the fields are also reciprocal (Negele and Orland, 1987). We define the matrices of second derivatives at finite fields as

$$\begin{aligned} \mathbf{G}^{(2)}[\eta, \bar{\eta}] &= -\begin{pmatrix} \frac{\partial^2 \mathcal{G}}{\partial \bar{\eta}(x) \partial \eta(x')} & -\frac{\partial^2 \mathcal{G}}{\partial \bar{\eta}(x) \partial \bar{\eta}(x')} \\ -\frac{\partial^2 \mathcal{G}}{\partial \eta(x) \partial \eta(x')} & \frac{\partial^2 \mathcal{G}}{\partial \eta(x) \partial \bar{\eta}(x')} \end{pmatrix} \\ &= -\begin{pmatrix} \langle \psi(x) \bar{\psi}(x') \rangle & \langle \psi(x) \psi(x') \rangle \\ \langle \bar{\psi}(x) \bar{\psi}(x') \rangle & \langle \bar{\psi}(x) \psi(x') \rangle \end{pmatrix} \end{aligned} \tag{14}$$

and

$$\begin{aligned} \mathbf{\Gamma}^{(2)}[\psi, \bar{\psi}] &= \begin{pmatrix} \frac{\partial^2 \Gamma}{\partial \bar{\psi}(x') \partial \psi(x)} & \frac{\partial^2 \Gamma}{\partial \bar{\psi}(x') \partial \bar{\psi}(x)} \\ \frac{\partial^2 \Gamma}{\partial \psi(x') \partial \psi(x)} & \frac{\partial^2 \Gamma}{\partial \psi(x') \partial \bar{\psi}(x)} \end{pmatrix} \\ &= \begin{pmatrix} \bar{\partial} \partial \Gamma[\psi, \bar{\psi}](x', x) & \bar{\partial}\, \bar{\partial}\, \Gamma[\psi, \bar{\psi}](x', x) \\ \partial \partial \Gamma[\psi, \bar{\psi}](x', x) & \partial \bar{\partial} \Gamma[\psi, \bar{\psi}](x', x) \end{pmatrix}, \end{aligned} \tag{15}$$

where the matrix elements in the second matrix of the last equation are just a more convenient notation for those in the first matrix. The reciprocity relation for the second derivatives reads

$$\mathbf{\Gamma}^{(2)}[\psi, \bar{\psi}] = (\mathbf{G}^{(2)}[\eta, \bar{\eta}])^{-1}. \tag{16}$$

Note that anomalous components are involved as long as the source fields are finite. Only at $\eta = \bar{\eta} = 0$ and $\psi = \bar{\psi} = 0$, and in the absence of U(1) charge symmetry breaking one has the simple relation $\Gamma^{(2)} = (G^{(2)})^{-1}$.

Another useful generating functional is the effective interaction (Salmhofer, 1999)

$$\mathcal{V}[\chi, \bar{\chi}] = -\ln \left\{ \frac{1}{\mathcal{Z}_0} \int \mathcal{D}\psi \mathcal{D}\bar{\psi} e^{(\bar{\psi}, G_0^{-1}\psi)} e^{-V[\psi+\chi, \bar{\psi}+\bar{\chi}]} \right\}. \tag{17}$$

A simple substitution of variables yields

$$\mathcal{V}[\chi,\bar{\chi}] = \mathcal{G}[\eta,\bar{\eta}] + \ln\mathcal{Z}_0 - (\bar{\eta}, G_0\eta), \tag{18}$$

where $\chi = G_0\eta$ and $\bar{\chi} = G_0^t\bar{\eta}$. Here G_0^t is the transposed bare propagator, that is, $G_0^t(x,x') = G_0(x',x)$. Hence, functional derivatives of $\mathcal{V}[\chi,\bar{\chi}]$ with respect to χ and $\bar{\chi}$ generate connected Green functions with bare propagators amputated from external legs in the corresponding Feynman diagrams. The term $\ln\mathcal{Z}_0 - (\bar{\eta}, G_0\eta)$ cancels the noninteracting part of $\mathcal{G}[\bar{\eta},\eta]$ such that $\mathcal{V}[\chi,\bar{\chi}] = 0$ for $V[\psi,\bar{\psi}] = 0$. The effective interaction $\mathcal{V}$ can also be expressed via functional derivatives, instead of a functional integral:

$$\begin{aligned} e^{-\mathcal{V}[\chi,\bar{\chi}]} &= \frac{1}{\mathcal{Z}_0}\int \mathcal{D}\psi\mathcal{D}\bar{\psi}\, e^{(\bar{\psi},G_0^{-1}\psi)} e^{-V[\psi+\chi,\bar{\psi}+\bar{\chi}]} \\ &= \frac{1}{\mathcal{Z}_0}\, e^{-V[\partial_{\bar{\eta}},\partial_\eta]}\int \mathcal{D}\psi\mathcal{D}\bar{\psi}\, e^{(\bar{\psi},G_0^{-1}\psi)} \\ &\quad\times e^{(\bar{\eta},\psi+\chi)+(\eta,\bar{\psi}+\bar{\chi})}\Big|_{\eta,\bar{\eta}=0} \\ &= e^{-V[\partial_{\bar{\eta}},\partial_\eta]} e^{(\bar{\eta},G_0\eta)} e^{(\bar{\eta},\chi)+(\eta,\bar{\chi})}\Big|_{\eta,\bar{\eta}=0} \\ &= e^{-V[\partial_{\bar{\eta}},\partial_\eta]} e^{(\partial_\chi,G_0\partial_{\bar{\chi}})} e^{(\bar{\eta},\chi)+(\eta,\bar{\chi})}\Big|_{\eta,\bar{\eta}=0} \\ &= e^{\Delta_{G_0}} e^{-V[\chi,\bar{\chi}]}, \end{aligned} \tag{19}$$

with the functional Laplacian

$$\Delta_{G_0} = (\partial_\chi, G_0\partial_{\bar{\chi}}) = \sum_{x,x'}\frac{\partial}{\partial\chi(x)} G_0(x,x')\frac{\partial}{\partial\bar{\chi}(x')}. \tag{20}$$

It is sometimes convenient (see Sec. II.G) to combine the fields ψ and $\bar{\psi}$ in a Nambu-type field

$$\Psi(x) = \begin{pmatrix}\psi(x)\\ \bar{\psi}(x)\end{pmatrix}, \tag{21}$$

and similarly for the source fields η and $\bar{\eta}$,

$$H(x) = \begin{pmatrix}\eta(x)\\ -\bar{\eta}(x)\end{pmatrix}. \tag{22}$$

The minus sign in the definition of H makes sure that the source term $(\bar{\eta},\psi) + (\bar{\psi},\eta)$ appearing in the definition of $\mathcal{G}$, and also in the Legendre transform relating $\mathcal{G}$ and Γ, can be written concisely as $(\bar{H},\Psi)$. In Nambu notation, the matrices of second derivatives of $\mathcal{G}$ and Γ have the compact form

$$\mathbf{G}^{(2)}[H] = -\frac{\partial^2\mathcal{G}}{\partial\bar{H}(x)\partial H(x')} \tag{23}$$

and

$$\mathbf{\Gamma}^{(2)}[\Psi] = \frac{\partial^2\Gamma}{\partial\bar{\Psi}(x')\partial\Psi(x)}, \tag{24}$$

respectively.

B. Exact fermionic flow equations

In this section we derive exact flow equations describing the evolution of the generating functionals defined above, as a function of a flow parameter Λ which parametrizes a modification of the bare propagator G_0. Usually Λ is an infrared cutoff or another scale dependence. For example, in a translation-invariant system one may impose a momentum cutoff, modifying G_0 to

$$G_0^\Lambda(k_0,\mathbf{k}) = \frac{\theta^\Lambda(\mathbf{k})}{ik_0 - \xi_\mathbf{k}}, \tag{25}$$

where $\theta^\Lambda(\mathbf{k})$ is a function that vanishes for $|\xi_\mathbf{k}| \ll \Lambda$ and tends to one for $|\xi_\mathbf{k}| \gg \Lambda$. In this way the infrared singularity of the propagator at $k_0 = 0$ and $\xi_\mathbf{k} = 0$ (corresponding to the noninteracting Fermi surface in $\mathbf{k}$ space) is cut off at the scale Λ. A simple choice for $\theta^\Lambda(\mathbf{k})$, which was often used in numerical solutions of truncated flow equations, is

$$\theta^\Lambda(\mathbf{k}) = \Theta(|\xi_\mathbf{k}| - \Lambda), \tag{26}$$

where Θ is the step function. With this choice momenta close to the Fermi surface are strictly excluded, as illustrated in Fig. 2 for a two-dimensional lattice fermion system.

Alternatively, one may also use a smooth cutoff function. In the absence of translation invariance it is more convenient to use a frequency cutoff instead of a momentum cutoff. The cutoff excludes "soft modes" below the scale Λ from the functional integral. Instead of a cutoff one can also choose other flow parameters such as temperature. The various possibilities will be discussed more extensively in Sec. II.D. For the derivation of the flow equations it does not matter how G_0^Λ depends on Λ.

The bare action constructed with G_0^Λ (instead of G_0) is denoted by $\mathcal{S}^\Lambda[\psi,\bar{\psi}]$, and the generating functionals introduced in Sec. II.A by $\mathcal{G}^\Lambda[\eta,\bar{\eta}]$, $\mathcal{V}^\Lambda[\chi,\bar{\chi}]$, and $\Gamma^\Lambda[\psi,\bar{\psi}]$, respectively. The original functionals $\mathcal{G}$, $\mathcal{V}$, and Γ are recovered in the limit $\Lambda\to 0$.

In the presence of a cutoff, Eq. (19) becomes

$$e^{-\mathcal{V}^\Lambda} = e^{\Delta_{G_0^\Lambda}} e^{-V}. \tag{27}$$

At the highest energy scale Λ_0 one has $G_0^{\Lambda_0} = 0$, and thus $\mathcal{V}^{\Lambda_0} = V$. Hence, $\mathcal{V}^\Lambda$ interpolates smoothly between the bare interaction V and the generating functional $\mathcal{V}$. Introducing the soft mode propagator

$$\bar{G}_0^\Lambda = G_0 - G_0^\Lambda, \tag{28}$$

which has support on scales below Λ, we write

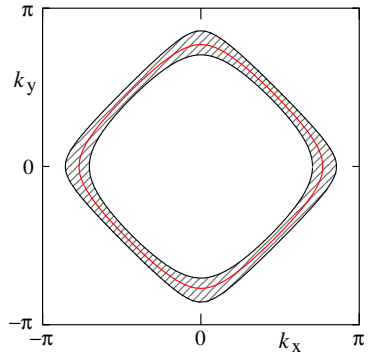

FIG. 2 (color online). Momentum space region around the Fermi surface excluded by a sharp momentum cutoff for fermions with a tight-binding dispersion on a two-dimensional square lattice (lattice constant = 1).

$$e^{-\mathcal{V}} = e^{\Delta_{G_0}} e^{-V} = e^{\Delta_{\tilde{G}_0^\Lambda} + \Delta_{G_0^\Lambda}} e^{-V} = e^{\Delta_{\tilde{G}_0^\Lambda}} e^{-\mathcal{V}^\Lambda}. \quad (29)$$

$\mathcal{V}^\Lambda$ obviously plays a dual role: It is the generating functional for (amputated) Green functions of a system with a cutoff Λ, and at the same time the interaction for the remaining low-energy degrees of freedom (Morris, 1994; Salmhofer, 1999).

The effective interaction satisfies the following exact renormalization group equation (Brydges and Wright, 1988; Salmhofer, 1999):

$$\frac{d}{d\Lambda}\mathcal{V}^\Lambda[\chi, \bar{\chi}] = -\left(\frac{\partial \mathcal{V}^\Lambda}{\partial \chi}, \dot{G}_0^\Lambda \frac{\partial \mathcal{V}^\Lambda}{\partial \bar{\chi}}\right) - \mathrm{tr}\left(\dot{G}_0^\Lambda \frac{\partial^2 \mathcal{V}^\Lambda}{\partial \bar{\chi}\partial \chi}\right), \quad (30)$$

where $\dot{G}_0^\Lambda = \frac{d}{d\Lambda} G_0^\Lambda$ and tr denotes the trace $\mathrm{tr}A = \sum_x A(x, x)$. Its derivation is simple:

$$\begin{aligned}\frac{d}{d\Lambda}\mathcal{V}^\Lambda &= -e^{\mathcal{V}^\Lambda}\frac{d}{d\Lambda}e^{-\mathcal{V}^\Lambda} \\ &= -e^{\mathcal{V}^\Lambda}\frac{d}{d\Lambda}(e^{\Delta_{\dot{G}_0^\Lambda}} e^{-V}) \\ &= -e^{\mathcal{V}^\Lambda}\Delta_{\dot{G}_0^\Lambda} e^{-\mathcal{V}^\Lambda} \\ &= \text{right-hand side of Eq. (30).}\end{aligned}$$

In the second step we used Eq. (27). With the initial condition

$$\mathcal{V}^{\Lambda_0}[\chi, \bar{\chi}] = V[\chi, \bar{\chi}], \quad (31)$$

the RG equation determines the flow of $\mathcal{V}^\Lambda$ uniquely for all $\Lambda < \Lambda_0$. The initial value Λ_0 must be chosen such that $G_0^{\Lambda_0}$ vanishes. For a sharp momentum cutoff, Λ_0 can be chosen as the maximal value of $|\xi_{\mathbf{k}}|$; for a frequency cutoff $\Lambda_0 = \infty$.

An expansion of the functional $\mathcal{V}^\Lambda[\chi, \bar{\chi}]$ in the renormalization group equation (30) in powers of χ and $\bar{\chi}$ leads to the fermionic analog of Polchinski's flow equations for amputated connected m-particle Green functions $V^{(2m)\Lambda}$ (Polchinski, 1984).

From the flow equation for $\mathcal{V}^\Lambda$, Eq. (30), and Eq. (18) applied to $\mathcal{V}^\Lambda$ and $\mathcal{G}^\Lambda$, one obtains an exact flow equation for $\mathcal{G}^\Lambda$:

$$\frac{d}{d\Lambda}\mathcal{G}^\Lambda[\eta, \bar{\eta}] = \left(\frac{\partial \mathcal{G}^\Lambda}{\partial \eta}, \dot{Q}_0^\Lambda \frac{\partial \mathcal{G}^\Lambda}{\partial \bar{\eta}}\right) + \mathrm{tr}\left(\dot{Q}_0^\Lambda \frac{\partial^2 \mathcal{G}^\Lambda}{\partial \bar{\eta}\partial \eta}\right), \quad (32)$$

where $Q_0^\Lambda = (G_0^\Lambda)^{-1}$ and the dot denotes a Λ derivative. This flow equation can also be derived more directly by applying a Λ derivative to the functional integral representation of $\mathcal{G}^\Lambda$.

The flow equations for $G^{(2m)\Lambda}$ and $V^{(2m)\Lambda}$ generate, among others, one-particle reducible terms, which require some special care. In this respect the flow equations for one-particle irreducible vertex functions $\Gamma^{(2m)\Lambda}$, obtained from the scale-dependent effective action,

$$\Gamma^\Lambda[\psi, \bar{\psi}] = (\bar{\eta}^\Lambda, \psi) + (\bar{\psi}, \eta^\Lambda) + \mathcal{G}^\Lambda[\eta^\Lambda, \bar{\eta}^\Lambda], \quad (33)$$

are easier to handle. Note that η^Λ and $\bar{\eta}^\Lambda$ are Λ-dependent functions of ψ and $\bar{\psi}$, as they are determined by the Λ-dependent equations $\psi = -\partial \mathcal{G}^\Lambda/\partial \bar{\eta}$ and $\bar{\psi} = \partial \mathcal{G}^\Lambda/\partial \eta$. Since the Λ dependence does not change the structure of the action as a function of the fields, all standard relations between the connected Green functions $G^{(2m)}$ and the vertex functions $\Gamma^{(2m)}$ carry over to the ones for $G^{(2m)\Lambda}$ and $\Gamma^{(2m)\Lambda}$.

The Λ derivative of Γ^Λ can be written as

$$\begin{aligned}\frac{d}{d\Lambda}\Gamma^\Lambda[\psi, \bar{\psi}] = &\left(\frac{d}{d\Lambda}\bar{\eta}^\Lambda, \psi\right) + \left(\bar{\psi}, \frac{d}{d\Lambda}\eta^\Lambda\right) \\ &+ \frac{d}{d\Lambda}\mathcal{G}^\Lambda[\eta^\Lambda, \bar{\eta}^\Lambda],\end{aligned}$$

where the derivative in front of $\mathcal{G}^\Lambda$ acts also on the Λ dependence of η^Λ and $\bar{\eta}^\Lambda$. Because of the relations $\partial \mathcal{G}^\Lambda/\partial \eta = \bar{\psi}$ and $\partial \mathcal{G}^\Lambda/\partial \bar{\eta} = -\psi$, most terms cancel and one obtains

$$\frac{d}{d\Lambda}\Gamma^\Lambda[\psi, \bar{\psi}] = \frac{d}{d\Lambda}\mathcal{G}^\Lambda[\eta^\Lambda, \bar{\eta}^\Lambda]\Big|_{\eta^\Lambda, \bar{\eta}^\Lambda \text{ fixed}}. \quad (34)$$

Inserting the flow equation (32) for $\mathcal{G}^\Lambda$ and using the reciprocity relations (13) and (16), one obtains the exact functional flow equation for the effective action

$$\frac{d}{d\Lambda}\Gamma^\Lambda[\psi, \bar{\psi}] = -(\bar{\psi}, \dot{Q}_0^\Lambda \psi) - \frac{1}{2}\mathrm{tr}\{\dot{\mathbf{Q}}_0^\Lambda (\mathbf{\Gamma}^{(2)\Lambda}[\psi, \bar{\psi}])^{-1}\}. \quad (35)$$

Here $\mathbf{\Gamma}^{(2)\Lambda}[\psi, \bar{\psi}]$ is the matrix of second functional derivatives defined in Eq. (15), and

$$\mathbf{Q}_0^\Lambda = \begin{pmatrix} Q_0^\Lambda & 0 \\ 0 & -Q_0^{\Lambda t}\end{pmatrix} = \mathrm{diag}(Q_0^\Lambda, -Q_0^{\Lambda t}), \quad (36)$$

where $Q_0^{\Lambda t}(x, x') = Q_0^\Lambda(x', x)$.

Alternative definitions of the effective action Γ^Λ, differing by interaction-independent terms, have also been used. One variant is to normalize the functional integral defining $\mathcal{G}^\Lambda$ at $V = 0$, dividing by $\mathcal{Z}_0^\Lambda$. This yields an additional contribution $\ln \mathcal{Z}_0^\Lambda$ to $\mathcal{G}^\Lambda$ and to its Legendre transform Γ^Λ. In the flow equation for Γ^Λ this leads to an additional term $\mathrm{tr}(\dot{Q}_0^\Lambda G_0^\Lambda)$, which is field independent and therefore does not couple to the other contributions (Salmhofer and Honerkamp, 2001). Another variant is (Ellwanger and Wetterich, 1994; Berges, Tetradis, and Wetterich, 2002)

$$\Gamma_R^\Lambda[\psi, \bar{\psi}] = \Gamma^\Lambda[\psi, \bar{\psi}] + (\bar{\psi}, R^\Lambda \psi), \quad (37)$$

where $R^\Lambda = Q_0^\Lambda - Q_0$. The additional quadratic term cancels the first (trivial) term in the flow equation (35) for Γ^Λ, and one obtains the equivalent flow equation

$$\frac{d}{d\Lambda}\Gamma_R^\Lambda[\psi, \bar{\psi}] = -\frac{1}{2}\mathrm{tr}\{\dot{\mathbf{R}}^\Lambda (\mathbf{\Gamma}_R^{(2)\Lambda}[\psi, \bar{\psi}] + \mathbf{R}^\Lambda)^{-1}\}, \quad (38)$$

where $\mathbf{R}^\Lambda = \mathrm{diag}(R^\Lambda, -R^{\Lambda t})$. The functional Γ_R^Λ and its analog for bosonic fields is known as effective average action in the literature (Berges, Tetradis, and Wetterich, 2002). Both Γ_R^Λ and Γ^Λ tend to the same effective action Γ in the limit $\Lambda \to 0$, where R^Λ vanishes. At the initial scale Λ_0, one has $\Gamma_R^{\Lambda_0}[\psi, \bar{\psi}] = \mathcal{S}[\psi, \bar{\psi}]$, while

$$\begin{aligned}\Gamma^{\Lambda_0}[\psi, \bar{\psi}] &= -(\bar{\psi}, Q_0^{\Lambda_0}\psi) + V[\psi, \bar{\psi}] = \mathcal{S}^{\Lambda_0}[\psi, \bar{\psi}] \\ &= \mathcal{S}[\psi, \bar{\psi}] - (\bar{\psi}, R^{\Lambda_0}\psi). \quad (39)\end{aligned}$$

Hence, Γ_R^Λ has the attractive feature that it interpolates smoothly between the (unregularized) bare action $\mathcal{S}$ and the final effective action Γ, while Γ^Λ interpolates between the *regularized* bare action $\mathcal{S}^{\Lambda_0}$ and Γ. On the other hand, the functional Γ^Λ has the advantage that its second functional derivative directly yields the inverse propagator $(G^\Lambda)^{-1}$ without the need to add R^Λ.

In Appendix A we present another version of exact flow equations, based on a *Wick-ordered* effective interaction. That version also contains one-particle reducible contributions, but it has the distinct advantage that the vertices are connected by propagators with an energy scale at or below Λ. This facilitates a systematic power counting (Salmhofer, 1999), and also a numerical evaluation of flow equations, since the integration regions shrink upon lowering Λ.

It is instructive to compare the functional RG flow equations with the traditional Wilsonian momentum-shell RG (Wilson and Kogut, 1974), which was applied to Fermi systems by Shankar (1991, 1994) and Polchinski (1993). In the commonly used version of Wilson's RG, the flow of the effective action is computed only for soft fields, that is, for fields with energy or momentum variables below the scale Λ, while in the functional RG the effective action with unrestricted source fields is computed. This allows for a direct calculation of correlation functions with arbitrary external variables such as momenta or Matsubara frequencies. Furthermore, in the traditional implementations of Wilson's RG the integration of degrees of freedom is combined with a rescaling of momenta and fields, which is chosen such that the momentum space and certain terms in the quadratic part of the action remain invariant during the flow. This facilitates the classification of interactions as relevant, marginal, or irrelevant, and helps to identify fixed points of the flow. The functional RG flow equations derived above do not involve any rescaling. Rescaling momentum space in a shell around the Fermi surface requires a nonlinear transformation in dimensions $d > 1$, which spoils the simple linear form of momentum conservation (Shankar, 1994; Metzner, Castellani, and Di Castro, 1998; Kopietz and Busche, 2001), and is therefore of questionable value. Power counting can be done also without rescaling, as shown in Sec. II.E. Rescaling of the fields can be implemented easily by a simple substitution of variables (Shankar, 1994; Kopietz and Busche, 2001). However, in many applications of the functional RG, quantitative results including power laws with anomalous scaling dimensions are obtained simply by direct calculation of the (unscaled) physical quantities.

C. Expansion in the fields

1. Hierarchy of flow equations

The functional flow equation for the effective action can be expanded in powers of the fields. To this end we expand the effective action as

$$\Gamma^\Lambda[\psi,\bar\psi] = \sum_{m=0}^{\infty} \mathcal{A}^{(2m)\Lambda}[\psi,\bar\psi], \tag{40}$$

where $\mathcal{A}^{(2m)\Lambda}[\psi,\bar\psi]$ is homogeneous of degree $2m$ in the fields,

$$\mathcal{A}^{(2m)\Lambda}[\psi,\bar\psi] = \frac{(-1)^m}{(m!)^2} \times \sum_{\substack{x_1,\ldots,x_m \\ x_1',\ldots,x_m'}} \Gamma^{(2m)\Lambda}(x_1',\ldots,x_m';x_1,\ldots,x_m) \times \bar\psi(x_1')\cdots\bar\psi(x_m')\psi(x_m)\cdots\psi(x_1), \tag{41}$$

for $m \geq 1$. The field-independent constant $\mathcal{A}^{(0)\Lambda}$ yields the grand canonical potential:

$$\mathcal{A}^{(0)\Lambda} = T^{-1}\Omega^\Lambda. \tag{42}$$

Here we restored the explicit temperature factor, since it is independent of the representation of the fields. To expand the inverse of $\mathbf{\Gamma}^{(2)\Lambda}$ on the right-hand side of the flow equation, we isolate the field-independent part of $\mathbf{\Gamma}^{(2)\Lambda}$ as

$$\mathbf{\Gamma}^{(2)\Lambda}[\psi,\bar\psi] = (\mathbf{G}^\Lambda)^{-1} - \tilde{\mathbf{\Sigma}}^\Lambda[\psi,\bar\psi], \tag{43}$$

where

$$\mathbf{G}^\Lambda = (\mathbf{\Gamma}^{(2)\Lambda}[\psi,\bar\psi]|_{\psi,\bar\psi=0})^{-1} = \mathrm{diag}(G^\Lambda, -G^{\Lambda t}) \tag{44}$$

is the full propagator, and [cf. Eq. (15)]

$$\tilde{\mathbf{\Sigma}}^\Lambda[\psi,\bar\psi] = -\begin{pmatrix} \bar\partial\partial\Gamma^\Lambda[\psi,\bar\psi] & \bar\partial\,\bar\partial\Gamma^\Lambda[\psi,\bar\psi] \\ \partial\partial\Gamma^\Lambda[\psi,\bar\psi] & \partial\bar\partial\Gamma^\Lambda[\psi,\bar\psi] \end{pmatrix} + (\mathbf{G}^\Lambda)^{-1}. \tag{45}$$

Note that $\tilde{\mathbf{\Sigma}}^\Lambda[\psi,\bar\psi]$ contains all contributions to $\mathbf{\Gamma}^{(2)\Lambda}[\psi,\bar\psi]$ which are at least quadratic in the fields. We now expand $(\mathbf{\Gamma}^{(2)\Lambda})^{-1} = (1 - \mathbf{G}^\Lambda\tilde{\mathbf{\Sigma}}^\Lambda)^{-1}\mathbf{G}^\Lambda$ as a geometric series. Inserted into Eq. (35), this yields

$$\frac{d}{d\Lambda}\Gamma^\Lambda[\psi,\bar\psi] = -\mathrm{tr}(\dot Q_0^\Lambda G^\Lambda) - (\bar\psi, \dot Q_0^\Lambda\psi) + \frac{1}{2}\,\mathrm{tr}\{\mathbf{S}^\Lambda(\tilde{\mathbf{\Sigma}}^\Lambda[\psi,\bar\psi] + \tilde{\mathbf{\Sigma}}^\Lambda[\psi,\bar\psi]\mathbf{G}^\Lambda\tilde{\mathbf{\Sigma}}^\Lambda[\psi,\bar\psi] + \cdots)\}, \tag{46}$$

where

$$\mathbf{S}^\Lambda = \mathrm{diag}(S^\Lambda, -S^{\Lambda t}) = -\mathbf{G}^\Lambda\dot{\mathbf{Q}}_0^\Lambda\mathbf{G}^\Lambda. \tag{47}$$

Using the Dyson equation $(G^\Lambda)^{-1} = Q_0^\Lambda - \Sigma^\Lambda$, the so-called single-scale propagator S^Λ can also be written as a Λ derivative of the propagator at fixed self-energy,

$$S^\Lambda = \frac{d}{d\Lambda}G^\Lambda\Big|_{\Sigma^\Lambda\ \mathrm{fixed}}. \tag{48}$$

The expansion of the flow equation in powers of ψ, $\bar\psi$ is now straightforward and leads to a hierarchy of flow equations for Σ^Λ, the two-particle vertex $\Gamma^{(4)\Lambda}$, and the higher-order vertices $\Gamma^{(6)\Lambda}$, $\Gamma^{(8)\Lambda}$, etc. The first three equations in this hierarchy are shown diagrammatically in Fig. 3. Note that only one-particle irreducible one-loop diagrams contribute, and internal lines are dressed by self-energy corrections. The hierarchy does not close at any finite order, since the flow of each vertex $\Gamma^{(2m)\Lambda}$ receives a contribution from a tadpole diagram involving $\Gamma^{(2m+2)\Lambda}$, and m-particle vertices with arbitrary m are generated by the flow, irrespective of their presence in the bare action.

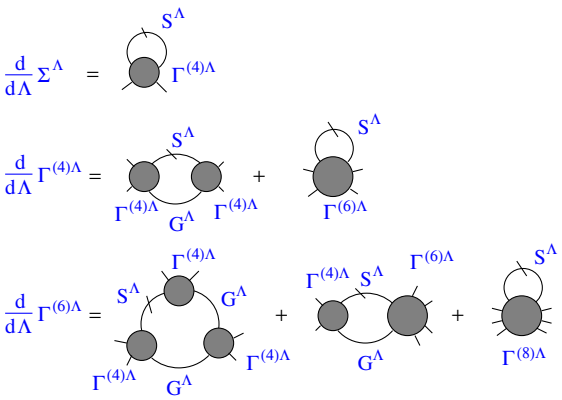

FIG. 3 (color online). Diagrammatic representation of the flow equations for the self-energy Σ^Λ, the two-particle vertex $\Gamma^{(4)\Lambda}$, and the three-particle vertex $\Gamma^{(6)\Lambda}$ in the one-particle irreducible version of the functional RG. Lines with a dash correspond to the single-scale propagator S^Λ, and the other lines to the full propagator G^Λ.

We now derive explicitly the first two flow equations from the hierarchy. Comparing coefficients of quadratic contributions (proportional to $\bar{\psi}\psi$) to the exact flow equation yields

$$\frac{d}{d\Lambda}\mathcal{A}^{(2)\Lambda} = -(\bar{\psi}, \dot{Q}_0^\Lambda \psi) - \mathrm{tr}(S^\Lambda \bar{\partial}\partial \mathcal{A}^{(4)\Lambda}). \tag{49}$$

Inserting Eq. (41), and using $\Gamma^{(2)\Lambda} = Q_0^\Lambda - \Sigma^\Lambda$, one obtains the flow equation for the self-energy,

$$\frac{d}{d\Lambda}\Sigma^\Lambda(x', x) = \sum_{y,y'} S^\Lambda(y, y')\Gamma^{(4)\Lambda}(x', y'; x, y). \tag{50}$$

Comparing coefficients of quartic contributions [proportional to $(\bar{\psi}\psi)^2$] yields

$$\begin{aligned}\frac{d}{d\Lambda}\mathcal{A}^{(4)\Lambda} = {} & \frac{1}{2}\,\mathrm{tr}(S^\Lambda \bar{\partial}\partial \mathcal{A}^{(4)\Lambda} G^\Lambda \bar{\partial}\partial \mathcal{A}^{(4)\Lambda} \\ & + S^{\Lambda t}\partial\bar{\partial}\mathcal{A}^{(4)\Lambda} G^{\Lambda t}\partial\bar{\partial}\mathcal{A}^{(4)\Lambda}) \\ & - \frac{1}{2}\,\mathrm{tr}(S^\Lambda \bar{\partial}\,\bar{\partial}\,\mathcal{A}^{(4)\Lambda} G^{\Lambda t}\partial\partial\mathcal{A}^{(4)\Lambda} \\ & + S^{\Lambda t}\partial\partial\mathcal{A}^{(4)\Lambda} G^\Lambda \bar{\partial}\,\bar{\partial}\,\mathcal{A}^{(4)\Lambda}) \\ & - \mathrm{tr}(S^\Lambda \bar{\partial}\partial \mathcal{A}^{(6)\Lambda}).\end{aligned} \tag{51}$$

Inserting Eq. (41), one obtains the flow equation for the two-particle vertex,

$$\begin{aligned}&\frac{d}{d\Lambda}\Gamma^{(4)\Lambda}(x_1', x_2'; x_1, x_2) \\ &= \sum_{y_1,y_1'}\sum_{y_2,y_2'} G^\Lambda(y_1, y_1')S^\Lambda(y_2, y_2') \\ &\quad \times \{\Gamma^{(4)\Lambda}(x_1', x_2'; y_1, y_2)\Gamma^{(4)\Lambda}(y_1', y_2'; x_1, x_2) \\ &\quad - [\Gamma^{(4)\Lambda}(x_1', y_2'; x_1, y_1)\Gamma^{(4)\Lambda}(y_1', x_2'; y_2, x_2) \\ &\quad + (y_1 \leftrightarrow y_2, y_1' \leftrightarrow y_2')] + [\Gamma^{(4)\Lambda}(x_2', y_2'; x_1, y_1) \\ &\quad \times \Gamma^{(4)\Lambda}(y_1', x_1'; y_2, x_2) + (y_1 \leftrightarrow y_2, y_1' \leftrightarrow y_2')]\} \\ &\quad - \sum_{y,y'} S^\Lambda(y, y')\Gamma^{(6)\Lambda}(x_1', x_2', y'; x_1, x_2, y).\end{aligned} \tag{52}$$

Note that there are several distinct contributions involving two two-particle vertices, corresponding to the familiar particle-particle, direct particle-hole, and crossed particle-hole channels, respectively, as shown diagrammatically in Fig. 4. Similarly, one can obtain the flow equation for $\Gamma^{(6)}$ and all higher vertices.

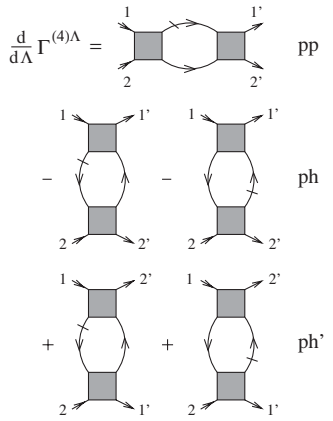

FIG. 4. Contributions to the flow of the two-particle vertex with particle-particle and particle-hole channels written explicitly, without the contribution from $\Gamma^{(6)\Lambda}$.

Since $\Gamma[\psi, \bar{\psi}]$ at $\psi = \bar{\psi} = 0$ is essentially (up to a factor T) the grand canonical potential Ω, the flow equation (35), evaluated at vanishing fields, yields also a flow equation for the grand canonical potential:

$$\frac{d}{d\Lambda}\Omega^\Lambda = -T\,\mathrm{tr}(\dot{Q}_0^\Lambda G^\Lambda). \tag{53}$$

The flow equation (35) and the ensuing equations for the vertex functions can be easily generalized to cases with U(1)-symmetry breaking by allowing for off-diagonal elements in the matrices $\mathbf{Q}_0^\Lambda$, $\mathbf{G}^\Lambda$, and $\mathbf{S}^\Lambda$.

2. Truncations

The exact hierarchy of flow equations for the vertex functions can be solved only for systems which can also be solved more directly, that is, without using flow equations. Usually truncations are unavoidable. A natural truncation is to neglect the flow of all vertices $\Gamma^{(2m)\Lambda}$ beyond a certain order m_0. We call this the level-m_0 truncation. The structure of the resulting equations and general properties of their solution will be discussed in Sec. II.E. Note that the level-m_0 truncation contains all perturbative contributions to order m_0 in the bare two-particle interaction.

In practice, in applications to physically interesting systems, vertices $\Gamma^{(2m)\Lambda}$ with $m > 3$ have so far been neglected, and the contributions from $\Gamma^{(6)\Lambda}$ to the flow of $\Gamma^{(4)\Lambda}$ are usually restricted to self-energy corrections (see below) or discarded completely. In particular, the analysis of competing instabilities (see Sec. III) is based entirely on a level-2 truncation given by the flow equation (52) for the two-particle vertex, with $\Gamma^{(6)\Lambda}$ replaced by zero, where the self-energy feedback is also neglected. This seemingly simple approximation captures the complex interplay of fluctuations in the particle-particle and particle-hole channel, which leads to interesting effects such as the generation of d-wave superconductivity from antiferromagnetic fluctuations. In the quantum transport phenomena reviewed in Sec. VI, the self-energy as given by the flow equation (50) plays a crucial

role. Some of the phenomena described there are already obtained by a level-1 approximation where the flowing two-particle vertex in Eq. (50) is approximated by the bare one. That truncation might look like a Hartree-Fock approximation, but it is, in fact, different, and it works well in cases where Hartree-Fock fails completely.

The truncated flow equations are still rather complicated. They involve the flow of functions, not just a limited number of running couplings. For example, the effective two-particle interaction in a translation-invariant system is a function of three independent momentum and energy variables. Hence, a simplified parametrization of effective interactions is necessary even for a numerical solution. A useful strategy is to neglect dependences which become irrelevant in the low-energy limit, that is, whose contributions to the flow scale to zero.

Contributions to the effective action are called "relevant," "marginal," and "irrelevant," if their importance increases, stays fixed, or decreases, respectively, upon lowering the scale Λ. This classification can be obtained from power counting. To this end, one traditionally considers a renormalization group transformation where one rescales momenta and fields after the integration over fields in a momentum shell of width $d\Lambda$ such that a certain quadratic part of the action (the Gaussian fixed point) remains invariant (Wilson and Kogut, 1974). From the behavior of the other terms of the action under this transformation one can directly assess whether they increase, remain invariant, or decrease compared to the quadratic part.

For Fermi systems in dimensions $d > 1$ the conventional RG transformation is not applicable, since the reduction of momentum space by the mode elimination cannot be compensated by a linear rescaling of momenta (Shankar, 1991, 1994). However, one can perform the power counting more directly by estimating the scale dependences of Feynman diagrams on the right-hand side of the flow equations. As described in Sec. II.E.3, this can be done rigorously and to all orders. At the crudest level the power counting is independent of dimensionality and corresponds to what one would get from the above-mentioned RG transformation applied to one-dimensional systems (Shankar, 1994), that is, (i) the self-energy has a relevant piece describing a Fermi surface shift, while linear dependences on frequency and momentum perpendicular to the Fermi surface are marginal; (ii) a regular two-particle interaction is marginal; its dependences on frequencies and momenta perpendicular to the Fermi surface are irrelevant, such that one can parametrize it by its static value on the Fermi surface; and (iii) regular m-particle interactions with $m \geq 3$ are irrelevant. This basic classification does not depend on dimensionality because the bare propagator G_0, Eq. (3), is singular on a $(d-1)$-dimensional surface, such that the codimension of the singularity in the $(d+1)$-dimensional space spanned by momentum and frequency is always two.

One should, however, not jump to the conclusion that the $m \geq 3$ terms can simply be discarded from the RG hierarchy in general. This is because effective interactions with $m \geq 3$ may diverge for small Λ even in the case of finite two-particle interactions. For example, the first contribution to the flow of $\Gamma^{(6)\Lambda}$ in Fig. 3 generates a three-particle interaction of order

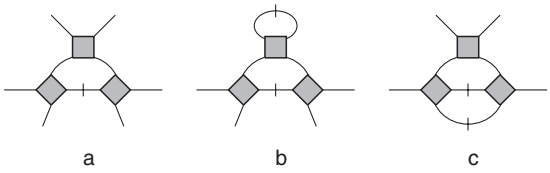

FIG. 5. (a) Third order graph contributing to $\Gamma^{(6)\Lambda}$. (b) Tadpole contraction. (c) Contraction to form a graph with overlapping loops.

Λ^{-1} if the external momenta add up to zero at each vertex. When inserted into the equation for $\Gamma^{(4)\Lambda}$ in Fig. 3, this may give rise to a marginal term of third order in $\Gamma^{(4)\Lambda}$. For $d = 1$, this term is indeed marginal. However, if $d \geq 2$ and the Fermi surface is curved, this and other contributions are suppressed below the basic power-counting estimate due to geometrically reduced integration volumes (Feldman and Trubowitz, 1990; Shankar, 1994). This improved power counting is described in Appendix B.3. It can also be used to give a precise, scale-dependent meaning to nesting of the Fermi surface.

A less obvious effect is that this improvement becomes uniform, that is, independent of the external momenta, in graphs with overlapping loops (Feldman, Salmhofer, and Trubowitz, 1996; Salmhofer, 1998a), so that their contribution gets further suppressed (see also Appendix B.3). It is this effect which implies that the derivative of the self-energy is not marginal, but irrelevant for curved Fermi surfaces in dimension $d \geq 2$. Moreover, it justifies truncated flows beyond the weak-coupling regime, as follows. Consider again the first contribution to the flow of $\Gamma^{(6)\Lambda}$, shown also in Fig. 5(a). When this term is inserted into the equation for $\Gamma^{(4)\Lambda}$, the two lines can be joined in two ways, shown in Figs. 5(b) and 5(c). Figure 5(b) gets no extra small factor, but Fig. 5(c) has overlapping loops and for positively curved Fermi surfaces in $d = 2$, its contribution gets suppressed by an additional small factor $\sim(\Lambda/\Lambda_I)\log(\Lambda_I/\Lambda)$ at scales below a scale Λ_I, which depends only on the geometry of the constant energy surfaces of the initial dispersion $\epsilon_{\mathbf{k}}$ (Feldman, Salmhofer, and Trubowitz, 1998). This suppression holds uniformly for all values of the external momenta. For $d = 3$, a similar bound holds, without the logarithm. Similar (in general, weaker) estimates are shown in Feldman, Salmhofer, and Trubowitz (1996) for general non-nested regular Fermi surfaces in $d \geq 2$ and for Fermi surfaces with van Hove singularities in Feldman and Salmhofer (2008a, 2008b). The contribution from Fig. 5(c) remains small compared to the second-order term if $|\Gamma^{(4)\Lambda}|(\Lambda/\Lambda_I)\log(\Lambda_I/\Lambda)$ is small. Note that this condition does not require $|\Gamma^{(4)\Lambda}|$ itself to be small: curvature effects justify dropping these terms beyond the weak-coupling regime, provided that the above condition is satisfied. This will be used in Sec. III. The detailed argument and a discussion of the consequences for the functional RG flow are given in Secs. 1 and 5 of Salmhofer and Honerkamp (2001).

In the theory of interacting Fermi systems, one is not only interested in low-energy fixed points and scaling, but also in the behavior at intermediate scales, and formally irrelevant terms may play an important role. There are cases where one wants to know the full temperature, momentum, or frequency dependence of physical quantities, because a low-energy

expansion contains insufficient information. One of the advantages of the functional RG framework is that such dependences can be computed directly.

In many situations, a comparison to standard resummations of the perturbation expansion is desirable, and it is also an interesting question to what extent such resummations can be reproduced by truncations of the functional RG flow equations. An important observation regarding this was made by Katanin (2004), who showed that a partial inclusion of the six-point vertex in the flow allows one to recover approximations of the type Hartree-plus-ladder summations (in cases where these approximations are a good starting point). This also allows one to continue fermionic flows into symmetry-broken phases (see Sec. IV). If we drop the eight-point vertex from the equation for $\Gamma^{(6)\Lambda}$, it is determined by a Feynman graph containing three four-point vertices, depicted in Fig. 5(a). When backsubstituted into the equation for the four-point vertex, two external legs get contracted in all possible ways. We have just discussed that the contribution from Fig. 5(c) is suppressed by improved power counting. When two legs of a single-four-point vertex are contracted to form a tadpole [see Fig. 5(b)], the value of the thus obtained subgraph is $\dot{\Sigma}^{\Lambda}$, by the flow equation for the self-energy. Thus a factor $G^{\Lambda}\dot{\Sigma}^{\Lambda}G^{\Lambda}$ appears in the integral for the value of the graph. By Dyson's equation,

$$\dot{G}^{\Lambda} = G^{\Lambda}\dot{\Sigma}^{\Lambda}G^{\Lambda} + S^{\Lambda}, \tag{54}$$

and this can be combined with the second-order contribution to replace S^{Λ} by $\dot{G}^{\Lambda}$. If all other effects of the six-point function, corresponding to graphs of the type shown in Fig. 5(c) are dropped, the equation for the four-point function gets changed to one where the product $G^{\Lambda}(k)S^{\Lambda}(k') + S^{\Lambda}(k)G^{\Lambda}(k')$ is replaced with $G^{\Lambda}(k)\dot{G}^{\Lambda}(k') + \dot{G}^{\Lambda}(k)G^{\Lambda}(k') = (d/d\Lambda)[G^{\Lambda}(k)G^{\Lambda}(k')]$. If one now restricts further to a single channel in the four-point equation, it becomes explicitly solvable by a ladder summation in that channel. Backsubstitution into the equation for the self-energy gives the corresponding Hartree-type term. This was explained by Katanin (2004), and, also in its extension to flows with symmetry breaking, by Salmhofer *et al.* (2004).

D. Flow parameters

In the derivation of the exact functional flow equation, the scale dependence of the bare propagator G_0^{Λ} was not specified. The derivation holds for any choice of G_0^{Λ}, provided all functions involved are indeed differentiable with respect to Λ, and provided that the resulting flow equation is well defined. These conditions are not trivial; in fact, badly chosen flow parameters may lead to divergences on the right-hand side of the flow equation. On the other hand, one can exploit the flexibility provided by the choice of the Λ dependence to ones own advantage. Besides regularity issues, the scale dependence of G_0^{Λ} is constrained only by the initial condition

$$G_0^{\Lambda_0} = 0, \tag{55}$$

and the final condition

$$G_0^{\Lambda\to 0} = G_0. \tag{56}$$

The functional $\Gamma = \Gamma^{\Lambda\to 0}$ reached at the end of the exact flow is independent of the choice of G_0^{Λ}. However, in most practical calculations, where approximations are unavoidable, a judicious choice of G_0^{Λ} is mandatory. Important aspects related to the choice of G_0^{Λ} are as follows: regularization of infrared singularities, minimization of truncation errors, respecting symmetries, and technical convenience. In the following we review the most frequently used cutoff schemes along with their merits and drawbacks.

1. Momentum and frequency cutoffs

For conciseness, we focus on translation and spin-rotation invariant one-band systems, such that the bare propagator G_0 can be written as a simple function of frequency and momentum as in Eq. (3). The scale dependence can then be introduced by multiplying G_0 with a suitable cutoff function θ^{Λ}:

$$G_0^{\Lambda}(k_0, \mathbf{k}) = \theta^{\Lambda}(k_0, \mathbf{k})G_0(k_0, \mathbf{k}), \tag{57}$$

with $\theta^{\Lambda_0} = 0$ and $\theta^{\Lambda\to 0} = 1$. To regularize the infrared divergence of G_0 at zero frequency and for momenta on the Fermi surface ($\xi_{\mathbf{k}} = 0$), the cutoff function $\theta^{\Lambda}(k_0, \mathbf{k})$ has to vanish sufficiently quickly for $k_0 \to 0$, $\xi_{\mathbf{k}} \to 0$ at fixed $\Lambda > 0$. The most frequently used cutoff functions are either pure momentum cutoffs of the form $\theta^{\Lambda}(\mathbf{k}) = \vartheta(|\xi_{\mathbf{k}}|/\Lambda)$ or frequency cutoffs $\theta^{\Lambda}(k_0) = \vartheta(|k_0|/\Lambda)$, where $\vartheta(x)$ is a function that vanishes for $x \ll 1$ and tends to 1 for $x \gg 1$. Mixed momentum and frequency cutoffs of the form $\theta^{\Lambda}(k_0, \mathbf{k}) = \vartheta[(k_0^2 + \xi_{\mathbf{k}}^2)/\Lambda^2]$ are preferred in the mathematical literature, as they facilitate power counting and rigorous estimates.

A technical advantage of momentum cutoffs compared to frequency cutoffs is that Matsubara sums on the right-hand side of the flow equations can often be performed analytically. Furthermore, a momentum cutoff does not spoil the analytic structure of propagators and vertex functions in the complex frequency plane. However, there are also serious drawbacks, which are specific to Fermi systems. Once self-energy effects are taken into account, the Fermi surface is usually deformed in the course of the flow, such that the momentum cutoff has to be continuously adapted to the new Fermi surface, which complicates the flow equations considerably. Second, particle-hole excitations with a small momentum transfer $\mathbf{q}$ are suppressed by the momentum cutoff for $|\xi_{\mathbf{k}+\mathbf{q}} - \xi_{\mathbf{k}}| < 2\Lambda$. As a consequence, the limit of vanishing momentum transfer $\mathbf{q} \to 0$ in interaction vertices and response functions does not commute with the limit $\Lambda \to 0$ (Metzner, Castellani, and Di Castro, 1998). In other words, forward scattering interactions and the response to homogeneous fields can be obtained only by taking the limit $\mathbf{q} \to 0$ at the end of the flow, at $\Lambda = 0$ (Honerkamp and Salmhofer, 2001a). This is a serious drawback in stability analyses (see Sec. III), where one compares the increase of the effective interaction in different momentum channels (including forward scattering), or different susceptibilities, upon lowering Λ until a divergence occurs in at least one channel at a finite scale $\Lambda_c > 0$.

A frequency cutoff has the advantage that it does not interfere with Fermi surface shifts, and that particle-hole processes with small momentum transfers are captured smoothly by the flow (Husemann and Salmhofer, 2009). It

can also be used in systems without translation invariance (Andergassen *et al.*, 2004), where a momentum cutoff is less useful since the propagator is not diagonal in momentum space. However, a frequency cutoff affects the analytic properties of propagators and vertex functions in the complex frequency plane. Depending on the sort of truncation used, this may pose a serious problem if one likes to continue results to real frequency. For a frequency cutoff the initial cutoff is $\Lambda_0 = \infty$. Since the contributions to the self-energy flow are of order Λ^{-1} at large Λ, one has to retain a convergence factor $e^{ik_0 0^+}$ on the right-hand side of the flow equation (Andergassen *et al.*, 2004), analogously to the convergence factor in the perturbation expansion of the self-energy (Negele and Orland, 1987); for a rigorous justification, see Pedra and Salmhofer (2008).

For a bare propagator $G_0(k_0, \mathbf{k}) = (ik_0 - \xi_\mathbf{k})^{-1}$ and a multiplicative cutoff as in Eq. (57), the full propagator has the form

$$G^\Lambda(k_0, \mathbf{k}) = \frac{\theta^\Lambda(k_0, \mathbf{k})}{ik_0 - \xi_\mathbf{k} - \theta^\Lambda(k_0, \mathbf{k})\Sigma^\Lambda(k_0, \mathbf{k})}, \tag{58}$$

and the single-scale propagator $S^\Lambda = -G^\Lambda \dot{Q}_0^\Lambda G^\Lambda$, see Eq. (47), reads

$$S^\Lambda(k_0, \mathbf{k}) = \frac{(ik_0 - \xi_\mathbf{k})\partial_\Lambda \theta^\Lambda(k_0, \mathbf{k})}{[ik_0 - \xi_\mathbf{k} - \theta^\Lambda(k_0, \mathbf{k})\Sigma^\Lambda(k_0, \mathbf{k})]^2}. \tag{59}$$

For a sharp cutoff function such as $\theta^\Lambda(k_0) = \Theta(|k_0| - \Lambda)$, the single-scale propagator seems ill defined, since $\partial_\Lambda \Theta(|k_0| - \Lambda) = -\delta(|k_0| - \Lambda)$, so that a delta peak in the numerator of Eq. (59) coincides with a discontinuity (due to the step function) in the denominator. However, this ambiguity can be easily removed by viewing the step function $\Theta(x)$ as a limit of increasingly sharp regularized step functions $\Theta_\epsilon(x)$, where the discontinuity is smeared over a width ϵ (Morris, 1994). With $\delta_\epsilon(x) = \partial_x \Theta_\epsilon(x)$, a simple substitution of variables yields

$$\delta_\epsilon(x) f(x, \Theta_\epsilon(x)) \overset{\epsilon \to 0}{\to} \delta(x) \int_0^1 du f(0, u), \tag{60}$$

for any continuous function f. Note that the right-hand side is unique; that is, it does not depend on the shape of the smeared step function $\Theta_\epsilon(x)$ for $\epsilon > 0$. For a sharp frequency cutoff $\theta^\Lambda(k_0) = \Theta(|k_0| - \Lambda)$, for example, the single-scale propagator thus simplifies to

$$S^\Lambda(k_0, \mathbf{k}) = -\frac{\delta(|k_0| - \Lambda)}{ik_0 - \xi_\mathbf{k} - \Sigma^\Lambda(k_0, \mathbf{k})}, \tag{61}$$

as long as it does not appear in products where other factors are also discontinuous at $|k_0| = \Lambda$. Otherwise, for example, in products of the form $S^\Lambda(k_0, \mathbf{k})[G^\Lambda(k_0, \mathbf{k})]^m$, one has to apply Eq. (60) to the entire product.

A sharp cutoff has the obvious technical advantage that the integration over the cutoff variable (k_0 or $\xi_\mathbf{k}$) can be carried out analytically, thanks to the delta function in the numerator of S^Λ. On the other hand, a sharp cutoff generates discontinuities in the momentum or frequency dependences of the vertex functions, corresponding to a pronounced nonlocality of the effective action (Morris, 1994), which is often not amenable to a simple parametrization. At finite temperature the flow equations are ill defined for a sharp frequency cutoff, since the Matsubara frequencies are discrete: $k_0 = (2n + 1)\pi T$ with integer n. Continuous cutoff functions at $T > 0$ are conveniently chosen such that the Λ derivative is nonzero only in a frequency range of width $2\pi T$, since then only two frequencies contribute to the Matsubara sum on the right-hand side of the flow equation (Enss *et al.*, 2005).

There are useful cutoff schemes which are formulated more naturally by *adding* a regulator function R^Λ to the inverse propagator (instead of multiplying):

$$Q_0^\Lambda(k_0, \mathbf{k}) = [G_0^\Lambda(k_0, \mathbf{k})]^{-1} = Q_0(k_0, \mathbf{k}) + R^\Lambda(k_0, \mathbf{k}), \tag{62}$$

with $R^{\Lambda_0} = \infty$ and $R^{\Lambda \to 0} = 0$. In particular, regulator functions of the form (Litim, 2001)

$$R^\Lambda(\mathbf{k}) = -Z^\Lambda[\mathrm{sgn}(\xi_\mathbf{k})\Lambda - \xi_\mathbf{k}]\Theta(\Lambda - |\xi_\mathbf{k}|), \tag{63}$$

or its frequency-dependent analog, $R^\Lambda(k_0) = iZ^\Lambda[\mathrm{sgn}(k_0)\Lambda - k_0]\Theta(\Lambda - |k_0|)$, have some distinct advantages. The prefactor Z^Λ is initially 1 and is then determined by a momentum (or frequency) derivative of the flowing self-energy $\Sigma^\Lambda(k_0, \mathbf{k})$. The Litim cutoff satisfies a criterion of "optimal" regularization of the infrared singularity of the propagator (Litim, 2001). For simple truncations it also leads to a convenient form of the integrands, facilitating the integrations.

It is easy to choose the cutoff function in a way that does not affect the global symmetries of the system, such as global charge conservation or global spin rotatation invariance. However, local conservation laws are typically spoiled. The corresponding Ward identities are modified by cutoff dependent additional terms, which vanish only in the limit $\Lambda \to 0$ (Enss, 2005). It is hard to devise truncations which satisfy the modified Ward identities at each scale Λ, and hence truncated flows often violate Ward identities also in the limit $\Lambda \to 0$ (Katanin, 2004). In these cases it is better to compute only independent quantities from the flow, and determine the remaining quantities, which are fixed by local conservation laws, via the Ward identity.

2. Temperature and interaction flows

For fermion systems the infrared singularity of the bare propagator can also be regularized by temperature, instead of a cutoff, since the fermionic Matsubara frequencies stay away from zero at a distance πT. A flow equation with temperature as a flow parameter can be obtained from the general flow equation derived in Sec. II.B, if one manages to shift all temperature dependences of the bare action to the quadratic part. This is indeed possible by a simple rescaling of the fields (Honerkamp and Salmhofer, 2001a). Consider a translation-invariant system of spin-$\frac{1}{2}$ fermions for definiteness, where the fields depend on a momentum $\mathbf{k}$, a spin index σ, and a Matsubara frequency $\omega_n = (2n + 1)\pi T$. Rescaling the fields as $\psi'_\sigma(n, \mathbf{k}) = T^{3/4}\psi_\sigma(\omega_n, \mathbf{k})$ and $\bar{\psi}'_\sigma(n, \mathbf{k}) = T^{3/4}\bar{\psi}_\sigma(\omega_n, \mathbf{k})$ removes all explicit T factors from the (quartic) interaction in the bare action. The temperature dependence is thereby shifted entirely to the quadratic part of the action, given by the inverse bare propagator for the rescaled fields,

$$Q_0^T(n,\mathbf{k}) = \frac{T^{1/2}}{i\omega_n - \xi_{\mathbf{k}}}. \tag{64}$$

The effective action $\Gamma^T[\psi', \bar{\psi}']$ for the rescaled fields obeys the exact flow equation (35), with temperature as the flow parameter. The unscaled vertex functions $\Gamma^{(2m)}$ are recovered from the vertex functions $\Gamma^{(2m)T}$ by multiplying with $T^{3m/2}$. The temperature flow has several advantageous features. First, it directly generates a temperature scan of the computed quantities. In cutoff schemes one has to run a full flow for each temperature separately. Second, the temperature flow includes particle-hole excitations with small momentum transfers uniformly at each scale. Third, local symmetries and the corresponding Ward identities are respected at each step at least for the exact flow, which makes the still difficult issue of Ward identities in truncated flows at least more transparent.

A particularly simple choice of a flow parameter is provided by a uniform factor λ scaling the bare propagator (Honerkamp *et al.*, 2004),

$$G_0^\lambda = \lambda G_0, \tag{65}$$

with $\lambda_0 = 0$, and $\lambda \to 1$ at the end of the flow. By a simple rescaling of the fields one can see that this is equivalent to multiplying the bare quartic interaction with a factor λ^2, which means that the interaction is scaled up continuously from 0 to its full strength in the course of the flow. Hence the name ''interaction flow'' for this scheme. In the absence of self-energy feedback the interaction flow has the technical advantage that the propagator has the same form at each scale, such that certain loop integrals need to be done only once. However, the global scaling of the propagator does not regularize the infrared singularities, such that one easily runs into infrared divergences. Nevertheless, for suitable problems and simple truncations the interaction flow has been shown to yield results similar to flows with a cutoff, and with less computational effort (Honerkamp *et al.*, 2004).

E. General properties of the RG equations

In this section we discuss the general structure of the RG hierarchy of equations and provide power-counting bounds for its solution. These bounds are simple, but mathematically exact, and they provide a strict sense of the notion of relevant and irrelevant terms. We also briefly discuss improved power-counting bounds, which provide sharper estimates for bulk Fermi systems in $d \geq 2$ and exhibit the role of Fermi surface geometry.

The generating functionals were introduced to obtain the Green functions and vertex functions of the model by differentiation, cf. Eqs. (7) and (10). In the framework of the RG as an iterated convolution, they acquire an independent importance. Indeed, in many situations in bosonic field theory, an expansion in the fields is avoided in favor of a gradient expansion (Berges, Tetradis, and Wetterich, 2002) or other types of parametrization (see also Sec. V), and the flow may lead to a nonanalytic function of the fields. Functions of Grassmann variables are, however, defined only by power series expansions in these variables, so in this case the meaning of the RG is strictly that of the infinite hierarchy. This is only a seeming disadvantage because by the anticommutation properties of Grassmann variables, the fully regularized functionals (as they appear in the flow equations) have convergent expansions in the fields (Gawedzki and Kupiainen, 1985; Feldman *et al.*, 1986; Lesniewski, 1987; Abdesselam and Rivasseau, 1998; Feldman, Knörrer, and Trubowitz, 1998, 2002; Salmhofer and Wieczerkowski, 2000). In contrast, the expansion in the fields of bosonic functionals is almost always divergent, even in the regularized theory. Convergent expansions then take the form of cluster expansions that distinguish between regions of small and large fields [see, e.g., Balaban *et al.* (2010) and references therein].

1. Inductive structure of the RG hierarchy

The functional $\tilde{\mathbf{\Sigma}}^\Lambda[\psi, \bar{\psi}]$ appearing in Eq. (46) has an expansion similar to Eq. (40), namely, $\tilde{\mathbf{\Sigma}}^\Lambda[\psi, \bar{\psi}](x', x) = \sum_{m\geq 1} \tilde{\mathbf{\Sigma}}^{(2m)\Lambda}[\psi, \bar{\psi}](x', x)$, where $\tilde{\mathbf{\Sigma}}^{(2m)\Lambda}$ is homogeneous of degree $2m$ in the fields, and hence has a representation with coefficient functions $\tilde{\mathbf{\Sigma}}^{(2m)\Lambda}$ similar to Eq. (41). By definition, Eq. (45) of $\tilde{\mathbf{\Sigma}}$, the $\tilde{\mathbf{\Sigma}}^{(2m)\Lambda}$ are determined by $\Gamma^{(2m+2)\Lambda}$, for example,

$$\begin{aligned}&(\tilde{\mathbf{\Sigma}}^{(2m)\Lambda}(x', x))_{11}(x'_1, \ldots, x'_m; x_1, \ldots, x_m)\\ &\quad = -\Gamma^{(2m+2)\Lambda}(x', x'_1, \ldots, x'_m; x_1, , \ldots, x_m, x).\end{aligned} \tag{66}$$

Here the indices refer to the matrix structure of Eq. (45). The other matrix elements are given by similar expressions.

We use this to expand Eq. (46) in homogeneous parts in ψ and $\bar{\psi}$ and compare coefficients. This gives

$$\begin{aligned}&\frac{d}{d\Lambda}\mathcal{A}^{(2m)\Lambda}[\psi, \bar{\psi}]\\ &= \frac{1}{2}\,\mathrm{tr}(\mathbf{S}^\Lambda \tilde{\mathbf{\Sigma}}^{(2m)\Lambda}[\psi, \bar{\psi}])\\ &\quad + \frac{1}{2}\,\mathrm{tr}(\mathbf{S}^\Lambda \tilde{\mathbf{\Sigma}}^{(2)\Lambda}[\psi, \bar{\psi}]\mathbf{G}^\Lambda \tilde{\mathbf{\Sigma}}^{(2m-2)\Lambda}[\psi, \bar{\psi}])\\ &\quad + \frac{1}{2}\sum_{p\geq 2}\sum_{\substack{m_0,\ldots,m_p\geq 1\\ m_0+\cdots+m_p=m}} \mathrm{tr}\Big(\mathbf{S}^\Lambda \tilde{\mathbf{\Sigma}}^{(2m_0)\Lambda}[\psi, \bar{\psi}]\\ &\quad \times \prod_{q=1}^{p} \mathbf{G}^\Lambda \tilde{\mathbf{\Sigma}}^{(2m_q)\Lambda}[\psi, \bar{\psi}]\Big).\end{aligned} \tag{67}$$

In the sum over p, each of $m_0, \ldots, m_p$ is at least 1 because $\tilde{\mathbf{\Sigma}}$ contains only field-dependent terms, and $m_0 + \cdots + m_p = m$ must hold since $\mathcal{A}^{(2m)\Lambda}$ is homogeneous of degree $2m$ in the fields $[\psi, \bar{\psi}]$. These two conditions imply that $p \leq m$ and that $m_q \leq m - p$ for all $0 \leq q \leq p$, so that for every given m, the sum runs only over finitely many terms. Since the coefficient in $\mathcal{A}^{(2m)\Lambda}$ is $\Gamma^{(2m)\Lambda}$ and $\tilde{\mathbf{\Sigma}}^{(2m)\Lambda} \sim \Gamma^{(2m+2)\Lambda}$, comparing coefficients of powers of ψ and $\bar{\psi}$ in Eq. (67) gives a hierarchy of differential equations for the $\Gamma^{(2m)\Lambda}$, labeled by m. We rewrite Eq. (67) as

$$\begin{aligned}\frac{d}{d\Lambda}\Gamma^{(2m)\Lambda} &= \mathcal{H}^\Lambda \Gamma^{(2m+2)\Lambda} + \mathcal{K}^\Lambda(\Gamma^{(4)\Lambda})\Gamma^{(2m)\Lambda}\\ &\quad + \sum_{p=2}^{m} \mathcal{L}_p^\Lambda(\Gamma^{(<2m)\Lambda}).\end{aligned} \tag{68}$$

The three summands on the right-hand side are obtained from the three terms in Eq. (67), and it is understood that both sides are functions of $2m$ variables $x_1, \ldots, x_{2m}$. The action of the operator $\mathcal{H}^\Lambda$ on $\Gamma^{(2m+2)\Lambda}$ is linear, as is that of $\mathcal{K}^\Lambda(\Gamma^{(4)\Lambda})$ on $\Gamma^{(2m)\Lambda}$, while $\mathcal{L}_p^\Lambda$ is nonlinear in the lower-m vertex functions $\Gamma^{(<2m)\Lambda} = \Gamma^{(4)\Lambda}, \ldots, \Gamma^{(2m-2)\Lambda}$. Specifically, the action of $\mathcal{H}^\Lambda$ is given by a tadpole-type contraction and summation, the action of $\mathcal{K}^\Lambda(\Gamma^{(4)\Lambda})$ is given by the evaluation of a one-loop diagram formed from $\Gamma^{(2m)\Lambda}$ and the four-point function $\Gamma^{(4)\Lambda}$, and $\mathcal{L}_p^\Lambda$ is given by a sum over one-loop diagrams involving $p+1$ vertex functions, each of which has $m_q < m$. Thus $\mathcal{H}^\Lambda$, $\mathcal{K}^\Lambda(\Gamma^{(4)\Lambda})$, and $\mathcal{L}_p^\Lambda$ also depend on Λ and on the self-energy Σ^Λ via the propagators S^Λ and G^Λ. The $\mathcal{H}^\Lambda$ term couples the higher vertex function $\Gamma^{(2m+2)\Lambda}$ into the equation for $\Gamma^{(2m)\Lambda}$. Thus the hierarchy does not close among finitely many m, and therefore truncations need to be employed to obtain solutions.

2. Truncated hierarchies and their iterative solution

If for some $m_0 \geq 1$, the initial vertex functions $\Gamma^{(2m)\Lambda_0}$ vanish for all $m > m_0 + 1$, one can employ the approximation of setting $\Gamma^{(2m)\Lambda} = \Gamma^{(2m)\Lambda_0}$ for all $m \geq m_0 + 1$. That is, all vertices with $m > m_0 + 1$ remain zero, and the (m_0+1)-particle vertex is kept fixed at its initial value. This level-m_0 truncation reduces the infinite hierarchy to a system of finitely many differential equations for $(\Gamma^{(2m)\Lambda})_{m \leq m_0}$. The vertex $\Gamma^{(2m_0+2)\Lambda_0}$ enters in the equation for $\Gamma^{(2m_0)\Lambda}$. Specifically, in the level-1 truncation, the two-particle vertex $\Gamma^{(4)\Lambda}$ is fixed to its bare value $\Gamma^{(4)\Lambda_0}$, and the self-energy is the solution of Eq. (50). The level-2 truncation is given by Eq. (52), with $\Gamma^{(6)\Lambda}$ fixed to its initial value $\Gamma^{(6)\Lambda_0}$ (which may vanish), together with Eq. (50). The term $\mathcal{K}^\Lambda(\Gamma^{(4)\Lambda})\Gamma^{(4)\Lambda}$ is quadratic in $\Gamma^{(4)\Lambda}$.

In the level-m_0 truncation of the hierarchy, with $m_0 > 2$, and at given Σ^Λ and $(\Gamma^{(2m')\Lambda})_{m'<m_0}$, Eq. (68) for $\Gamma^{(2m_0)\Lambda}$ becomes a linear inhomogeneous differential equation for $\Gamma^{(2m_0)\Lambda}$, which can be solved by an operator version of the standard method of variation of the constant: when all sums and integrals corresponding to the traces in Eq. (67) are written out, it takes the form of a linear integro-differential equation which is, viewed more abstractly, a linear ordinary differential equation in a suitable space of functions, to which standard techniques apply. Together with the initial condition $\Gamma^{(2m)\Lambda_0}$, this determines $\Gamma^{(2m)\Lambda}$ uniquely in terms of $(\Gamma^{(2m')\Lambda})_{m'<m_0}$. Backsubstitution of this solution into the $\mathcal{H}^\Lambda$ term for the equation for $\Gamma^{(2m_0-2)\Lambda}$ then yields an equation for $\Gamma^{(2m_0-2)\Lambda}$, which can be solved in terms of the not yet determined lower vertex functions $(\Gamma^{(2m')\Lambda})_{m'<m_0-1}$. Proceeding downward in m in this way, one can formally solve the truncated hierarchy, with the final equation determining Σ^Λ. We write "formally" here because after at most two steps of this iteration, the differential equations become nonlinear, so that existence of the solution is typically known only for short flow times, and because the question of blowup of solutions is rather nontrivial. Indeed, we see below that blowup generically occurs in RG equations if relevant terms have not been taken into account. This phenomenon is related to the infrared divergences of unrenormalized perturbation theory. The major advantage of the RG method is that the growing terms can be identified and studied long before they get singular and then removed by taking into account appropriately chosen relevant parts in the flowing action.

Increasing m_0 to improve the accuracy is then a natural strategy for approximation of the true solution; however, explicit and numerical calculations can be done only for small m_0, because the number of variables increases rapidly with m. Nevertheless, one can get useful information in the form of bounds for the maximal possible value of the vertex functions (or other norms that measure their size). This is done in the following section.

3. Running coupling expansion and power counting

We turn to the standard situation of a model with two-body interactions, where the initial interaction of the fermion system is quartic, i.e., $\Gamma^{(2m)\Lambda_0} = 0$ for all $m \geq 3$. We also assume that this interaction is short range so that its Fourier transform is bounded (e.g., an unscreened Coulomb interaction is long range). In a perturbative expansion in powers of the initial four-point interaction $V^{\Lambda_0} = \Gamma^{(4)\Lambda_0}$, the vertices are given by sums over irreducible graphs. An irreducible Feynman graph formed with r four-legged vertices can have at most $2r$ external legs, so that in order r in that expansion, all vertex functions with $m > r$ vanish.

As we now explain, one can solve the RG hierarchy in terms of a similar expansion in the *scale-dependent* four-point function $V^\Lambda = \Gamma^{(4)\Lambda}$, again by integrating the RG hierarchy downward in scale, but keeping the $2m$-point functions for $m > 2$ only to a fixed order in V^Λ. The equation for V^Λ itself then becomes an integro-differential equation with a power r nonlinearity on the right-hand side (the equation for Σ^Λ remains unchanged). This leads in a natural way to power-counting estimates for the higher $2m$-point functions in terms of the maximal value of the four-point vertex that occurs in the flow.

We denote the $O((V^\Lambda)^r)$ contribution to $\Gamma^{(2m)\Lambda}$ by $\Gamma_r^{(2m)\Lambda}$. Its scale derivative equals

$$\frac{d}{d\Lambda}\Gamma_r^{(2m)\Lambda} = \mathcal{H}^\Lambda \Gamma_r^{(2m+2)\Lambda} + \mathcal{K}^\Lambda(V^\Lambda)\Gamma_{r-1}^{(2m)\Lambda} + \sum_{p\geq 2}{}' \sum' \mathcal{L}_p^\Lambda(\Gamma_{r_0}^{(2m_0)\Lambda}, \ldots, \Gamma_{r_p}^{(2m_p)\Lambda}). \quad (69)$$

The primed sum runs over all sequences $(m_0, \ldots, m_p)$ and all sequences $(r_0, \ldots, r_p)$ with $m_q \geq 1$ and $r_q \geq 1$ for all $1 \leq q \leq p$, $m_0 + \cdots + m_p = m + p$ and $r_0 + \cdots + r_p = r$. The solution of the RG hierarchy for an initial quartic interaction has the property that $\Gamma_r^{(2m)\Lambda} = 0$ for all $m > r$. Therefore, for $m = r$, the $\mathcal{H}^\Lambda$ term drops out of Eq. (68), and all remaining terms contain only V^Λ or terms of order at most $r-1$ in V^Λ. Thus, given these lower-order Γ's, $\Gamma_r^{(2r)\Lambda}$ can be obtained by integration. Then the right-hand side of the equation for $m = r-1$ is determined, so $\Gamma_r^{(2r-2)\Lambda}$ can be determined, and so on. Successive backsubstitution then leads to a system of equations where $d\Gamma_r^{(2m)\Lambda}/d\Lambda$ gets contributions from a sum of graphs with r vertices of type $V^{\Lambda'}$, where $\Lambda_0 \geq \Lambda' \geq \Lambda$, and propagators $G^{\Lambda''}$ and $S^{\Lambda'''}$, all the intermediate scales Λ', etc. are integrated. Thus the equation becomes nonlocal in the flow parameter Λ, but the right-hand side is known once V^Λ and Σ^Λ are known. V^Λ is given

by a degree r nonlinear equation, with a similar graphical background as discussed above, and Σ^Λ by the standard self-energy equation (50). While more restricted than the level-m truncation, the running coupling scheme also captures effects that cannot be seen in any fixed order of bare perturbation theory, such as screening or asymptotic freedom of certain coupling functions.

We use this inductive structure to derive basic power-counting bounds for the vertex functions in terms of the flowing four-point function, for a d-dimensional bulk fermion system ($d \geq 1$). For simplicity, we focus on spin-$\frac{1}{2}$ fermions with translation-invariant action, so that we can use $x_i = (k_i, \sigma_i) = (k_{0,i}, \mathbf{k}_i, \sigma_i)$, as discussed at the beginning of Sec. II.A. We also assume that the symmetries of the action remain unbroken. These specific assumptions are for presentation only; power counting can be done without them. By translation invariance,

$$\Gamma_r^{(2m)\Lambda}[(k_1, \sigma_1), \ldots, (k_{2m}, \sigma_{2m})] = \delta\Big(\sum_i k_i\Big)\hat{\Gamma}_r^{(2m)\Lambda}(\underline{k}, \underline{\sigma}),$$

where the delta function forces conservation of the spatial momentum $\mathbf{k}$ (up to reciprocal lattice vectors) and conservation of the frequency variable k_0, and we have introduced the abbreviations $\underline{\sigma} = (\sigma_1, \ldots, \sigma_{2m})$ and $\underline{k} = (k_1, \ldots, k_{2m-1})$. For $\Lambda = \Lambda_0$, the function $\hat{\Gamma}_r^{(2m)\Lambda}$ is smooth and bounded because the initial interaction is short range, and this stays so during the flow above critical scales.

Consider the maximal size of the vertex functions, $\|\Gamma_r^{(2m)\Lambda}\| = \sup_{\underline{k},\underline{\sigma}}|\hat{\Gamma}_r^{(2m)\Lambda}(\underline{k}, \underline{\sigma})|$. Then, for $m \geq 3$,

$$\|\Gamma_r^{(2m)\Lambda}\| \leq \gamma_r^{(2m)} s_\Lambda^{r-m+1} f_\Lambda^r \Lambda^{2-m}, \tag{70}$$

where $\gamma_r^{(2m)}$ is independent of Λ and β,

$$f_\Lambda = \sup_{\Lambda \leq \ell \leq \Lambda_0} \|V^\ell\| \tag{71}$$

is the maximal value of the four-point coupling on all scales between Λ and Λ_0, and

$$s_\Lambda = \max_\alpha \sum_{\alpha'} \int đk |\hat{S}^\Lambda_{\alpha,\alpha'}(k)|, \tag{72}$$

with $\int đk \cdots = T\sum_{k_0} \int d^dk/(2\pi)^d \cdots$ (for the general power counting, we do not need to assume that the propagator is diagonal in the spin indices α, α', so $\hat{S}^\Lambda$ also carries these indices). The dependence of s_Λ on Λ is determined by the shape of the Fermi surface. As shown in Appendix B.1, s_Λ is of the order of 1 for regular Fermi surfaces. If the Fermi surface contains van Hove points, s_Λ grows logarithmically in Λ for $\Lambda \to 0$.

At first sight, one may worry about the factor Λ^{2-m}, which diverges for $m \geq 3$ as $\Lambda \to 0$. For the maximum value of the vertex functions, it is indeed true, and easily verified in examples, that there are always particular values of the external momenta where these vertex functions become large in $\beta = 1/T$ (and diverge at zero temperature). However, this happens only on a "small" set of momenta. For a general m-point function, it is involved to determine this set, but this is not necessary for power counting. One can use the L^1 norm instead, i.e., consider $\|\Gamma_r^{(2m)\Lambda}\|_1 = \sum_{\underline{\sigma}} \int đk_1 \cdots đk_m |\Gamma_r^{(2m)\Lambda}(\underline{k}, \underline{\sigma})|$. Using generalizations of Eq. (70), one can then show that if f_Λ remains finite

$$\|\Gamma_r^{(2m)\Lambda}\|_1 \leq c_r^{(2m)} f_\Lambda^r \tag{73}$$

with constants $c_r^{(2m)}$ that are independent of Λ, β, and the system size L [see Salmhofer (1999), Sec. 4.4.3]. This implies that, even in the limit $\beta \to \infty$, the $2m$-point vertices can become singular only on a set of zero Lebesgue measure in momentum space. In general, this set can be rather complicated, but, loosely speaking, it will have a codimension of at least 1.

It is one of the appealing features of the flow-equation RG that exact statements such as Eq. (70) can be proven in a few lines; see Appendix B. The argument given there also implies an at-most logarithmic growth of the coefficients in the equation for f_Λ itself. The self-energy then comes out of order f_Λ, provided that renormalization is done correctly; see Sec. II.E.4. At small f_Λ, the size of the vertices $\Gamma^{(2m)\Lambda}$ with $m \geq 3$ is thus determined by f_Λ. The terms with $m \geq 3$ are the RG-irrelevant ones, $m = 2$ is marginal, and $m = 1$ is relevant. This classification is explained in detail in Appendix B. In a Taylor expansion of the vertex functions in the Matsubara frequency around zero, and in momentum around the Fermi surface, additional small factors arise, which cancel the small denominators of the propagators; at the same time, the vertex function is replaced by a differentiated one. Hence, the flow obtained by projecting the frequencies to zero and the momenta to the Fermi surface gives the dominant contribution for small Λ. This is expected from a simple counting of bare scaling dimensions and can be established more rigorously by power-counting arguments similar to those used above and in Appendix B.

In the case of a curved Fermi surface in $d \geq 2$, f_Λ indeed stays small in a weakly interacting system above a BCS-like temperature [see, e.g., Salmhofer (1998b)], indicating the absence of symmetry breaking. At zero temperature, f_Λ grows as Λ decreases, and the four-point function has singularities at points corresponding to nesting vectors of the Fermi surface; for details, see Appendix B.3. This growth of f_Λ with decreasing scale Λ is usually called the "flow to strong coupling" in RG studies and is described in more detail in Sec. III. A singularity of the two-particle vertex in momentum space means that the interaction becomes long range in position space. This is associated with the formation of critical fluctuations, and in case of spontaneous breaking of a continuous symmetry, with the appearance of Goldstone bosons (see Sec. IV).

4. Self-energy and Fermi surface shift

The self-energy is important for all effective one-particle properties of the system, and it can cause drastic effects, as compared to the noninteracting fermions. Accordingly, in the RG flow, the self-energy is a relevant term. In the absence of symmetry breaking, it modifies the inverse propagator to $ik_0 - \xi_{\mathbf{k}} - \Sigma(k_0, \mathbf{k})$. The long-distance behavior of the fermionic propagator is determined by the behavior of this function around its zero set. A Taylor expansion around $k_0 = 0$ gives

$$ik_0 - \xi_{\mathbf{k}} - \Sigma(k_0, \mathbf{k}) = \frac{ik_0 - e_{\mathbf{k}}}{Z_{\mathbf{k}}} + \rho(k_0, \mathbf{k}) \tag{74}$$

with $Z_{\mathbf{k}}^{-1} = 1 + i(\partial_0\Sigma)(0, \mathbf{k})$, $Z_{\mathbf{k}}^{-1} e_{\mathbf{k}} = \xi_{\mathbf{k}} + \Sigma(0, \mathbf{k})$, and a Taylor remainder ρ. If ρ vanishes faster than linearly in k_0 as $k_0 \to 0$, we thus obtain an effective description in terms of quasiparticles with dispersion relation $e_{\mathbf{k}}$, hence "interacting" Fermi surface $\{\mathbf{k}:\xi_{\mathbf{k}} + \Sigma(0, \mathbf{k}) = 0\}$, Fermi velocity $\nabla e_{\mathbf{k}}$, and quasiparticle weight $Z_{\mathbf{k}}$. If $Z_{\mathbf{k}}$ is bounded and nonvanishing for all $\mathbf{k}$, the long-distance decay of the fermion propagator in position space is the same as for the free theory.

The question whether Σ is smooth enough for the above to hold is nontrivial. In the one-dimensional Luttinger model, $\partial_0\Sigma(0, k_F)$ diverges, and the small-k_0 behavior of the self-energy, $\Sigma(k_0, k_F) \sim |k_0|^\alpha$ with $\alpha < 1$ depending on the interaction strength, implies that the self-energy effects dominate at small k_0 and the decay in position space becomes more rapid, so that the occupation number density $n(\mathbf{k})$ becomes a continuous function of $\mathbf{k}$ even at zero temperature (Giamarchi, 2004). An even more drastic change is spontaneous symmetry breaking, where the propagator cannot be written any more in the simple form given above (see Sec. IV).

In the RG flow, Σ is replaced by the Λ-dependent self-energy $\Sigma^\Lambda = (G_0^\Lambda)^{-1} - (G^\Lambda)^{-1}$. An important phenomenon in this context is the shift in the Fermi surface entailed by Σ^Λ. In terms of power counting, this shift is the most relevant term. Cutting off the propagator around the free Fermi surface then fails to regularize the propagator, which leads to spurious singularities in the RG flow. A convenient method to avoid this is to introduce a counterterm. In the context of the bare perturbation expansion, the counterterm method was already described by Nozières (1964). The main idea is to anticipate the form that the propagator takes at the end of the flow and to rearrange the flow such that this form, not the bare one, is used as the starting point for the RG analysis, hence the Fermi surface is fixed to that of the interacting system in the flow. The difference between the two dispersion functions appears as a (finite) counterterm. To obtain a one-to-one relation between the model given by the Hamiltonian and the one with fixed interacting Fermi surface, one has to solve a self-consistency equation. Feldman and Trubowitz (1990) used the counterterm method for the radius shift of a circular Fermi surface in a RG flow. Feldman, Salmhofer, and Trubowitz (1996, 1998b, 1999, 2000) generalized this to the case of noncircular curved Fermi surfaces, solved the self-consistency equation, and showed that $Z_{\mathbf{k}}$ remains finite for $d \geq 2$ to all orders. The corresponding fixed-point problem for the Fermi surface was also considered by Ledowski and Kopietz (2003). The role of van Hove singularities was analyzed by Feldman and Salmhofer (2008a, 2008b). Feldman and Trubowitz (1991) also used the counterterm method to derive the equation for the superconducting gap from an RG flow; for further work in that direction, see also Sec. IV. Alternatively to counterterms, one can try to avoid a momentum space cutoff altogether (Honerkamp and Salmhofer, 2001a, 2001b; Husemann and Salmhofer, 2009), or to use an adaptive scheme [see the appendix in Honerkamp *et al.* (2001), Benfatto, Giuliani, and Mastropietro (2006), and Salmhofer (2007)].

F. Flow equations for observables and correlation functions

All observables of the fermionic system are given by polynomials in the fields, so they can be calculated from the connected Green functions $G^{(2m)\Lambda}$, hence by the above-mentioned tree relations also from the irreducible vertex functions $\Gamma^{(2m)\Lambda}$. It is nevertheless convenient, and due to the limitations of approximations often mandatory, to calculate the flow of observables and their correlation (or response) functions by separate flow equations, which we derive and discuss now.

For simplicity we restrict the presentation to the particularly important class of observables that are correlations of fermionic bilinears. Charge-invariant bilinears are of the form

$$\mathcal{B}(x) = \sum_{y,y'} \bar{\psi}(y) B(x; y, y') \psi(y'). \tag{75}$$

Charge-noninvariant bilinears are of the form

$$\mathcal{B}(x) = \sum_{y,y'} [\psi(y) B(x; y, y') \psi(y') + \bar{\psi}(y) \tilde{B}(x; y, y') \bar{\psi}(y')]. \tag{76}$$

The functions B and $\tilde{B}$ determine the spatial and spin structures of these bilinears. For translation-invariant systems, we choose a momentum representation where $x = (k_0, \mathbf{k})$ and $y = (p_0, \mathbf{p}, \sigma)$, as explained above Eq. (3). With the notations $p = (p_0, \mathbf{p})$ and $\int đp = T\sum_{p_0} \int d\mathbf{p}$, a charge-invariant bilinear is of the form

$$\mathcal{B}(k) = \int đp\, \bar{\psi}_\sigma(p) b_{\sigma,\sigma'}(p, k) \psi_{\sigma'}(p + k). \tag{77}$$

The frequency k_0 is an integer multiple of $2\pi T$. The case $k = 0$ and $b = \sigma_i$, where σ_i denotes the ith Pauli matrix, corresponds to a uniform spin density. The case $k_0 = 0$, $\mathbf{k} = (\pi, \pi, \ldots, \pi)$, and $b = \sigma_i$ corresponds to a staggered spin density. Similarly, the same choices of k but with $b_{\sigma,\sigma'} = \delta_{\sigma,\sigma'}$ correspond to charge densities. Other choices of $\mathbf{k}$ can be used to test tendencies toward noncommensurate magnetic or charge ordering. Cooper pair fields correspond to the noncharge-invariant combinations

$$\mathcal{B}(k) = \int đp [\bar{\psi}_\sigma(p) \Delta_{\sigma,\sigma'}(p, k) \bar{\psi}_{\sigma'}(-p + k) + \psi_\sigma(p) \bar{\Delta}_{\sigma',\sigma}(-p + k, k) \psi_{\sigma'}(-p + k)]. \tag{78}$$

Again, the simplest choice is uniform singlet pairing, where $k = 0$ and $\Delta_{\sigma,\sigma'}(p, k) = \Delta(\mathbf{p})\varepsilon_{\sigma,\sigma'}$. In this case $\Delta(\mathbf{p})$ is the gap function. Triplet pairing, extended Cooper pairs, and spatially nonuniform gaps are described by suitable generalizations.

A convenient way of generating correlation functions of the bilinears $\mathcal{B}$ is to couple the $\mathcal{B}(x)$ to external source fields $J(x)$, i.e., to add a term $(J, \mathcal{B}) = \sum_x J(x)\mathcal{B}(x)$ to the action. The external field J is not an integration variable, so it can be regarded as a (functional) parameter on which $\mathcal{G}$ depends. Writing $\mathcal{G} = \mathcal{G}(J, \eta, \bar{\eta})$, we then have

$$\langle \mathcal{B}(x)\mathcal{B}(y)\rangle - \langle \mathcal{B}(x)\rangle\langle \mathcal{B}(y)\rangle = -\frac{\partial^2 \mathcal{G}(J,\eta,\bar{\eta})}{\partial J(x)\partial J(y)}\Bigg|_{\substack{J=0\\ \eta,\bar{\eta}=0}}. \tag{79}$$

In the presence of J, the effective action $\Gamma = \Gamma(J, \psi, \bar{\psi})$, as well as all other quantities appearing in the fermionic Legendre transform (9), depends on J as well. Since relations such as $(\partial\Gamma/\partial\bar{\psi})(J, \psi, \bar{\psi}) = \eta(J, \psi, \bar{\psi})$ remain valid for any J, straightforward differentiation yields

$$\frac{\partial^2 \mathcal{G}(J,\eta,\bar{\eta})}{\partial J(x)\partial J(y)}\Bigg|_{\substack{J=0\\ \eta,\bar{\eta}=0}} = \frac{\partial^2 \Gamma(J,\psi,\bar{\psi})}{\partial J(x)\partial J(y)}\Bigg|_{\substack{J=0\\ \psi,\bar{\psi}=0}}. \tag{80}$$

Graphically, this relation is intuitive in that the bilinears always couple to the (effective) vertices by two lines, and the fermionic vertices are all even, so that the graphs that contribute are automatically irreducible.

Again, because J plays the role of a parameter, the flow equation (35) is unchanged. Flow equations for the response functions are then obtained simply by expanding Γ in the fields J and comparing coefficients. This again leads to a hierarchy of equations for the vertex functions $\Gamma^{(2m,n)}$ that have $2m$ fermionic and n external bosonic lines. The J-independent term corresponds to the standard fermionic hierarchy for the $\Gamma^{(2m,0)} = \Gamma^{(2m)}$, which therefore remains unchanged. When counting powers in the fermionic fields, each J corresponds to a bilinear, so that the truncation $\Gamma^{(2m)} = 0$ for $m \geq m_0$ for the fermionic vertices corresponds to a truncation $\Gamma^{(2m,n)} = 0$ for $m + n \geq m_0$. The flow equations remaining after a truncation for $m_0 = 3$ are shown diagrammatically in Fig. 6.

The two-point correlation $\langle \mathcal{B}(x)\mathcal{B}(y)\rangle - \langle \mathcal{B}(x)\rangle\langle \mathcal{B}(y)\rangle$ of any fermionic bilinear $\mathcal{B}$ involves only the fermionic two- and four-point functions, and hence could simply be calculated from the knowledge of $\Gamma^{(2)}$ and $\Gamma^{(4)}$ by the reciprocity relation and Eq. (12). Equation (80) shows that the route via external fields in the one-particle irreducible equations is strictly equivalent to this if the hierarchy is treated exactly. When making truncations to the hierarchy and other approximations, the two are no longer the same. Anomalous scaling dimensions of fermionic bilinears (or other composite objects) are captured easily by separate flow equations for these quantities, while they are hard to obtain from $\Gamma^{(2)}$ and $\Gamma^{(4)}$, if the latter are computed from a truncated flow equation. An instructive example is given by the calculation of the density

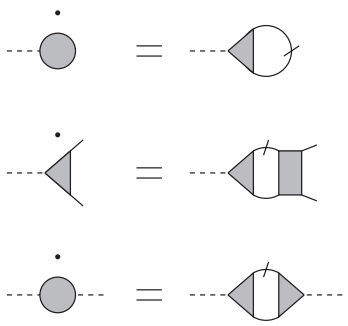

FIG. 6. The truncation of the hierarchy for the response function that corresponds to keeping only the irreducible two-particle vertex in the fermionic hierarchy.

profile near a static impurity in a Luttinger liquid in Andergassen *et al.* (2004).

G. Flow equations for coupled boson-fermion systems

The focus of this review is on fermion systems. However, even if the bare action involves only fermionic fields, bosonic degrees of freedom are frequently generated as fermion composites and order parameter fields. For example, Cooper pairs and the order parameter in a superconductor are bosons. Technically, bosonic fields are introduced in an originally purely fermionic theory by a Hubbard-Stratonovich decoupling of an interaction between fermions (Popov, 1987). Often the fermionic fields are subsequently intregrated out, such that an effective action involving only bosons remains. Otherwise one has to deal with a coupled theory of fermions and bosons. In this section we generalize the flow equations derived in Sec. II.B to interacting boson-fermion systems. Flow equations for coupled boson-fermions systems have been derived by various groups, with slight differences in the notation (Berges, Tetradis, and Wetterich, 2002; Kopietz, Bartosch, and Schütz, 2010).

We first introduce some notation for bosons and write down the bosonic analogs of some of the most important equations from Sec. II.B. Bosonic particles are described by complex fields ϕ. It is convenient to combine ϕ and its complex conjugate ϕ^* in a bosonic Nambu field

$$\Phi(x) = \begin{pmatrix} \phi(x) \\ \phi^*(x) \end{pmatrix}. \tag{81}$$

The generating functional for connected Green functions can be written as (Negele and Orland, 1987)

$$\mathcal{G}[H] = -\ln \int \mathcal{D}\Phi e^{-\mathcal{S}[\Phi]} e^{(H^*,\Phi)}, \tag{82}$$

where $\mathcal{S}[\Phi]$ is the bare action, and

$$H(x) = \begin{pmatrix} h(x) \\ h^*(x) \end{pmatrix} \tag{83}$$

is the source field. Connected Green functions are obtained as functional derivatives

$$\begin{aligned} &G^{(2m)}(x_1,\ldots,x_m;x_1',\ldots,x_m') \\ &\quad = \langle \phi(x_1)\cdots\phi(x_m)\phi^*(x_m')\cdots\phi^*(x_1')\rangle_c \\ &\quad = -\frac{\partial^{2m}\mathcal{G}[H]}{\partial h^*(x_1)\cdots\partial h^*(x_m)\partial h(x_m')\cdots\partial h(x_1')}\Bigg|_{H=0}. \end{aligned} \tag{84}$$

The effective action is defined as Legendre transform

$$\Gamma[\Phi] = (H^*, \Phi) + \mathcal{G}[H], \tag{85}$$

with $\Phi = -\partial\mathcal{G}/\partial H^*$. Functional derivatives of $\Gamma[\Phi]$ yield the bosonic m-particle vertex functions

$$\begin{aligned} &\Gamma^{(2m)}(x_1,\ldots,x_m;x_1',\ldots,x_m') \\ &\quad = \frac{\partial^{2m}\Gamma[\Phi]}{\partial\phi^*(x_1)\cdots\partial\phi^*(x_m)\partial\phi(x_m')\cdots\partial\phi(x_1')}\Bigg|_{\Phi=0}. \end{aligned} \tag{86}$$

The matrices of second derivatives at finite fields

$$\mathbf{G}^{(2)}[H] = -\frac{\partial^2 \mathcal{G}}{\partial H^*(x)\partial H(x')} = \begin{pmatrix} \langle \phi(x)\phi^*(x')\rangle & \langle \phi(x)\phi(x')\rangle \\ \langle \phi^*(x)\phi^*(x')\rangle & \langle \phi^*(x)\phi(x')\rangle \end{pmatrix} \tag{87}$$

and

$$\mathbf{\Gamma}^{(2)}[\Phi] = \frac{\partial^2 \Gamma}{\partial \Phi^*(x)\partial \Phi(x')} \tag{88}$$

obey the reciprocity relation $\mathbf{\Gamma}^{(2)}[\Phi] = (\mathbf{G}^{(2)}[H])^{-1}$.

Endowing the bare propagator G_0 with a cutoff or another scale dependence, one can derive exact flow equations for the generating functionals in complete analogy to the fermionic case. In particular, the flow equation for the effective action $\Gamma^\Lambda[\Phi]$ has the form

$$\frac{d}{d\Lambda}\Gamma^\Lambda[\Phi] = \frac{1}{2}(\Phi^*, \dot{\mathbf{Q}}_0^\Lambda \Phi) + \frac{1}{2}\,\mathrm{tr}\{\dot{\mathbf{Q}}_0^\Lambda (\mathbf{\Gamma}^{(2)\Lambda}[\Phi])^{-1}\}, \tag{89}$$

where $\mathbf{Q}_0^\Lambda = \mathrm{diag}(Q_0^\Lambda, Q_0^{\Lambda t})$ with $Q_0^\Lambda = (G_0^\Lambda)^{-1}$. Note that the first term on the right-hand side can also be written as $(\phi^*, \dot{Q}_0^\Lambda \phi)$. The above flow equation is equivalent to the frequently used flow equation for the effective average action (Berges, Tetradis, and Wetterich, 2002)

$$\Gamma_R^\Lambda[\Phi] = \Gamma^\Lambda[\Phi] - \tfrac{1}{2}(\Phi^*, \mathbf{R}^\Lambda \Phi), \tag{90}$$

with $R^\Lambda = Q_0^\Lambda - Q_0$, which reads (Wetterich, 1993)

$$\frac{d}{d\Lambda}\Gamma_R^\Lambda[\Phi] = \frac{1}{2}\,\mathrm{tr}\{\dot{\mathbf{R}}^\Lambda (\mathbf{\Gamma}_R^{(2)\Lambda}[\Phi] + \mathbf{R}^\Lambda)^{-1}\}. \tag{91}$$

Order parameters are often associated with real (not complex) bosonic fields. In that simpler case the above equations are still valid if one replaces the complex Nambu fields Φ and H by the real fields ϕ and h.

A generalization to coupled fermion-boson systems is now straightforward. Bosonic and fermionic fields are conventiently collected in a ''superfield''

$$\Xi = \begin{pmatrix} \Phi \\ \Psi \end{pmatrix}, \tag{92}$$

where Φ and Ψ are the bosonic and fermionic Nambu fields defined above (see Sec. II.A). The conjugate superfield is given by

$$\bar{\Xi} = \begin{pmatrix} \Phi^* \\ \bar{\Psi} \end{pmatrix}. \tag{93}$$

The generating functional for connected Green functions involving both bosons and fermions reads

$$\mathcal{G}[H_b, H_f] = -\ln \int \mathcal{D}\Phi \mathcal{D}\Psi e^{-\mathcal{S}[\Phi,\Psi]} e^{(H_b^*,\Phi)+(\bar{H}_f,\Psi)}, \tag{94}$$

where $\mathcal{S}[\Phi, \Psi]$ is the bare action, and H_b and H_f are the Nambu source fields for bosons and fermions, respectively. Functional derivatives with respect to the source fields generate connected Green functions with an arbitrary number of bosonic and fermionic fields, the only general constraint being that the number of fermion fields is always even.

The effective action $\Gamma[\Phi, \Psi]$ is given by the Legendre transform

$$\Gamma[\Phi, \Psi] = (H_b^*, \Phi) + (\bar{H}_f, \Psi) + \mathcal{G}(H_b, H_f), \tag{95}$$

where $\Phi = -\partial \mathcal{G}/\partial H_b^*$ and $\Psi = -\partial \mathcal{G}/\partial \bar{H}_f$. The source fields may also be collected in a superfield

$$\mathcal{H} = \begin{pmatrix} H_b \\ H_f \end{pmatrix}. \tag{96}$$

The Legendre transform can then be written more concisely as $\Gamma[\Xi] = (\bar{\mathcal{H}}, \Xi) + \mathcal{G}(\mathcal{H})$.

The matrix of second functional derivatives of $\mathcal{G}$ at finite fields

$$\mathbf{G}^{(2)}[\mathcal{H}] = -\frac{\partial^2 \mathcal{G}}{\partial \bar{\mathcal{H}}(x)\partial \mathcal{H}(x')} = \begin{pmatrix} \langle \Phi(x)\Phi^*(x')\rangle & -\langle \Phi(x)\bar{\Psi}(x')\rangle \\ \langle \Psi(x)\Phi^*(x')\rangle & -\langle \Psi(x)\bar{\Psi}(x')\rangle \end{pmatrix} \tag{97}$$

involves also mixed boson-fermion propagators, which vanish only for $\mathcal{H} = 0$. The matrix of second derivatives of the effective action

$$\mathbf{\Gamma}^{(2)}[\Xi] = \frac{\partial^2 \Gamma}{\partial \bar{\Xi}(x)\Xi(x')} = \begin{pmatrix} \frac{\partial^2\Gamma}{\partial\Phi^*(x)\partial\Phi(x')} & \frac{\partial^2\Gamma}{\partial\Phi^*(x)\partial\Psi(x')} \\ \frac{\partial^2\Gamma}{\partial\bar{\Psi}(x)\partial\Phi(x')} & \frac{\partial^2\Gamma}{\partial\bar{\Psi}(x)\partial\Psi(x')} \end{pmatrix} \tag{98}$$

is related to $\mathbf{G}^{(2)}[\mathcal{H}]$ by the reciprocity relation $\mathbf{\Gamma}^{(2)}[\Xi] = (\mathbf{G}^{(2)}[\mathcal{H}])^{-1}$.

A flow of the generating functionals is generated by modifying the bare propagators for bosons and fermions G_{b0} and G_{f0} such that they depend on some scale parameter Λ. We denote the scale-dependent bare propagators by G_{b0}^Λ and G_{f0}^Λ, and their inverse by Q_{b0}^Λ and Q_{f0}^Λ. The generalization of the exact flow equations for the effective action in purely bosonic or fermionic systems to coupled boson-fermion systems reads

$$\frac{d}{d\Lambda}\Gamma^\Lambda[\Phi, \Psi] = \frac{1}{2}(\Phi^*, \dot{\mathbf{Q}}_{b0}^\Lambda \Phi) - \frac{1}{2}(\bar{\Psi}, \dot{\mathbf{Q}}_{f0}^\Lambda \Psi) + \frac{1}{2}\,\mathrm{Str}\{\dot{\mathbf{Q}}_0^\Lambda (\mathbf{\Gamma}^{(2)\Lambda}[\Phi, \Psi])^{-1}\}, \tag{99}$$

where

$$\mathbf{Q}_0^\Lambda = \begin{pmatrix} \mathbf{Q}_{b0}^\Lambda & 0 \\ 0 & \mathbf{Q}_{f0}^\Lambda \end{pmatrix}. \tag{100}$$

The supertrace Str incorporates a minus sign in the fermionic sector. The flow equation (99) is equivalent to the flow equation (Berges, Tetradis, and Wetterich, 2002)

$$\frac{d}{d\Lambda}\Gamma_R^\Lambda[\Phi, \Psi] = \frac{1}{2}\,\mathrm{Str}\{\dot{\mathbf{R}}^\Lambda (\mathbf{\Gamma}_R^{(2)\Lambda}[\Phi, \Psi] + \mathbf{R}^\Lambda)^{-1}\}, \tag{101}$$

with $\mathbf{R}^\Lambda = \mathbf{Q}_0^\Lambda - \mathbf{Q}_0$, for the effective average action

$$\Gamma_R^\Lambda[\Phi, \Psi] = \Gamma^\Lambda[\Phi, \Psi] - \tfrac{1}{2}(\Phi^*, \mathbf{R}_b^\Lambda \Phi) + \tfrac{1}{2}(\bar{\Psi}, \mathbf{R}_f^\Lambda \Psi). \tag{102}$$

The expansion of the exact functional flow equation (99) proceeds in complete analogy to the purely fermionic case. Inserting

$$\mathbf{\Gamma}^{(2)\Lambda}[\Phi,\Psi] = (\mathbf{G}^{\Lambda})^{-1} - \tilde{\mathbf{\Sigma}}^{\Lambda}[\Phi,\Psi], \tag{103}$$

with

$$\mathbf{G}^{\Lambda} = (\mathbf{\Gamma}^{(2)\Lambda}[\Phi,\Psi]|_{\Phi=\Psi=0})^{-1} = \mathrm{diag}(\mathbf{G}_b^{\Lambda}, \mathbf{G}_f^{\Lambda}) \tag{104}$$

into the functional flow equation (99), one obtains

$$\begin{aligned}\frac{d}{d\Lambda}\Gamma^{\Lambda}[\Phi,\Psi] = {} & \frac{1}{2}\,\mathrm{Str}(\dot{\mathbf{Q}}_0^{\Lambda}\mathbf{G}^{\Lambda}) \\ & + \frac{1}{2}(\Phi^*, \dot{\mathbf{Q}}_{b0}^{\Lambda}\Phi) - \frac{1}{2}(\bar{\Psi}, \dot{\mathbf{Q}}_{f0}^{\Lambda}\Psi) \\ & - \frac{1}{2}\,\mathrm{Str}\{\mathbf{S}^{\Lambda}(\tilde{\mathbf{\Sigma}}^{\Lambda}[\Phi,\Psi] \\ & + \tilde{\mathbf{\Sigma}}^{\Lambda}[\Phi,\Psi]\mathbf{G}^{\Lambda}\tilde{\mathbf{\Sigma}}^{\Lambda}[\Phi,\Psi] + \cdots)\},\end{aligned} \tag{105}$$

with the single-scale propagator

$$\mathbf{S}^{\Lambda} = -\mathbf{G}^{\Lambda}\dot{\mathbf{Q}}_0^{\Lambda}\mathbf{G}^{\Lambda} = \mathrm{diag}(\mathbf{S}_b^{\Lambda}, \mathbf{S}_f^{\Lambda}). \tag{106}$$

The expansion in powers of the fields is now straightforward and leads to a hierarchy of flow equations for all vertex functions. The first few terms are shown diagrammatically in Fig. 7.

The flow equations derived above are also valid in the case of U(1) symmetry breaking, if one allows for off-diagonal elements in the matrices $\mathbf{Q}_{b0}^{\Lambda}$, $\mathbf{Q}_{f0}^{\Lambda}$, $\mathbf{G}_b^{\Lambda}$, $\mathbf{G}_f^{\Lambda}$, etc. (Berges, Tetradis, and Wetterich, 2002; Schütz and Kopietz, 2006).

Coupled flow equations for fermions and bosonic Hubbard-Stratonovich fields are particularly convenient to treat fluctuations associated with spontaneous symmetry breaking (see Sec. IV) and quantum criticality (see Sec. V), but they may also be used to study Luttinger liquids and other symmetric states in interacting Fermi systems (Schütz, Bartosch, and Kopietz, 2005; Ledowski and Kopietz, 2007a, 2007b; Bartosch *et al.*, 2009).

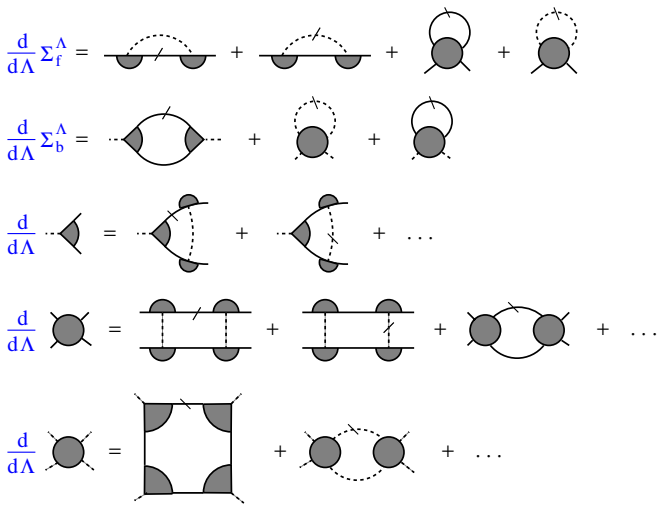

FIG. 7 (color online). Diagrammatic representation of the flow equations for the (fermionic and bosonic) self-energies and some of the interaction vertices in a coupled boson-fermion theory. Solid lines denote fermionic, and dashed lines denote bosonic propagators. Propagators with a dash are single-scale propagators.

III. COMPETING INSTABILITIES

In this section we describe how one can apply the level-2 truncation of the fermionic RG, mainly without self-energy corrections, to two-dimensional fermion systems, and study the interplay of ordering tendencies. In resummations of perturbation theory, their manifestation are singularities in the four-point function and in certain susceptibilities. In the RG, the precursor to a singularity is the growth of some parts of the vertex function (often termed flow to strong coupling). Since singularities in the vertex function change the power counting drastically, this truncated flow then has to be stopped before a singularity happens, at a scale $\Lambda_* > 0$, where one can read off the dominant interactions and infer a tentative phase diagram (in this, susceptibilities are used to compare the strength of different ordering tendencies and to determine Λ_*). As discussed in Sec. II.C.2, curvature effects of the Fermi surface imply that the truncations discussed here can be used also when the interaction is no longer small, provided that the power-counting improvement factor times the interaction strength remains small. To obtain a true phase diagram, however, one needs to integrate over all degrees of freedom, also those with scales below Λ_*. This has been achieved in some cases (see Sec. IV), but much remains to be done.

This first step of monitoring the flow to strong coupling above Λ_*, as described in this section, is important for the following reasons: (1) It allows one to determine the effective interaction just above transition scales from the given microscopic model without any additional *a priori* assumptions about the nature of symmetry breaking, and thereby provides an initial condition for the integration at scales below Λ_*. (2) It exhibits how the interplay of the scale-dependent scattering processes on different parts of the Fermi surface gradually builds up the effective interaction. (3) It has by now become a versatile tool for analyzing models with an elaborate microscopic structure, such as multiple bands.

A. Hubbard model and *N*-patch RG schemes

The Hubbard model and its extensions have become standard in correlated fermion systems: on the square lattice as a candidate model for high-temperature superconducting cuprates (Fulde, 1991; Anderson, 1997), in a multiband generalization, for the newly discovered iron superconductors (Miyake *et al.*, 2010), on triangular lattices for organic crystals (Kino and Fukuyama, 1996; McKenzie, 1997), and on the honeycomb lattice for graphene (Herbut, 2006; Lopez-Sancho, de Juan, and Vozmediano, 2009). The Hamiltonian for the simplest one-band Hubbard model reads

$$H = -\sum_{i,j,s} t_{i-j} c_{i,s}^{\dagger} c_{j,s} + U \sum_i n_{i,\uparrow} n_{i,\downarrow}, \tag{107}$$

where $t_{i-j} = t_{j-i}$ is the hopping amplitude between sites i and j and U is the Hubbard on-site repulsion. We consider here mainly the case with only nearest-neighbor hopping t and next-to-nearest-neighbor hopping t' on a square lattice. Additional hopping terms can be added if a more detailed description of the band structure is required, and other interaction terms may be added. The chemical potential μ and t

and t' determine the band structure $\xi_{\mathbf{k}} = -2t(\cos k_x + \cos k_y) - 4t' \cos k_x \cos k_y - \mu$, and hence the shape of the Fermi surface.

Resummations of perturbation theory in U suggest singularities in different channels, arising from Fermi surface nesting and van Hove singularities (Schulz, 1987), hence competing effects, which are best treated by RG methods. After two-patch studies, which provided a crude approximation to the momentum dependence of the four-point vertex (Dzyaloshinskii, 1987; Lederer, Montambaux, and Poilblanc, 1987; Schulz, 1987; Gonzalez, Guinea, and Vozmediano, 1996; Furukawa, Rice, and Salmhofer, 1998), more careful analyses with momentum-dependent vertices were done using the Polchinski (Zanchi and Schulz, 1997, 1998, 2000), the Wick-ordered (Halboth and Metzner, 2000a, 2000b), and the one-particle irreducible flow equations (Honerkamp *et al.*, 2001), all with a momentum space regulator. To include ferromagnetism, the temperature flow was introduced by Honerkamp and Salmhofer (2001a, 2001b) and further developed by Honerkamp (2001) and Katanin and Kampf (2003). The results of these studies at van Hove filling were confirmed using a refined parametrization of the wave vector dependence (Husemann and Salmhofer, 2009). The decoupling of the various ordering tendencies in the limit of small U very close to the instability and the influence of nonlocal interactions were discussed by Binz, Baeriswyl, and Douçot (2002, 2003).

In the general RG setup of Sec. II, the fermion fields now carry a spin index s and a multiindex K consisting of Matsubara frequencies ω, wave vectors $\mathbf{k}$, and possibly a band index b. To avoid bias, the action is required to retain all symmetries of the initial action. This implies [see Honerkamp *et al.* (2001) and Salmhofer and Honerkamp (2001)] that

$$\Gamma^{(4)\Lambda}_{s_1 s_2 s_3 s_4}(K_1, K_2; K_3, K_4) = V^\Lambda(K_1, K_2; K_3, K_4)\delta_{s_1 s_3}\delta_{s_2 s_4} - V^\Lambda(K_2, K_1; K_3, K_4)\delta_{s_1 s_4}\delta_{s_2 s_3} \tag{108}$$

for a spin-rotation invariant system. By lattice- and time-translation invariance, K_4 is fixed by K_1, K_2, and K_3 in the one-band model (in multiband models, the fourth band index b_4 still remains free). We therefore abbreviate the notation to $V^\Lambda(K_1, K_2, K_3)$. In the truncation $\Gamma^{(6)\Lambda} = 0$, the flow equations for the self-energy and for the coupling function become

$$\frac{d}{d\Lambda}\Sigma^\Lambda(K) = -\int dK'[2V^\Lambda(K, K', K) - V^\Lambda(K, K', K')]S^\Lambda(K'),$$
$$\frac{d}{d\Lambda}V^\Lambda = \mathcal{T}^\Lambda_{PP} + \mathcal{T}^\Lambda_{PH,d} + \mathcal{T}^\Lambda_{PH,cr} \tag{109}$$

with the particle-particle term $\mathcal{T}^\Lambda_{PP}$ and the direct and crossed particle-hole terms $\mathcal{T}^\Lambda_{PH,d}$ and $\mathcal{T}^\Lambda_{PH,cr}$:

$$\mathcal{T}^\Lambda_{PP}(K_1, K_2; K_3, K_4) = \int dK\, V^\Lambda(K_1, K_2, K)L^\Lambda(K, -K + K_1 + K_2) \times V^\Lambda(K, -K + K_1 + K_2, K_3), \tag{110}$$

$$\mathcal{T}^\Lambda_{PH,d}(K_1, K_2; K_3, K_4) = \int dK[-2V^\Lambda(K_1, K, K_3)L^\Lambda(K, K + K_1 - K_3) \times V^\Lambda(K + K_1 - K_3, K_2, K) + V^\Lambda(K_1, K, K + K_1 - K_3) \times L^\Lambda(K, K + K_1 - K_3)V^\Lambda(K + K_1 - K_3, K_2, K) + V^\Lambda(K_1, K, K_3)L^\Lambda(K, K + K_1 - K_3) \times V^\Lambda(K_2, K + K_1 - K_3, K)], \tag{111}$$

$$\mathcal{T}^\Lambda_{PH,cr}(K_1, K_2; K_3, K_4) = \int dK\, V^\Lambda(K_1, K + K_2 - K_3, K) \times L^\Lambda(K, K + K_2 - K_3)V^\Lambda(K, K_2, K_3). \tag{112}$$

Here $L^\Lambda(K, K') = S^\Lambda(K)G^\Lambda(K') + G^\Lambda(K)S^\Lambda(K')$ is the product of single-scale propagators S^Λ and full propagators G^Λ with momentum assignments corresponding to the diagrams in Fig. 8.

For the Hubbard Hamiltonian (107), the initial condition is $V^{\Lambda_0}(K_1, K_2, K_3) = U$. Other interactions can be dealt with by modifying this initial condition. The truncation $\Gamma^{(6)\Lambda} = 0$ is justified only for a sufficiently small bare coupling, since a contribution to $\Gamma^{(6)\Lambda}$ is generated at third order in the two-particle interaction, which leads to third-order contributions to the flow of V^Λ (see Sec. II). In most studies the self-energy feedback into the flow of V^Λ was also neglected, since it also affects the flow only at third order in V^Λ.

The coupling function $V^\Lambda(K_1, K_2, K_3)$ depends on three wave vectors and three Matsubara frequencies, so that the RG

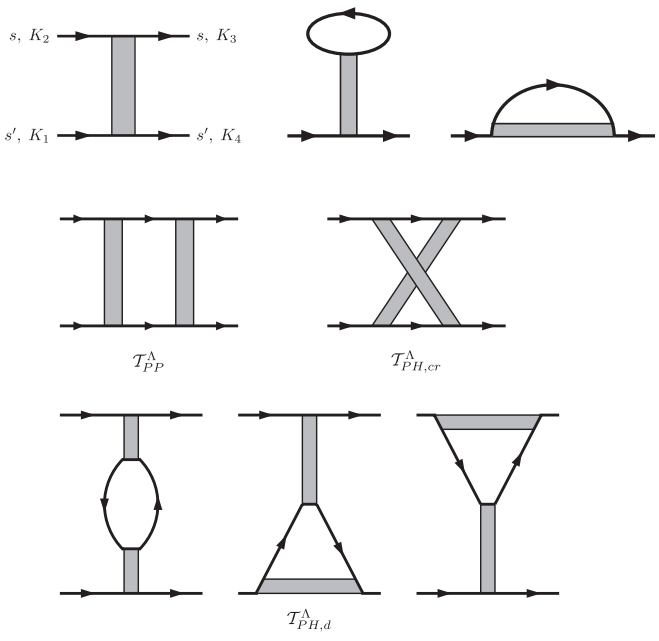

FIG. 8. Top row: The coupling function $V^\Lambda(K_1, K_2, K_3)$ with the spin convention, and the diagrams entering in the flow equation for the self-energy (middle and right diagrams). Middle and bottom rows: The diagrams for the flow of the coupling function. The internal lines are either full propagators G^Λ or single-scale propagators S^Λ.

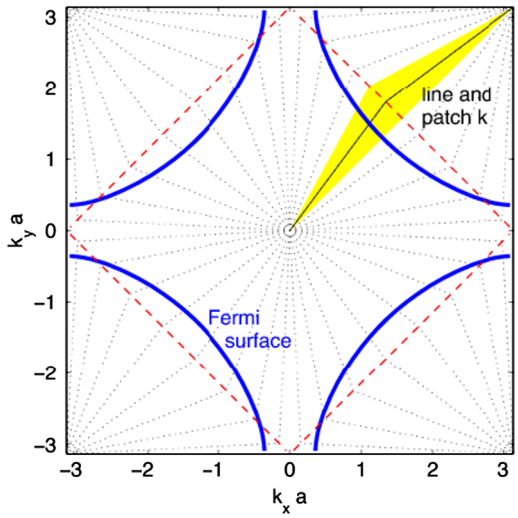

FIG. 9 (color online). N-patch discretization of the Brillouin zone for the one-band Hubbard model on the 2D square lattice. The colored region is a patch in which the coupling function is approximated as a constant.

equation for a two-dimensional system is a differential equation in a nine-dimensional space. As discussed in Sec. II.E, its most singular part sits at zero Matsubara frequency. Hence one may neglect the frequency dependence. Then V^Λ defines an effective Hamiltonian. Similarly, the $\mathbf{k}$ dependence is most important in the angular direction along the Fermi surface. This dependence can then be taken into account by a discretization, i.e., by devising patches in the Brillouin zone in which the coupling function is kept constant. Feldman *et al.* (1992) showed that using N patches leads to a natural N-vector model in two dimensions. Zanchi and Schulz (1998, 2000) were the first to use it in studies of the Hubbard model.

Usually one forms elongated patches that extend roughly perpendicular to the Fermi surface but are rather narrow parallel to the Fermi surface (see Fig. 9). The coupling function is then computed for wave vectors $\mathbf{k}_1$ to $\mathbf{k}_3$ at the Fermi surface in the center of the patches. We label the patches by $\kappa_i = 1, \ldots, N$. The function V^Λ is thus approximated by $O(N^3)$ interpatch couplings $V^\Lambda(\kappa_1, \kappa_2, \kappa_3)$. Even if $\mathbf{k}_1$, $\mathbf{k}_2$, and $\mathbf{k}_3$ are on the Fermi surface, $\mathbf{k}_4$ can be anywhere. In the calculation of the loop integrals it is however necessary to assign a patch number κ_4 to $\mathbf{k}_4$, which amounts to an approximation of projecting $\mathbf{k}_4$ on the Fermi surface. Note that this projected N-patch discretized coupling function $V^\Lambda(\kappa_1, \kappa_2, \kappa_3)$ then has fewer symmetries; for instance, $V^\Lambda(\kappa_1, \kappa_2, \kappa_3) \neq V^\Lambda(\kappa_2, \kappa_1, \kappa_4)$ in general, as in the latter object $\mathbf{k}_3$ is not necessarily on the Fermi surface. For sufficiently large N, this discretization captures the angular variation of the coupling function along the Fermi surface with good precision.

The results obtained within this approximation, described in the following, have been found to be robust when the dependence on frequencies ω_i (Klironomos and Tsai, 2006; Honerkamp, Fu, and Lee, 2007) and the component of $\mathbf{k}_i$ transversal to the Fermi surface (Halboth and Metzner, 2000a; Honerkamp, 2001; Honerkamp *et al.*, 2004) are included. Katanin (2009) performed a flow to third order in the scale-dependent four-point vertex (see Sec. II.E.3), with the frequency dependence in the same approximation as Honerkamp and Salmhofer (2003).

B. Results for the two-dimensional Hubbard model

Starting from the initial condition given by the Hubbard model, the flow is run from Λ_0 down to a characteristic scale Λ_*, where the largest coupling reaches some multiple α of the bandwidth. The choice of α varies widely in the literature; the discussion here is based on the comparably cautious choice $\alpha = 2$ or 3, as well as on the consistency check that the results do not change drastically as α is changed. The characteristic scale Λ_* corresponds to a temperature T_*. If T is clearly above T_*, the flow can be integrated to scale zero without any instabilities. T_* is only an upper bound for the temperature where ordering can set in because of order parameter fluctuations at scales below Λ_*. In two dimensions they are so strong that long-range order that breaks continuous symmetries does not occur at any $T > 0$, thus "ordering" means either short-range order with a large correlation length, or ordering in a related system with a small coupling in the third direction, as is present in most materials.

1. Antiferromagnetism and superconductivity

The results discussed here are obtained with a slightly smeared-out step function as cutoff on $\mathbf{k}$ (no cutoff on the frequencies) and by dropping the self-energy.

a. Antiferromagnetism

For $t' = 0$ and $\mu = 0$, the band is half filled, and the Fermi surface is a perfect square. Every vector connecting parallel sides of the Fermi surface is a nesting vector, and $\nabla\xi_{\mathbf{k}} = 0$ at $(\pi, 0)$ and $(0, \pi)$. This strongly enhances particle-hole terms at wave vector $\mathbf{Q} = (\pi, \pi)$. A random-phase approximation summation of these bubbles results in a divergent static spin susceptibility at $\mathbf{Q}$ for any $U > 0$ at sufficiently low T, indicating the formation of an antiferromagnetic (AF) spin-density wave (SDW), in accordance with mean-field studies (Fulde, 1991). The basic RG results at low T are shown for $U = 2t$ in Fig. 10. The labeling of the $N = 32$ patches along the Fermi surface can be read off Fig. 10(a). Figure 10(b) shows V^Λ as a function of the patch indices κ_1 and κ_2, at $\Lambda_* \sim 0.16t$ and with $\kappa_3 = 1$ [i.e., $\mathbf{k}_3$ near $(-\pi, 0)$]. Strongly enhanced repulsive interactions appear as a vertical line at $\kappa_2 = 24$ (i.e., for $\mathbf{k}_2 - \mathbf{k}_3 = \mathbf{Q}$), almost κ_1 independent, and as a horizontal line at $\kappa_1 = 24$ (corresponding to $\mathbf{k}_1 - \mathbf{k}_3 = \mathbf{Q}$) with only a weak dependence on κ_2, roughly half as large as the vertical feature. In an extrapolation where the regular profiles are narrowed down to delta functions with an appropriate prefactor J, $V^\Lambda(\kappa_1, \kappa_2, \kappa_3) = (J/4)(2\delta_{\mathbf{k}_2-\mathbf{k}_3,\mathbf{Q}} + \delta_{\mathbf{k}_1-\mathbf{k}_3,\mathbf{Q}})$, corresponding to a mean-field AF-spin interaction Hamiltonian $J\sum_{\langle i,j\rangle} e^{i\mathbf{Q}\cdot(\mathbf{R}_i-\mathbf{R}_j)}\mathbf{S}_i \cdot \mathbf{S}_j$, with $\mathbf{S}_i = \frac{1}{2}c_i^+\boldsymbol{\sigma}c_i$. The effective Hamiltonian consisting of the low-scale hopping term and this interaction exhibits AF long-range order at sufficiently low T. An analysis of the flow of susceptibilities (Halboth and Metzner, 2000a; Honerkamp *et al.*, 2001) as described in Sec. II.F confirms this picture.

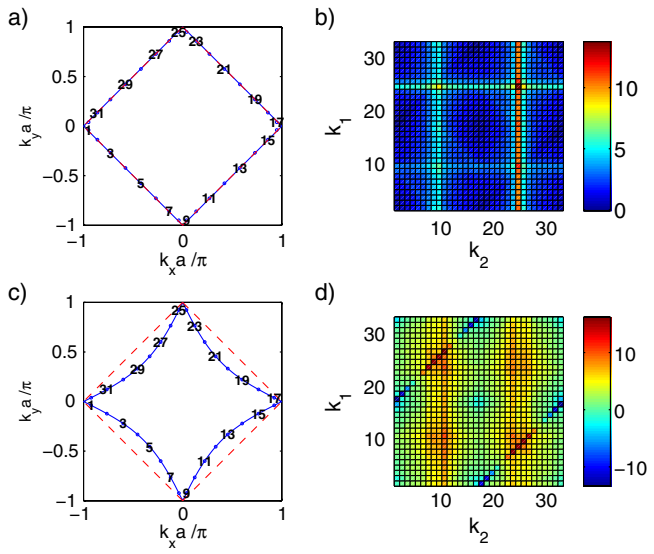

FIG. 10 (color online). N-patch functional RG data obtained with the momentum-shell functional RG for the repulsive Hubbard model on the 2D square lattice. Upper plots: $\mu = 0$, $t' = 0$, and initial $U = 2t$; lower plots: $\mu = 1.2t$, $t' = -0.3t$, and $U = 3t$. Left: Fermi surfaces for the two cases and the $N = 32$ discretization points for the two incoming $\mathbf{k}_1$, $\mathbf{k}_2$ and the first outgoing wave vector $\mathbf{k}_3$. Right: The coupling function $V^{\Lambda_*}(\kappa_1, \kappa_2, \kappa_3)$ with $\kappa_3 = 1$ and κ_1 and κ_2 moving around the Fermi surface. The color bars on the right indicate the values of the interactions.

The extrapolation to a mean-field Hamiltonian is a drastic oversimplification, in which the spin fluctuations are lost, but they are retained in the V^Λ obtained by the RG flow. As the leading instability is clearly exposed by this analysis, one can also resort to a bosonized description that treats the collective infrared physics (Baier, Bick, and Wetterich, 2004).

b. d-wave Cooper pairing

For $t' = -0.3t$ and $\mu = -1.2t$, the Fermi surface still contains the saddle points $(\pi, 0)$ and $(0, \pi)$ but is curved away from these points [Fig. 10(c)]. Now Cooper pair scattering dominates, well visible in Fig. 10(d) on the diagonal lines $\mathbf{k}_1 + \mathbf{k}_2 = 0$ ($|\kappa_1 - \kappa_2| = N/2$ in terms of patch indices). It is attractive when the incoming pair $\mathbf{k}_1, -\mathbf{k}_1$ is near the same saddle point $(\pm\pi, 0)$ as the outgoing pair $\mathbf{k}_3, -\mathbf{k}_3$, and repulsive when incoming and outgoing pairs are at different saddle points. This is the symmetry of the form factor $d(\mathbf{k}) = d_0(\cos k_x - \cos k_y)$ for $d_{x^2-y^2}$ Cooper pairing. In an extrapolation as above, $V^\Lambda(\mathbf{k}_1, \mathbf{k}_2, \mathbf{k}_3)$ gives rise to the mean-field Hamiltonian

$$H^\Lambda_{d\mathrm{SC}} = V_{d\mathrm{SC}} \sum_{\mathbf{k},\mathbf{k}'} d(\mathbf{k}) d(\mathbf{k}') c^\dagger_{\mathbf{k}',\uparrow} c^\dagger_{-\mathbf{k}',\downarrow} c_{-\mathbf{k},\downarrow} c_{\mathbf{k},\uparrow},$$

which has a d-wave singlet-paired ground state. This d-wave pairing instability was found in a number of studies using different functional RG schemes (Zanchi and Schulz, 1998, 2000; Halboth and Metzner, 2000a, 2000b; Honerkamp, 2001; Honerkamp *et al.*, 2001; Honerkamp and Salmhofer, 2001a, 2001b; Tsai and Marston, 2001), in a rather large parameter region. This constitutes convincing evidence that the weakly coupled Hubbard model possesses a d-wave superconducting ground state.

c. Interplay of AF and SC

In Fig. 10(d), the sign structure of the d-wave term goes together, and fits perfectly with, enhanced repulsive interactions near $\kappa_1 = 8$ and $\kappa_2 = 24$, which are the remnants of the SDW feature in Fig. 10(b). Their larger width is due to the Fermi surface curvature. As Λ is decreased, these SDW features appear first, due to approximate nesting at high scales, and then create an attractive component in the $d_{x^2-y^2}$-pairing channel, which then grows as Λ is lowered further, while the SDW is cut off by Fermi surface curvature, as discussed also in Appendix B.3. When the SDW-enhancing terms are removed by hand from the right-hand side of the RG equation, the d-wave terms are suppressed as well. Thus the d-wave pairing interaction is induced by AF-spin fluctuations that appear on higher scales.

At fixed U, t, and t', there is a sizable interval of μ for which the Fermi surface remains close to the saddle points. Since both AF-SDW and d-wave SC are driven by repulsive scattering between $(\pi, 0)$ and $(0, \pi)$, both grow and reinforce one another. In the *saddle point regime*, it becomes impossible to single out one over the other in the truncation used here. By analogy with the quasi-one-dimensional ladder systems, it has been argued that in this regime the Fermi surface gets truncated (Furukawa, Rice, and Salmhofer, 1998; Honerkamp *et al.*, 2001; Läuchli, Honerkamp, and Rice, 2004).

2. Ferromagnetism versus superconductivity

At the van Hove filling, ferromagnetic (FM) tendencies are enhanced by the logarithmic divergence of the density of states, and the Stoner criterion for the bare interaction suggests an FM ordered state at arbitrarily small U. However, the van Hove singularities also make the $O(U^2)$ Cooper pair scattering $\log^2$ divergent, hence putting the two terms into direct competition.

As discussed in Sec. II.D.1, the momentum-shell cutoff artificially suppresses FM. For this reason, the T flow (see Sec. II.D.2) was invented (Honerkamp and Salmhofer, 2001a, 2001b), and we discuss results obtained by T flow here. The main difference to the AF and SC scenario discussed above is that at zero transfer momentum, scattering processes driving FM must have the opposite sign from those driving singlet SC, hence mutually suppressing one another. This simple picture is confirmed by the RG with momentum-dependent vertices, in a study where t' and μ are varied at fixed U and t, such that the Fermi surface always contains the saddle points: near to $t' = -t/3$, T_* gets strongly suppressed, hinting at a quantum critical point between the d-wave SC and FM phases (lower left plot in Fig. 11). These results were later confirmed by a two-particle self-consistent approach (Hankyevych, Kyung, and Termblay, 2003) and in the so-called Ω scheme, which employs a soft infrared regulator on the Matsubara frequencies (Husemann and Salmhofer, 2009); see the lower right plot in Fig. 11. In the latter study, the N-patch scheme was replaced by a parametrization of the vertex functions in terms of exchange bosons. The much higher value of Λ_* in the transitional regime near $t' = -t/3$

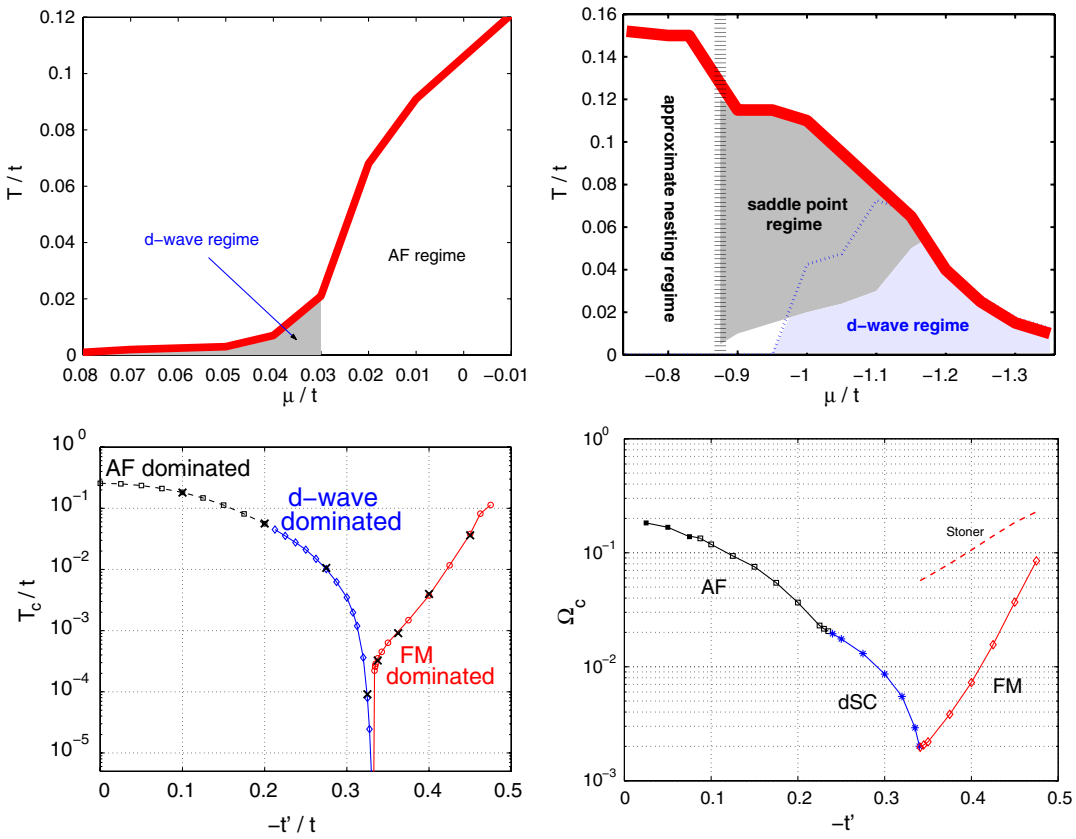

FIG. 11 (color online). Leading instabilities as found by N-patch functional RG in the t-t'-Hubbard model. Left upper plot: T_* vs μ for band filling larger than unity, at $t' = -0.3t$ and $U = 3t$. There is a high-energy-scale AF-SDW instability with a weaker $d_{x^2-y^2}$-wave pairing instability when the AF-SDW is cut off. From Honerkamp, 2001. Right upper plot: Data for the same t' and U on the "hole-doped" side with band fillings smaller than 1. From Honerkamp *et al.*, 2001. Now there is a broad crossover "saddle point regime" between the nesting-driven AF-SDW instability and the $d_{x^2-y^2}$-wave pairing regime. Lower left plot: T_* vs t' at the van Hove filling where the Fermi surface contains the points $(\pi, 0)$ and $(0, \pi)$. For large t' one finds a ferromagnetic instability. From Honerkamp and Salmhofer, 2001a, 2001b, obtained with the T flow. Right lower plot: Ω_* vs t' at van Hove filling, now obtained with the simplified vertex parametrization of Husemann and Salmhofer (2009) and with a soft frequency regulator Ω.

is believed to be due to a form factor that was not fully resolved there.

3. Charge instabilities

The effective interaction develops a pronounced momentum dependence also in the charge sector. In the forward scattering channel, this amounts to the formation of nonuniform contributions to the Landau interaction. If strong enough, the latter can lead to a *Pomeranchuk instability* (Pomeranchuk, 1959), that is, a symmetry-breaking deformation of the Fermi surface.

In particular, the antiferromagnetic peak drives the combination of couplings $V_c^\Lambda(\kappa_1, \kappa_2, \kappa_3) = 2V^\Lambda(\kappa_1, \kappa_2, \kappa_3) - V^\Lambda(\kappa_2, \kappa_1, \kappa_3)$ at certain $\mathbf{Q} = \mathbf{k}_3 - \mathbf{k}_1$. Near to $\mathbf{Q} \approx \mathbf{0}$ and $\mathbf{Q} \approx (\pi, \pi)$,

$$V_c^\Lambda(\kappa_1, \kappa_2, \kappa_3) \approx -f_d(\mathbf{k}_1) f_d(\mathbf{k}_2) V_d(\mathbf{k}_3 - \mathbf{k}_1), \qquad (113)$$

where $f_d(\mathbf{k})$ has the same symmetries as $d(\mathbf{k}) = \cos k_x - \cos k_y$, but is more strongly peaked near the saddle points. For $\mathbf{Q} = (\pi, \pi)$ the corresponding mean-field state is the d-density wave state, which breaks time-reversal invariance (Chakravarty *et al.*, 2001) and gaps the single-particle states, except at nodal points on the Brillouin zone diagonal. For forward scattering, $\mathbf{Q} = \mathbf{0}$, the mean-field state breaks only the lattice rotational symmetry of the electronic dispersion and hence of the Fermi surface. This tendency to form a *nematic* state (Fradkin *et al.*, 2010) via a d-wave Pomeranchuk instability driven by forward scattering interactions was discovered using functional RG (Halboth and Metzner, 2000b). Although the Pomeranchuk instability is not leading in the flow for the Hubbard model (Honerkamp, Salmhofer, and Rice, 2002), a nematic state can coexist with the superconducting state (Neumayr and Metzner, 2003; Yamase and Metzner, 2007), and it may get less suppressed by fluctuations since it breaks no continuous symmetry. The d-wave Pomeranchuk instability has been investigated as a possible source of nematicity of the electronic state in relation with experiments on various correlated electron systems (Honerkamp, 2005; Yamase and Metzner, 2006; Yamase, 2009; Metlitski and Sachdev, 2010c; Okamoto *et al.*, 2010).

4. Flows with self-energy effects

We briefly summarize functional RG studies where the self-energy has been included. If a frequency-independent vertex function V^Λ is directly inserted in the right-hand side

of Eq. (50), then Σ^{Λ} is real and independent of the frequency, and hence only changes the dispersion. This was taken into account in the appendix of Honerkamp *et al.* (2001), where the adaptive scale decomposition method later detailed by Salmhofer (2007) was used. To keep the density fixed, μ is adjusted as a function of Λ. Since the interaction grows in the flow, it is a nontrivial check of the validity of the truncation in which the feedback from the interaction does not lift the low-kinetic-energy modes to high energies, which would drastically shift the Fermi surface and lead to spurious divergences. The first study by Honerkamp *et al.* (2001) showed that the Fermi surface tends to become flatter as Λ decreases, but that it indeed shifts very little before the flow is stopped at Λ_*. Thus, including the real part of the self-energy does not lead to any essential changes in the AF and SC scenario described above. However, correlations that feed only on the immediate vicinity of the saddle points, such as FM, are affected more strongly, and a full analysis of the coupled flow of self-energy and vertex directly at the saddle points remains an open problem, in spite of partial results (Feldman and Salmhofer, 2008b).

The imaginary part and the frequency dependence of the self-energy can be approximated by inserting the integrated flow of the interaction vertex in the self-energy equation (Honerkamp, 2001). This effectively includes two-loop frequency-dependence effects, and captures the T^2 dependence of the quasiparticle scattering rate in a Fermi-liquid situation and the exponent of the vanishing quasiparticle weight in the Luttinger liquid up to second order in the bare couplings (Honerkamp and Salmhofer, 2003). For the 2D Hubbard model, the quasiparticle lifetime and renormalization factor were calculated by Honerkamp (2001) and Honerkamp and Salmhofer (2003), exhibiting a strongly $\mathbf{k}$-dependent quasiparticle degradation as Λ_* is approached. This trend was also found by Zanchi (2001) in a slightly different approximation for the self-energy and is also robust in a more elaborate treatment (Katanin, 2009), where the six-point vertex was partially included. The anisotropy of the quasiparticle lifetime was found to have a non-Fermi-liquid temperature dependence and to correlate with the strength of the generated d-wave pairing interaction (Ossadnik *et al.*, 2008), similar to what is observed experimentally in overdoped cuprates. More refined studies of the frequency dependence revealed, however, that a simple parametrization in terms of a quasiparticle weight is insufficient (Katanin and Kampf, 2004; Rohe and Metzner, 2005). It was shown that near Λ_* the small-$|\omega|$ behavior of $\Sigma^{\Lambda}(\omega, \mathbf{k})$ leads to a splitup of the quasiparticle peak. All these findings are consistent with an anisotropic breakup of the Fermi surface that one would like to connect with the phenomenology of the high-T_c cuprates (Honerkamp *et al.*, 2001; Lee, Nagaosa, and Wen, 2006), but a quantitative comparison is difficult due to the strongly coupled nature of the cuprates.

C. Pnictide superconductors

The functional RG has been useful in the study of the newly discovered iron-pnictide superconductors (Norman, 2008; Ishida, Nakai, and Hosono, 2009; Hirschfeld and Scalapino, 2010). Here the functional RG may work even better, as the pnictides are less strongly correlated than the high-T_c cuprates. This can already be inferred from the experimental phase diagram, where one finds only metallic antiferromagnetic phases (if at all), but never Mott insulating antiferromagnetism. Theoretical works that try to assess the iron d-orbital onsite-interaction strengths find values that put the materials into the range of weak to moderate correlations (Anisimov *et al.*, 2009; Miyake *et al.*, 2010). Regarding the electronic structure, the pnictides are more complex than the cuprates. At least three of the five iron d orbitals have non-negligible weight near the Fermi level (Mazin *et al.*, 2008; Daghofer *et al.*, 2010). Therefore, even if one is interested only in the vicinity of the Fermi surface, the multiband character has to be kept. The Fermi surface [see Fig. 12(b)] is divided into two hole pockets, centered around the origin of the Brillouin zone at $\mathbf{k} = \mathbf{0}$, and two electron pockets around $\mathbf{k} = (\pi, 0)$ and $\mathbf{k} = (0, \pi)$ in the unfolded zone corresponding to the small unit cell with one iron atom [or $\mathbf{k} = (\pi, \pi)$ in the folded zone corresponding to the large unit cell with two iron atoms]. As pointed out earlier (Kuroki *et al.*, 2008; Mazin *et al.*, 2008), there is approximate nesting of electron and hole pockets which enhances particle-hole susceptibilities with the wave vector connecting these pockets. In addition, depending on the parameters and approximations (Ikeda, Arita, and Kunes, 2010), there can be a third hole pocket at (π, π) in the unfolded zone.

The first N-patch studies of the pnictides were performed by Wang *et al.* (2009) and further elaborated in Wang, Zhai,

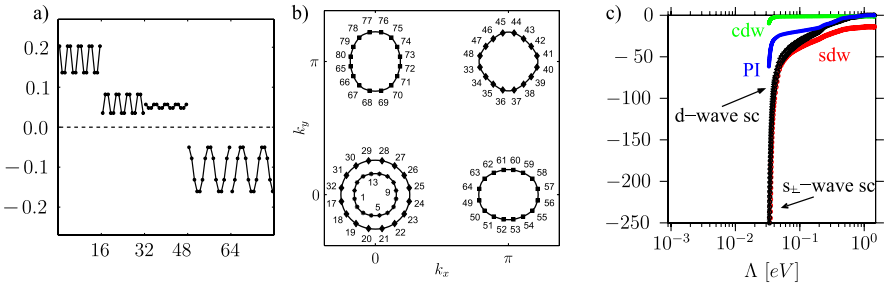

FIG. 12 (color online). Functional renormalization group results for the iron-pnictide compound LaFeAsO at moderate hole doping. (a) Superconducting form factor as the outcome of functional RG, plotted versus the position on the hole pockets at Γ and M and electron pockets at X, numbered as depicted in (b). The competing fluctuations manifest themselves in diverging ordering susceptibilities at low RG scales as shown in (c), including, in particular, spin-density wave (SDW), superconductivity (SC), Pomeranchuk (PI), and charge-density-wave (CDW) instabilities. From Thomale, Platt, Hanke, Bernevig, 2011a.

and Lee (2009, 2010) for a five-band model. They obtained a sign-changing s-wave pairing instability driven by AF fluctuations as the dominant pairing instability. Further they found strongly anisotropic gaps around the electron pockets, with the possibility of node formation. The basic structure of the phase diagram with the sign-changing pairing gap between electron and hole pockets can be understood already from simplified few-patch RG approaches (Chubukov, Efremov, and Eremin, 2008). However, this would predict isotropic gaps around these pockets (Platt, Honerkamp, and Hanke, 2009). To understand the gap anisotropy one has to take into account the multiorbital nature of the electronic spectrum in the iron pnictides, as done in the initial studies (Wang, Zhai, and Lee, 2009, 2010; Wang *et al.*, 2009). In order to understand this point, we start with a single-particle Hamiltonian in wave vector-Fe-d-orbital space

$$H = \sum_{\mathbf{k},s,o} h(\mathbf{k})_{oo'} c^{\dagger}_{\mathbf{k},o,s} c_{\mathbf{k},o',s}, \tag{114}$$

where the matrices $h(\mathbf{k})_{oo'}$ take into account intraorbital and interorbital terms for orbital index $o = o'$ or $o \neq o'$, respectively. s is the spin quantum number. The energy bands are obtained by a unitary transformation from orbital to band operators (index b), $c_{\mathbf{k},b,s} = \sum_o u_{bo}(\mathbf{k}) c_{\mathbf{k},o,s}$. The standard choice for the interaction between the electrons is to introduce orbital-dependent intraorbital and interorbital on-site repulsions, plus Hund's rule and pair hopping terms. While these local terms lead to $\mathbf{k}$-independent interactions in the orbital basis, parametrized by a tensor $V_{o1,o2,o3,o4}$, after the transformation to bands one arrives at a $\mathbf{k}$-dependent interaction function

$$\begin{aligned} &V_{b1,b2,b3,b4}(\mathbf{k}_1, \mathbf{k}_2, \mathbf{k}_3, \mathbf{k}_4) \\ &= \sum_{o1,o2,o3,o4} V_{o1,o2,o3,o4} u_{b1,o1}(\mathbf{k}_1) u_{b2,o2}(\mathbf{k}_2) \\ &\quad \times u^*_{b3,o3}(\mathbf{k}_3) u^*_{b4,o4}(\mathbf{k}_4). \end{aligned} \tag{115}$$

The combination of u_{bo}s behind the interaction tensor is sometimes called the "orbital makeup" (Graser *et al.*, 2009; Maier *et al.*, 2009). These prefactors cause a marked $\mathbf{k}$ structure already in the initial interaction which is then renormalized during the functional RG flow. It turns out that this orbital makeup has an essential influence on the competition between different channels in the flow and is responsible for the gap anisotropies found in the multiband functional RG studies by Wang, Zhai, and Lee (2009, 2010) and Wang *et al.* (2009), and in subsequent functional RG studies (Platt, Thomale, and Hanke, 2011a; Thomale, Platt, Hanke, and Bernevig, 2011a). A typical result for the predicted pairing gaps is shown in Fig. 12(a). Note that, according to the functional RG analysis, the pairing state should be strongly doping dependent (Thomale *et al.*, 2009, 2011b; Thomale, Platt, Hanke, and Bernevig, 2011a).

Summarizing, the iron superconductors pose an interesting problem where the functional RG has been instrumental in obtaining the main ordering tendencies in good agreement with current experiments. For future research, one goal should be to make the functional RG a useful bridge between *ab initio* descriptions providing the effective model at intermediate energy scales and the many-body effects seen in the experiments at low scales. In particular, it will be interesting to relate experimentally observed material trends in, e.g., the gap structure or the energy scales of the different systems, to changes in the microscopic Hamiltonian taken from *ab initio* descriptions. Furthermore, the functional RG studies may have to be extended to include the dispersion orthogonal to the iron-pnictide planes, as this would yield additional possibilities for nodes in the gap function (Norman, 2008; Ishida, Nakai, and Hosono, 2009; Hirschfeld and Scalapino, 2010; Platt, Thomale, and Hanke, 2011b).

D. Other systems

Besides the above-described two larger fields of application, the functional RG truncations described in this section have also been employed in a number of other models in strongly correlated electron physics. Here we briefly list some of these activities.

In relation to possible unconventional superconductivity in organic crystals and layered cobaltates, Hubbard-type models on the triangular lattice have been studied (Tsai and Marston, 2001; Honerkamp, 2003). At large U, the spin exchange interaction between the sites of the triangular lattice is geometrically frustrated, leading to a much weaker appearance of antiferromagnetism and a possible nonmagnetic insulating phase (Morita, Watanabe, and Imada, 2002; Sahebsara and Sénéchal, 2008; Yoshioka, Koga, and Kawakami, 2009). At weak coupling and for nearest-neighbor hopping, Fermi surface nesting is absent, so that near to or at half band filling only low-scale Kohn-Luttinger-like superconducting instabilities occur out of an innocuous Fermi liquid. However, there appears to be a strong dependence on details of the microscopic modeling.

To study interaction effects in graphene, the N-patch functional RG has been applied to the extended Hubbard model on the honeycomb lattice. In nominally undoped graphene, the Fermi surface becomes a set of *Dirac points* where the density of states vanishes, and no instabilities are found for sufficiently small interactions. If the interaction strength exceeds a certain value, various instabilities driven by particle-hole fluctuations between the two Dirac points (Honerkamp, 2008) are found. Interestingly, for larger second-nearest-neighbor interactions, there is the possibility of an instability toward a quantum spin Hall phase (Raghu *et al.*, 2008). However, a spin-liquid phase for intermediate strength of the Hubbard on-site repulsion that was recently found in quantum Monte Carlo calculations (Meng *et al.*, 2010) is not reflected in the functional RG results on this level of approximation. When the Fermi level is moved away from the Dirac points, the functional RG again detects pairing instabilities. In the case of dominant nearest-neighbor repulsion, the leading pairing tendency is in the f-wave triplet channel (Honerkamp, 2008).

The unbiasedness of the functional RG, and the access it gives to $\mathbf{k}$ and ω dependences of vertex functions, is also of great use in (quasi-)one-dimensional models. The half-filled extended Hubbard model in one dimension has been studied in the search for bond-order-wave phases, which could indeed

be found with a refined patching of the **k** dependence of the interaction away from the Fermi points (Tam, Tsai, and Campbell, 2006). For quasi-1D models with a small transverse hopping in a second direction the change from a gapless Luttinger liquid in a strictly one-dimensional situation to Fermi-liquid instabilities toward ordering can be monitored as a function of the transverse hopping (Honerkamp and Salmhofer, 2003). The Fermi surface in coupled metallic chains was studied by Ledowski, Kopietz, and Ferraz (2005) and Ledowski and Kopietz (2007a, 2007b). The possibility of triplet pairing driven by density wave fluctuations was explored in such situations (Nickel *et al.*, 2005, 2006). In these quasi-one-dimensional systems, including the frequency dependence of the interaction vertex is numerically more feasible than in two dimensions. This was used to study the interplay of phonon-mediated and direct electron-electron interactions for chains (Tam *et al.*, 2007a), ladders (Tam *et al.*, 2007b), and systems with small transverse hopping (Bakrim and Bourbonnais, 2010).

Many-fermion lattice Hamiltonians can also be realized with ultracold atoms in optical lattices, opening up new directions. For example, mixtures of more than two hyperfine states (Honerkamp and Hofstetter, 2004) and boson-mediated pairing on two-dimensional lattices (Mathey, Tsai, and Castro Neto, 2006, 2007; Klironomos and Tsai, 2007) have been investigated using fermionic N-patch methods.

Another promising development is the application of the functional RG to quantum spin systems (Reuther and Wölfle, 2010). Here, an auxiliary-fermion representation is used for the spins in generalized Heisenberg models, and the functional RG can be formulated in terms of these fermions. An important difference to systems of itinerant electrons, in the quantum spin system the kinetic energy for the pseudofermions is zero and the interactions depend only on one spatial or wave vector variable. This allows one to keep the full frequency dependence of the self-energy and interaction vertex on the imaginary axis, in the usual truncation where the six-point vertex is neglected. The Katanin modification (Katanin, 2004, see also Sec. II.C.2) of the flow hierarchy turns out to be crucial here. If it is employed, the auxiliary-fermion functional RG describes the transitions from Néel order to collinear order through an intermediate paramagnetic phase in the J_1-J_2 spin-1/2 model on the square lattice as a function of J_1/J_2 in good agreement with numerical approaches. Furthermore, similar systems on the triangular lattice (Reuther and Thomale, 2011) and with longer-ranged couplings (Reuther *et al.*, 2011) were studied. The success of a relatively simple truncation in such an intrinsically strongly coupled system is explained by these authors in that the diagrams summed in this flow contain the leading contributions in both $1/N$ and $1/S$ expansions plus particle-particle diagrams, hence those contributions that are believed to be most important.

IV. SPONTANEOUS SYMMETRY BREAKING

In many interacting Fermi systems a symmetry of the bare action is spontaneously broken at sufficiently low temperatures and, in particular, in the ground state. In the fermionic flow equations, the common types of spontaneous symmetry breaking such as magnetic order or superconductivity are associated with a divergence of the effective two-particle interaction at a finite scale $\Lambda_c > 0$, in a specific momentum channel. In Sec. III we discussed several examples for such divergences. The truncation for the effective two-particle vertex leading to the N-patch scheme described and used in Sec. III is insufficient to describe the symmetry-broken phase. To continue the flow below the scale Λ_c, an appropriate order parameter has to be introduced.

There are two distinct ways of implementing spontaneous symmetry breaking in the functional RG. In one approach the fermionic flow is computed in the presence of a small (ideally infinitesimal) symmetry-breaking term added to the bare action, which is promoted to a finite order parameter below the scale Λ_c (Salmhofer *et al.*, 2004). A relatively simple truncation of the exact flow equation captures spontaneous symmetry breaking in mean-field models such as the reduced BCS model exactly, although the effective two-particle interactions diverge. Another possibility is to decouple the interaction by a bosonic order parameter field, via a Hubbard-Stratonovich transformation, and to study the coupled flow of the fermionic and order parameter fields (Baier, Bick, and Wetterich, 2004).

In the case of competing instabilities a reliable calculation based on either of the above-mentioned routes to symmetry breaking is quite involved. For a rough estimate of order parameters and phase diagrams, one may also neglect low-energy fluctuations and combine flow equations at high scales with a mean-field treatment at low scales. In this functional RG + mean-field approach, one stops the flow of the effective two-particle interaction at a scale $\Lambda_{\mathrm{MF}} > \Lambda_c$, that is, before it diverges. The remaining low-energy degrees of freedom are treated in mean-field approximation, with a reduced effective interaction extracted from the effective two-particle vertex $\Gamma^{(4)\Lambda_{\mathrm{MF}}}$. In the first application of this "poor man's" approach to symmetry breaking the interplay and possible coexistence of antiferromagnetism and d-wave superconductivity in the (repulsive) two-dimensional Hubbard model were studied (Reiss, Rohe, and Metzner, 2007). As in any hybrid method, the results depend quantitatively on the choice of the intermediate scale Λ_{MF} (except for mean-field models), and there is no unique criterion for this choice.

We now review the purely fermionic and the Hubbard-Stratonovich approaches to spontaneous symmetry breaking in the functional RG. The methods will be explained for the case of a superconductor as a prototype for continuous symmetry breaking, and the interested reader is referred to the literature on applications involving other order parameters.

A. Fermionic flows

The effective action Γ^{Λ} obtained from the exact flow equation or from symmetry-conserving truncations thereof exhibits the same symmetries as the bare action $\mathcal{S}$. To analyze spontaneous symmetry breaking, one therefore has to add a symmetry-breaking term $\delta\mathcal{S}$ to the bare action and compute the flow of Γ^{Λ} in the presence of this term. In the case of spontaneous symmetry breaking an arbitrarily small symmetry-breaking term is promoted to a finite order parameter at a scale Λ_c, which survives until the end of the flow.

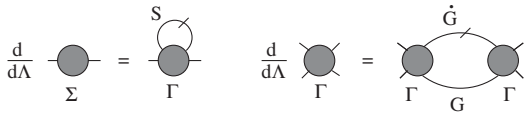

FIG. 13. Coupled flow equations for the self-energy and the two-particle vertex determining the fermionic flow with symmetry breaking.

A crucial issue is then to find a manageable truncation of the exact flow equation which captures the essential features of the flow into the symmetry-broken phase. This is nontrivial since the effective two-particle interactions driving the symmetry breaking become large. Indeed, truncations based on neglecting vertices $\Gamma^{(2m)\Lambda}$ with $m > 2$ in the hierarchy of flow equations fail miserably. A benchmark for truncations is the requirement that they should at least provide a decent solution for mean-field models. This requirement is met by an approximation introduced by Katanin (2004) to implement Ward identities in truncated flow equations. Katanin's truncation, which was described already in Sec. II.C, consists of two coupled flow equations for the self-energy Σ^Λ and the two-particle vertex $\Gamma^{(4)\Lambda}$; see Fig. 13.

They are almost identical to the first two equations in the hierarchy described in Sec. II.C, with $\Gamma^{(6)\Lambda} = 0$, but in the flow equation for $\Gamma^{(4)\Lambda}$ the single-scale propagator S^Λ is replaced by $\partial_\Lambda G^\Lambda = S^\Lambda + G^\Lambda \partial_\Lambda \Sigma^\Lambda G^\Lambda$. This modification takes tadpole contributions obtained from contractions of the three-particle vertex $\Gamma^{(6)\Lambda}$ into account.

It is easy to see that the Katanin truncation solves mean-field models for symmetry breaking such as the Stoner model for ferromagnetism or the reduced BCS model exactly (Salmhofer *et al.*, 2004). The exact self-energy in such models is given by the Hartree-Fock term $\Sigma = VG$ (schematically), where V is the bare interaction, and the two-particle vertex by a ladder sum of the form $\Gamma^{(4)} = V(1 - GGV)^{-1}$. These equations hold also in the presence of a cutoff Λ. Applying Λ derivatives one immediately finds that Σ^Λ and $\Gamma^{(4)\Lambda}$ obey flow equations of the (schematic) form $\partial_\Lambda \Sigma^\Lambda = \Gamma^{(4)\Lambda} S^\Lambda$ and $\partial_\Lambda \Gamma^{(4)\Lambda} = \Gamma^{(4)\Lambda} \partial_\Lambda (G^\Lambda G^\Lambda) \Gamma^{(4)\Lambda}$, which corresponds exactly to Katanin's truncation.

To be more specific, we consider the case of singlet superconductivity, where the continuous U(1) symmetry associated with charge conservation is spontaneously broken, while spin-rotation invariance remains conserved. Superconductivity can be induced by adding a term of the form

$$\delta\mathcal{S} = \sum_k [\Delta_0(k)\bar{\psi}_\uparrow(k)\bar{\psi}_\downarrow(-k) + \Delta_0^*(k)\psi_\downarrow(-k)\psi_\uparrow(k)], \tag{116}$$

with a (generally complex) external pairing field $\Delta_0(k)$, to the bare action. It is convenient to use Nambu spinors $\Psi_\alpha(k)$ and $\bar{\Psi}_\alpha(k)$ with $\bar{\Psi}_+(k) = \bar{\psi}_\uparrow(k)$, $\Psi_+(k) = \psi_\uparrow(k)$, $\bar{\Psi}_-(k) = \psi_\downarrow(-k)$, and $\Psi_-(k) = \bar{\psi}_\downarrow(-k)$. The effective action as a functional of the Nambu fields, truncated beyond two-particle terms, has the form

$$\Gamma^\Lambda[\Psi, \bar{\Psi}] = \Gamma^{(0)\Lambda} - \sum_k \sum_{\alpha_1,\alpha_2} \Gamma^{(2)\Lambda}_{\alpha_1\alpha_2}(k)\bar{\Psi}_{\alpha_1}(k)\Psi_{\alpha_2}(k) + \frac{1}{4}\sum_{k_1,\ldots,k_4} \sum_{\alpha_1,\ldots,\alpha_4} \Gamma^{(4)\Lambda}_{\alpha_1\alpha_2\alpha_3\alpha_4}(k_1,k_2,k_3,k_4) \times \bar{\Psi}_{\alpha_1}(k_1)\bar{\Psi}_{\alpha_2}(k_2)\Psi_{\alpha_3}(k_3)\Psi_{\alpha_4}(k_4). \tag{117}$$

Because of spin-rotation invariance only terms with an equal number of Ψ and $\bar{\Psi}$ fields contribute. The Nambu propagator $\mathbf{G}^\Lambda = (\mathbf{\Gamma}^{(2)\Lambda})^{-1}$ can be written as a 2×2 matrix of the form

$$\mathbf{G}^\Lambda(k) = \begin{pmatrix} G^\Lambda_{++}(k) & G^\Lambda_{+-}(k) \\ G^\Lambda_{-+}(k) & G^\Lambda_{--}(k) \end{pmatrix} = \begin{pmatrix} G^\Lambda(k) & F^\Lambda(k) \\ F^{*\Lambda}(k) & -G^\Lambda(-k) \end{pmatrix}. \tag{118}$$

It is instructive to discuss the flow of the superconducting gap and the two-particle vertex for the reduced BCS model (Salmhofer *et al.*, 2004), which is defined by an action of the form

$$\mathcal{S}[\psi, \bar{\psi}] = \sum_{k,\sigma}(-ik_0 + \xi_{\mathbf{k}})\bar{\psi}_\sigma(k)\psi_\sigma(k) + \sum_{k,k'} V(k,k')\bar{\psi}_\uparrow(k)\bar{\psi}_\downarrow(-k)\psi_\downarrow(-k')\psi_\uparrow(k'). \tag{119}$$

Note that the interaction is restricted to particles with strictly opposite momenta and spins. It is well known that mean-field theory solves this model exactly in the thermodynamical limit (Haag, 1962; Mühlschlegel, 1962). The restricted momentum dependence of the bare interaction carries over to similar restrictions for the effective two-particle vertex $\Gamma^{(4)\Lambda}$ in Eq. (117). Only two independent components appear, namely,

$$V^\Lambda(k,k') = \Gamma^{(4)\Lambda}_{+-+-}(k,k',k',k), \tag{120}$$

$$W^\Lambda(k,k') = \Gamma^{(4)\Lambda}_{++--}(k,k',k',k). \tag{121}$$

The first component is a normal interaction between two particles, and its initial value $V^{\Lambda_0}(k,k')$ is the bare interaction. The second component is an anomalous term describing the creation of four particles. It is initially zero, but is generated by charge symmetry-breaking terms in the course of the flow. Another anomalous term describing the destruction of four particles is given by the complex conjugate of $W^\Lambda(k,k')$. The diagonal element of the Nambu self-energy vanishes for the reduced BCS model, while the off-diagonal element is given by the gap function $\Delta^\Lambda(k)$.

For the special case of a momentum-independent s-wave interaction V, the flow equations obtained from the procedure described above are particularly simple. Choosing a momentum-independent and real bare gap $\Delta_0 > 0$, the flowing quantities Δ^Λ, V^Λ, and W^Λ are real and momentum independent, too. Their (exact) flow is given by

$$\frac{d}{d\Lambda}\Delta^\Lambda = -(V^\Lambda + W^\Lambda)\sum_k \frac{d}{d\Lambda}F^\Lambda\Big|_{\Delta^\Lambda \text{ fixed}}, \tag{122}$$

where $\frac{d}{d\Lambda}F^\Lambda|_{\Delta^\Lambda \text{ fixed}}$ is the anomalous Nambu single-scale propagator, and

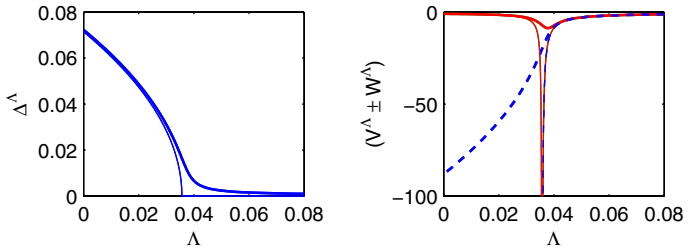

FIG. 14 (color online). Flow for a reduced BCS model with a constant density of states at zero temperature; the bandwidth is 1 and the bare interaction $V = -0.3$. Left: Flow of the gap Δ^Λ; the thick line is for a bare gap $\Delta_0 = 2.4 \times 10^{-4}$ and the thin line for $\Delta_0 = 6 \times 10^{-8}$, in units of the bandwidth. Right: Flow of the linear combinations $V^\Lambda + W^\Lambda$ (solid lines) and $V^\Lambda - W^\Lambda$ (dashed lines) of normal and anomalous vertices. Thick lines are again for $\Delta_0 = 2.4 \times 10^{-4}$ and thin lines for $\Delta_0 = 6 \times 10^{-8}$.

$$\frac{d}{d\Lambda}(V^\Lambda \pm W^\Lambda) = -(V^\Lambda \pm W^\Lambda)^2 \times \sum_k \frac{d}{d\Lambda}[|G^\Lambda(k)|^2 \mp |F^\Lambda(k)|^2]. \quad (123)$$

A typical flow for an attractive bare interaction $V < 0$ is shown in Fig. 14, for two different choices of the bare gap Δ_0. The gap increases monotonically from the initial value Δ_0 upon lowering Λ, and reaches a finite value $\Delta \gg \Delta_0$ for $\Lambda \to 0$. A finite Δ_0 regularizes the square-root singularity in the gap flow at $\Lambda = \Lambda_c$. The normal vertex V^Λ reaches a large negative value at the critical scale Λ_c, while the anomalous vertex W^Λ becomes large and positive. The linear combination $V^\Lambda + W^\Lambda$, which drives the gap flow, is also strongly negative at Λ_c, but it saturates at a moderately negative value for Λ below Λ_c. By contrast, $V^\Lambda - W^\Lambda$ decreases monotonically and reaches a final value of order $1/\Delta_0$ for $\Lambda \to 0$, which diverges for $\Delta_0 \to 0$. This divergence is the mean-field remnant of the Goldstone mode associated with the broken continuous symmetry.

In the case of a discrete broken symmetry, the effective interaction becomes large only at the critical scale, while no large components remain for $\Lambda \to 0$. This has been exemplified in a study of the RG flow of a mean-field model for a commensurate charge-density wave (Gersch *et al.*, 2005).

The performance of the Katanin truncation for models with full (not reduced) interactions has not yet been fully explored, since an accurate parametrization of the flowing vertex is quite demanding. However, the results obtained so far are encouraging. Staying with superconductivity as an example, the Nambu vertex contains 16 components, most of them corresponding to anomalous interactions. In addition to the anomalous terms appearing already in the reduced BCS model, there are anomalous interactions corresponding to the creation of three particles and the destruction of one particle, and vice versa (Salmhofer *et al.*, 2004; Gersch, Honerkamp, and Metzner, 2008). Making full use of spin-rotation invariance, all the Nambu components can be actually expressed by only three independent functions of momenta and frequencies (Eberlein and Metzner, 2010). The main challenge is an adequate parametrization of the (threefold) momentum and frequency dependence, since singularities associated with symmetry breaking and the Goldstone mode appear in the course of the flow. Surprisingly, in a test case study for the weakly attractive Hubbard model, a rather crude parametrization using the N-patch discretization described in Sec. III turned out to yield a reasonable flow into the superconducting phase, with results for the gap in good agreement with results obtained earlier by other means (Gersch, Honerkamp, and Metzner, 2008). This is encouraging, but the low-energy fluctuations are clearly not well described in such a parametrization. To deal with the singular momentum and frequency dependence in the Cooper channel (and possibly also in the forward scattering channel), the channel decomposition devised by Husemann and Salmhofer (2009) seems useful, since it allows one to isolate singular dependences in functions of only one momentum and frequency variable, similar to a description of singular interactions by exchange bosons. The channel decomposition has been formally extended already to the superconducting state (Eberlein and Metzner, 2010), but a concrete calculation beyond mean-field models has not yet been performed.

In systems with a first order phase transition one may miss the symmetry-broken phase if one tests only for local stability of the symmetric phase by offering a small symmetry-breaking field, since the latter may be metastable. However, one can escape from the metastable state by adding a scale-dependent symmetry-breaking counterterm R^Λ to the effective action, which has to be chosen sufficiently large at the beginning of the flow and fades out for $\Lambda \to 0$, such that the system is ultimately not modified. Formally this is just another choice of regularization within the general framework described in Sec. II.B. The counterterm method has been implemented for the exactly soluble test case of a charge-density wave mean-field model by Gersch, Reiss, and Honerkamp (2006).

Popular approximations also beyond mean-field theory can be retrieved from the functional RG by keeping a suitable subset of contributions. In particular, the Eliashberg theory for frequency-dependent (usually phonon-induced) pairing interactions can be obtained as an approximation to the exact flow equations both in the symmetric (Tsai *et al.*, 2005) and in the symmetry-broken state (Honerkamp and Salmhofer, 2005). This is achieved by keeping the Cooper channel for zero total momentum and frequency and the crossed particle-hole channel for zero transfer in the flow of the interaction, and the Fock term for the self-energy.

B. Flows with Hubbard-Stratonovich fields

Collective order parameter fluctuations associated with spontaneous symmetry breaking in interacting many-body systems are often treated by introducing an auxiliary order parameter field via a Hubbard-Stratonovich transformation (Popov, 1987). A combination of the functional RG with the Hubbard-Stratonovich route to spontaneous symmetry breaking in an interacting Fermi system was first used by Baier, Bick, and Wetterich (2004). They studied the formation of an antiferromagnetic state in the repulsive two-dimensional Hubbard model at half filling and managed to recover the low-energy collective behavior (described by a nonlinear sigma model) from a truncated set of coupled flow equations

for the fermions and the order parameter field. In the following we describe the method for the case of a superfluid phase, summarizing the work of several groups.

We consider an interacting continuum or lattice Fermi system with a local attraction $V < 0$. For continuum systems a suitable ultraviolet regularization is necessary. A local attraction can act only between particles with opposite spin and leads to singlet pairing. It is thus natural to decouple this interaction by a Hubbard-Stratonovich transformation with a complex bosonic field $\phi(q)$ corresponding to the bilinear composite of fermionic fields $V\sum_k \psi_\downarrow(-k)\psi_\uparrow(k+q)$. This leads to an action of the form

$$\begin{aligned}\mathcal{S}[\phi,\psi,\bar{\psi}] = &-\sum_{k,\sigma}\bar{\psi}_\sigma(k)(ik_0-\xi_{\mathbf{k}})\psi_\sigma(k)\\ &+\frac{m_b}{2}\sum_q \phi^*(q)\phi(q)\\ &+\sum_{k,q}[\bar{\psi}_\uparrow(k+q)\bar{\psi}_\downarrow(-k)\phi(q)+\text{H.c.}],\end{aligned} \tag{124}$$

where ϕ^* is the complex conjugate of ϕ and $m_b = -1/V > 0$.

Spontaneous symmetry breaking can now be studied by using the flow equation for the effective action $\Gamma^\Lambda[\phi,\psi,\bar{\psi}]$ for coupled bosonic and fermionic fields derived in Sec. II.G. Relatively simple truncations capture several nontrivial fluctuation effects. Effective interactions beyond quartic order in the fields are generally neglected. Also boson-fermion vertices beyond the order appearing already in the bare action are discarded. The truncations are usually formulated as an ansatz for the effective average action

$$\begin{aligned}\Gamma_R^\Lambda[\phi,\psi,\bar{\psi}] &= \Gamma^\Lambda[\phi,\psi,\bar{\psi}] - \text{regulator term}\\ &= \Gamma_b^\Lambda[\phi]+\Gamma_f^\Lambda[\psi,\bar{\psi}]+\Gamma_{bf}^\Lambda[\phi,\psi,\bar{\psi}],\end{aligned} \tag{125}$$

which obeys the initial condition $\Gamma_R^{\Lambda_0} = \mathcal{S}$; see Sec. II.G.

The ansatz used for the bosonic part is guided by the usual strategy of a double expansion in ϕ and gradients [see, e.g., Tetradis and Wetterich (1994)]:

$$\Gamma_b^\Lambda[\phi] = \sum_x U_{\text{loc}}^\Lambda[\phi(x)] + \text{gradient terms}, \tag{126}$$

where $x = (x_0, x_1, \ldots, x_d)$ collects imaginary time and real space coordinates. Note that we use the same letter ϕ for the real space and momentum space representations of the bosonic field. The shape of the local potential $U_{\text{loc}}^\Lambda(\phi)$ depends on the scale. For Λ above a critical scale Λ_c it has the convex form

$$U_{\text{loc}}^\Lambda(\phi) = m_b^\Lambda|\phi|^2 + u^\Lambda|\phi|^4, \tag{127}$$

with a minimum at $\phi = 0$. For $\Lambda < \Lambda_c$ the potential assumes a Mexican hat shape

$$U_{\text{loc}}^\Lambda(\phi) = u^\Lambda[|\phi|^2 - |\alpha^\Lambda|^2]^2, \tag{128}$$

with a circle of minima at $|\phi| = |\alpha^\Lambda|$, where α^Λ is the (flowing) bosonic order parameter. The regime $\Lambda > \Lambda_c$ is called the *symmetric* regime. At $\Lambda = \Lambda_c$ the bosonic mass m_b vanishes. In the *symmetry-broken* regime, for $\Lambda < \Lambda_c$, the order parameter α^Λ rises continuously from zero to a finite value. Its flow can be computed by tracing the minimum of the flowing potential U_{loc}^Λ or, equivalently, by the condition that the bosonic one-point vertex $\Gamma_b^{(1)\Lambda}$ vanishes.

For the gradient terms in $\Gamma_b^\Lambda[\phi]$ various choices have been made. The simplest one (Birse *et al.*, 2005; Diehl *et al.*, 2007; Krippa, 2007) compatible with the U(1) symmetry has the form of an inverse bare propagator for free bosons,

$$\begin{aligned}&\sum_x[Z_b^\Lambda\phi^*(x)\partial_{x_0}\phi(x) - A_b^\Lambda\phi^*(x)\nabla^2\phi(x)]\\ &\quad = \sum_q \phi^*(q)[-iZ_b^\Lambda q_0 + A_b^\Lambda\mathbf{q}^2]\phi(q),\end{aligned} \tag{129}$$

where $\nabla = (\partial_{x_1},\ldots,\partial_{x_d})$. For lattice fermions one may replace $\mathbf{q}^2$ by a periodic dispersion $\omega_{\mathbf{q}}$ which is proportional to $\mathbf{q}^2$ only at small $\mathbf{q}$ (Strack, Gersch, and Metzner, 2008). The term linear in q_0 is absent in particle-hole symmetric systems (Strack, Gersch, and Metzner, 2008), such that contributions of order q_0^2 become important. Additional gradient terms have to be taken into account to fully capture the effects of the Goldstone mode, as discussed below.

The normal fermionic part of the effective action is usually kept in its bare form, sometimes adjusted by renormalization factors for the frequency and momentum dependences. In the symmetry-broken regime, an anomalous term is generated, such that Γ_f^Λ becomes

$$\begin{aligned}\Gamma_f^\Lambda[\psi,\bar{\psi}] = &-\sum_{k,\sigma}\bar{\psi}_\sigma(k)(iZ_f^\Lambda k_0 - A_f^\Lambda\xi_{\mathbf{k}})\psi_\sigma(k)\\ &+\sum_k[\Delta^\Lambda(k)\bar{\psi}_\uparrow(k)\bar{\psi}_\downarrow(-k)+\text{H.c.}].\end{aligned} \tag{130}$$

For a local interaction the k dependence of the gap function $\Delta^\Lambda(k)$ is weak and in simple truncations fully absent. Quartic terms corresponding to effective two-fermion interactions are absent in the bare action by virtue of the Hubbard-Stratonovich decoupling, but are generated again in the course of the flow. These generated terms are neglected in lowest-order truncations, and sometimes they are treated by a dynamical decoupling procedure called dynamical bosonization, see below.

For the effective boson-fermion interaction one also maintains the bare form of a local three-point function,

$$\begin{aligned}\Gamma_{bf}^\Lambda[\phi,\psi,\bar{\psi}] = &\sum_{k,q} g^\Lambda[\bar{\psi}_\uparrow(k+q)\bar{\psi}_\downarrow(-k)\phi(q)+\text{H.c.}]\\ &+\text{anomalous terms},\end{aligned} \tag{131}$$

with anomalous terms of the form $\psi\psi\phi$ and $\bar{\psi}\,\bar{\psi}\,\phi^*$ contributing only in the symmetry-broken regime. The coupling g^Λ is frequently referred to as "Yukawa coupling." The anomalous terms in the boson-fermion interaction are usually neglected. If taken into account, they remain indeed rather small (Strack, Gersch, and Metzner, 2008).

Instead of using a U(1)-symmetric ansatz for the effective action, one may also start from the hierarchy of flow equations for the vertex functions and implement the U(1) symmetry by Ward identities (Bartosch, Kopietz, and Ferraz, 2009).

Even with the simple ansatz (129) for the bosonic gradient terms, the effective action described above yields sensible results not only at weak coupling, but actually in the

entire regime from BCS superfluidity to Bose-Einstein condensation of tightly bound pairs (Diehl *et al.*, 2007). In particular, the transition temperature T_c increases exponentially with the interaction in the weak-coupling regime, reaches a maximum, and finally saturates in the strong coupling limit, as it should.

The bosonic interaction u^Λ and also the bosonic renormalization factors A_b^Λ and Z_b^Λ vanish in the limit $\Lambda \to 0$ (Birse *et al.*, 2005; Krippa, 2007). This fluctuation effect reflects the drastic renormalization of longitudinal order parameter correlations, which are well known from the interacting Bose gas in dimensions $d \leq 3$ [see, e.g., Pistolesi *et al.* (2004)]. Note that for a nodeless gap function the low-energy behavior of a fermionic superfluid is equivalent to that of an interacting Bose gas, since fermionic excitations are fully gapped. However, with the simple ansatz (129) the transverse order parameter fluctuations corresponding to the Goldstone mode are also strongly renormalized, which is not correct. To distinguish between longitudinal and transverse fluctuations, one can fix the phase of the order parameter α^Λ such that α^Λ is real, decompose the complex order parameter field in real and imaginary parts $\phi(q) = \sigma(q) + i\pi(q)$ with $\sigma(-q) = \sigma^*(q)$ and $\pi(-q) = \pi^*(q)$, and introduce different renormalization factors for σ and π fields (Pistolesi *et al.*, 2004). Using this decomposition, the correct infrared behavior was obtained by Strack, Gersch, and Metzner (2008) where, however, the cancellation of singular contributions to the renormalization factors for the transverse π fields was implemented by hand. To capture this cancellation intrinsically, one has to include an additional U(1) symmetric gradient term of the form $[\sigma(\partial_{x_0}, \nabla)\sigma + \pi(\partial_{x_0}, \nabla)\pi]^2$ (Tetradis and Wetterich, 1994; Strack, 2009).

The fermionic flow based on the Katanin truncation described in Sec. IV.A reproduces the exact solution of the reduced BCS model (and other mean-field models). Within the truncation described above, the bosonized flow yields a reasonable solution without artificial features, but the gap comes out a bit too small. The reason for this is the truncation of $U_{\mathrm{loc}}^\Lambda(\phi)$ at quartic order. To recover the exact solution, one has to keep all orders in ϕ (Strack, Gersch, and Metzner, 2008).

The ansatz (130) for $\Gamma_f^\Lambda[\psi, \bar{\psi}]$ neglects the generation of fermionic interactions by the flow. In particular, quartic (two-fermion) interactions are generated by box diagrams with four boson-fermion vertices. These terms contain contributions from particle-hole fluctuations which, among other effects, lead to a significant reduction of the transition temperature. The (re)generated two-fermion interaction can be decoupled at each step in the flow by a procedure called dynamical bosonization (Gies and Wetterich, 2002, 2004; Floerchinger and Wetterich, 2009). A general two-fermion interaction cannot be decoupled exactly by a single Hubbard-Stratonovich field, such that several fields may be needed to obtain accurate results. Dynamical bosonization was used to include effects from particle-hole fluctuations in attractively interacting Fermi systems by Floerchinger *et al.* (2008).

Following the work of Baier, Bick, and Wetterich (2004) on the repulsive Hubbard model at half filling, functional RG flow equations with Hubbard-Stratonovich fields were also applied to the Hubbard model away from half filling. Commensurate and incommensurate antiferromagnetic fluctuations were investigated (Krahl, Friederich, and Wetterich, 2009). More importantly, it was clarified how the generation of d-wave pairing from antiferromagnetic fluctuations can be captured by a bosonized flow (Krahl, Müller, and Wetterich, 2009), and the flow was continued into the symmetry-broken phase, with coupled order parameter fields describing antiferromagnetism and d-wave superconductivity (Friederich, Krahl, and Wetterich, 2010, 2011).

Compared to the purely fermionic RG described in Sec. IV.A, the treatment of order parameter fluctuations is facilitated considerably by the Hubbard-Stratonovich field. On the other hand, fluctuation effects associated with other channels (the particle-hole channel in case of superfluidity) look more complicated. For systems with competing instabilities the choice of an adequate Hubbard-Stratonovich field becomes problematic, since the fermionic interaction can be decoupled in different ways, which, in combination with truncations, may lead to ambiguities in the results. In general, several Hubbard-Stratonovich fields must be used, and the analysis done in Sec. III indicates which ones are the most important. The decomposition of the interaction by Husemann and Salmhofer (2009) allows one to switch to Hubbard-Stratonovich fields after the fermionic flow has been performed down to a certain scale, and may thus be used to combine the two flow representations.

V. QUANTUM CRITICALITY

Instabilities of the normal metallic state lead to a rich variety of quantum phase transitions (Sachdev, 1999) in the ground state of interacting electron systems, which can be tuned by a control parameter such as pressure, doping, or a magnetic field. Most interesting are *continuous* transitions which lead to quantum critical fluctuations (Belitz, Kirkpatrick, and Vojta, 2005). Near a quantum critical point (QCP) electronic excitations are strongly scattered by order parameter fluctuations such that Fermi-liquid theory breaks down (Vojta, 2003; von Loehneysen *et al.*, 2007). Quantum critical fluctuations are therefore frequently invoked as a mechanism for non-Fermi-liquid behavior observed in strongly correlated electron compounds.

Quantum phase transitions in interacting Fermi systems are traditionally described by an effective order parameter theory pioneered by Hertz (1976) and Millis (1993). An order parameter field ϕ is introduced by a Hubbard-Stratonovich decoupling of the fermionic interaction, and the fermionic fields are subsequently integrated out. The resulting effective action for the order parameter is truncated at quartic order and analyzed by standard scaling and RG techniques. However, more recent studies revealed that the Hertz-Millis approach is not always applicable, especially in low-dimensional systems (Belitz, Kirkpatrick, and Vojta, 2005; von Loehneysen *et al.*, 2007). Since electronic excitations in a metal are gapless, integrating out the electrons can lead to singular interactions in the effective order parameter action which cannot be approximated by a local quartic term. The nature of the problem was identified and essential aspects of its solution were presented first for disordered ferromagnets by Kirkpatrick and Belitz (1996), and later elaborated on by

Belitz *et al.* (2001a, 2001b). For clean ferromagnets, Belitz, Kirkpatrick, and Vojta (1997) showed that Hertz-Millis theory breaks down, and no continuous quantum phase transition can exist, in any dimension $d \leq 3$; the transition is generically of first order (Belitz, Kirkpatrick, and Vojta, 1999). The Hertz-Millis approach was also shown to be invalid for the quantum antiferromagnetic transition in two dimensions (Abanov, Chubukov, and Schmalian, 2003; Abanov and Chubukov, 2004; Metlitski and Sachdev, 2010a). In that case a continuous transition survives, but the QCP becomes non-Gaussian.

Applications of the functional RG to quantum phase transitions and quantum criticality in interacting Fermi systems have appeared only recently. In Sec. V.A we explain how the Hertz-Millis theory fits into the functional RG framework and we review some extensions relying on an effective order parameter action truncated at quartic or hexatic order. An application of a nonperturbative truncation, where all orders in ϕ are (and must be) kept, is discussed in Sec. V.B. Finally, in Sec. V.C we briefly discuss the possibility of studying coupled flow equations for fermions and their critical order parameter fluctuations in the functional RG framework, and we refer to first steps in this direction.

A. Hertz-Millis theory

In his seminal work on quantum phase transitions in metallic electron systems, Hertz (1976) proposed to decouple the electron-electron interaction by introducing an order parameter field ϕ via a Hubbard-Stratonovich transformation. The resulting action is quadratic in the fermionic variables ψ and $\bar{\psi}$, which can therefore be integrated out. One thus obtains an effective action which depends only on ϕ. Truncating at quartic order in ϕ, and discarding irrelevant momentum and frequency dependences (in the sense of standard power counting), leads to the Hertz action,

$$\mathcal{S}[\phi] = \mathcal{S}^{(0)} + \sum_q \phi(-q)\left[A\mathbf{q}^2 + Z\frac{|q_0|}{|\mathbf{q}|^{z-2}}\right]\phi(q) + \sum_x U_{\mathrm{loc}}[\phi(x)], \tag{132}$$

where $\mathcal{S}^{(0)}$ is a field-independent term, and

$$U_{\mathrm{loc}}(\phi) = r\phi^2 + u\phi^4. \tag{133}$$

We write our equations for the case of a real scalar order parameter for simplicity, using again the same letter ϕ for the real and momentum space representations of the field. Except for the frequency dependence, the action has the form of a ϕ^4 theory for thermal phase transitions. The frequency-dependent term stems from low-energy particle-hole excitations. Here the dynamical exponent z is an integer number ≥ 2 depending on the type of transition. Tuning the parameter r one can approach the phase transition, in particular, the quantum phase transition at $T = 0$.

The action (132) has been analyzed by standard scaling and RG techniques. Because of the frequency dependence, the scaling behavior at the QCP corresponds to a system with an effective dimensionality $d_{\mathrm{eff}} = d + z$, where d is the spatial dimension (Hertz, 1976). As a consequence, the QCP appears to be Gaussian in three- and even in two-dimensional systems. An important insight by Millis (1993) was that the ϕ^4 term in the action is nevertheless crucial to obtain the correct temperature dependences near the QCP. He derived the temperature dependence of the correlation length ξ and other quantities by using a perturbative RG with a mixed momentum and frequency cutoff. From a functional RG perspective, Millis's scaling theory can be viewed as a simple truncation of the effective average action $\Gamma_R^\Lambda[\phi]$ evolving from $\mathcal{S}[\phi]$, namely,

$$\Gamma_R^\Lambda[\phi] = \Gamma^{(0)\Lambda} + \sum_q \phi(-q)\left[A^\Lambda\mathbf{q}^2 + Z^\Lambda\frac{|q_0|}{|\mathbf{q}|^{z-2}}\right]\phi(q) + \sum_x U_{\mathrm{loc}}^\Lambda[\phi(x)], \tag{134}$$

where

$$U_{\mathrm{loc}}^\Lambda(\phi) = r^\Lambda\phi^2 + u^\Lambda\phi^4, \tag{135}$$

and Λ parametrizes a mixed momentum and frequency cutoff. The flow equations for the parameters in Eq. (134) are obtained by inserting $\Gamma_R^\Lambda[\phi]$ in the exact functional flow equation (91) and comparing coefficients. Because of the local form of the ϕ^4 interaction, the self-energy is momentum and frequency independent such that the parameters A^Λ and Z^Λ remain invariant. The flow of u^Λ, which is driven by a contribution of order $(u^\Lambda)^2$, is important only in the marginal case $d + z = 4$ and near the thermal phase transition at $T_c > 0$. Hence, most of Millis's results on the region around the QCP in the phase diagram are based on an analysis of the flow of r^Λ and the thermodynamic potential $\Omega^\Lambda = T\Gamma^{(0)\Lambda}$ [for a review, see von Loehneysen *et al.* (2007)].

Various extensions of Millis's analysis were derived within the functional RG framework. In particular, an extension to the symmetry-broken phase was formulated, for cases where the broken symmetry is *discrete* and does not gap out the fermionic excitations (Jakubczyk *et al.*, 2008). One such case is a nematic transition driven by a Pomeranchuk instability of interacting electrons on a lattice, where the discrete point-group symmetry of the lattice is spontaneously broken (Fradkin *et al.*, 2010). The symmetry-broken regime was described by the ansatz (134) for $\Gamma_R^\Lambda[\phi]$, with a quartic local potential which has a minimum away from zero:

$$U_{\mathrm{loc}}^\Lambda(\phi) = u^\Lambda[\phi^2 - (\phi_0^\Lambda)^2]^2. \tag{136}$$

The resulting flow equations were used to compute T_c and the Ginzburg temperature $T_G^<$ below T_c as a function of the control parameter r. To access the non-Gaussian thermal critical regime near T_c, it is crucial to take the flow of the quartic coupling u^Λ into account. The parameters A^Λ and Z^Λ are now scale dependent, too. While Z^Λ remains almost invariant, the flow of A^Λ is important near T_c and gives rise to an anomalous scaling dimension. A main result of the calculation was that the leading r dependence of T_c is the same as that of the Ginzburg temperatures below and above T_c (the latter was calculated by Millis, 1993), but a fairly large Ginzburg region opens in two dimensions (Jakubczyk *et al.*, 2008; Bauer, Jakubczyk, and Metzner, 2011).

In another extension a ϕ^6 interaction was included in U_{loc}^Λ to study a possible change of the order of the transition by

fluctuations (Jakubczyk, 2009), as well as quantum tricritical points in metals (Jakubczyk, Bauer, and Metzner, 2010).

Note that the extensions mentioned above are based on perturbative truncations resulting in flow equations with few running couplings, which could also have been obtained by more conventional RG methods.

B. Full potential flow

We now review an application to a problem where the effective action cannot be truncated at any finite order in ϕ, such that the possibility to make nonperturbative truncations becomes crucial (Jakubczyk, Metzner, and Yamase, 2009).

The problem arises when asking how a nematic transition caused by a d-wave Pomeranchuk instability in two dimensions is affected by fluctuations. Such a transition can be modeled by tight-binding electrons on a square lattice with an attractive d-wave forward scattering interaction (Metzner, Rohe, and Andergassen, 2003):

$$H = \sum_{\mathbf{k}} \epsilon_{\mathbf{k}} n_{\mathbf{k}} + \frac{1}{2L} \sum_{\mathbf{k},\mathbf{k}',\mathbf{q}} f_{\mathbf{k}\mathbf{k}'}(\mathbf{q}) n_{\mathbf{k}}(\mathbf{q}) n_{\mathbf{k}'}(-\mathbf{q}), \tag{137}$$

where $n_{\mathbf{k}}(\mathbf{q}) = \sum_{\sigma} c^{\dagger}_{\mathbf{k}-\mathbf{q}/2,\sigma} c_{\mathbf{k}+\mathbf{q}/2,\sigma}$ and L is the number of lattice sites. The interaction has the form

$$f_{\mathbf{k}\mathbf{k}'}(\mathbf{q}) = -g(\mathbf{q}) d_{\mathbf{k}} d_{\mathbf{k}'}, \tag{138}$$

where $d_{\mathbf{k}} = \cos k_x - \cos k_y$ is a form factor with $d_{x^2-y^2}$ symmetry. The coupling function $g(\mathbf{q}) \geq 0$ has a maximum at $\mathbf{q} = \mathbf{0}$ and is restricted to small momentum transfers by a cutoff Λ_0. For sufficiently large $g = g(\mathbf{0})$ the interaction drives a d-wave Pomeranchuk instability leading to a nematic state with broken orientation symmetry, which can be described by the order parameter

$$\phi = \frac{g}{L} \sum_{\mathbf{k}} d_{\mathbf{k}} \langle n_{\mathbf{k}} \rangle. \tag{139}$$

In the plane spanned by the chemical potential and temperature a nematic phase is formed below a dome-shaped transition line $T_c(\mu)$ with a maximal transition temperature near van Hove filling. In mean-field theory, the phase transition is usually first order near the edges of the transition line, that is, where T_c is relatively low, and second order at the roof of the dome (Kee, Kim, and Chung, 2003; Khavkine *et al.*, 2004; Yamase, Oganesyan, and Metzner, 2005).

Introducing an order parameter field via a Hubbard-Stratonovich transformation, integrating out the fermions, and keeping only the leading momentum and frequency dependences for small $\mathbf{q}$ and small $q_0/|\mathbf{q}|$ leads to a Hertz-type action $\mathcal{S}[\phi]$ of the form (132), with $z = 3$ and a local potential given by the mean-field potential

$$U_{\mathrm{loc}}(\phi) = \frac{\phi^2}{2g} - \frac{2T}{L} \sum_{\mathbf{k}} \ln(1 + e^{-(\epsilon_{\mathbf{k}} - \phi d_{\mathbf{k}} - \mu)/T}). \tag{140}$$

At low temperatures, the coefficients of a Landau expansion of $U_{\mathrm{loc}}(\phi)$ in powers of the field, $U(\phi) = a_0 + a_2\phi^2 + a_4\phi^4 + \cdots$, are typically negative for all exponents $2m \geq 4$. Hence, $\mathcal{S}[\phi]$ and consequently also the effective action $\Gamma_R^{\Lambda}[\phi]$ cannot be truncated at any finite order in ϕ. Fortunately, for bosonic fields the functional RG allows also for nonperturbative approximations, where one expands only in gradients, and not in powers of ϕ (Berges, Tetradis, and Wetterich, 2002). In particular, one can use the ansatz (134) for $\Gamma_R^{\Lambda}[\phi]$ without expanding the local potential $U_{\mathrm{loc}}^{\Lambda}(\phi)$. The flow of $U_{\mathrm{loc}}^{\Lambda}(\phi)$ is then determined by a *partial* differential equation which contains a second derivative of the potential with respect to ϕ.

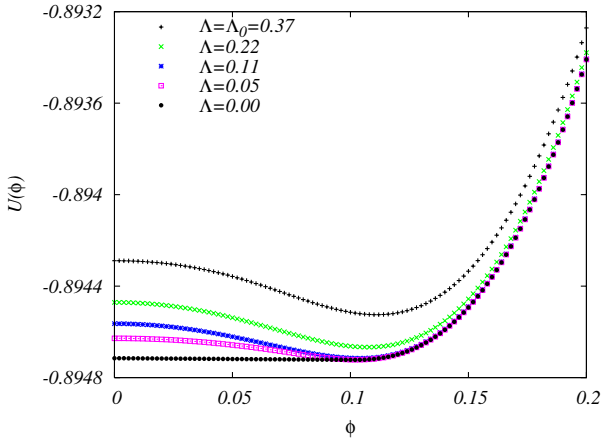

FIG. 15 (color online). Flowing effective potential $U_{\mathrm{loc}}^{\Lambda}(\phi)$ for various values of Λ between $\Lambda_0 = e^{-1}$ and 0, at $\mu = -0.78$ and $T = 0.05$. From Jakubczyk, Metzner, and Yamase, 2009.

In Fig. 15 an exemplary plot of the evolution of the flowing effective potential $U_{\mathrm{loc}}^{\Lambda}(\phi)$ is shown for Λ ranging from the ultraviolet cutoff $\Lambda_0 = e^{-1} \approx 0.37$ to the final value $\Lambda = 0$. The flow has been computed for electrons on a square lattice with nearest-neighbor hopping $t = 1$, next-to-nearest-neighbor hopping $t' = -\frac{1}{6}$, and a coupling strength $g = 0.8$. The initial (mean-field) potential has a minimum at $\phi_0 = 0.112$. The final potential exhibits spontaneous symmetry breaking with an order parameter $\phi_0 = 0.102$. Fluctuations shift ϕ_0 toward a slightly smaller value compared to the mean-field solutions. The flat shape of $U_{\mathrm{loc}}^{\Lambda}(\phi)$ for $\phi \leq \phi_0$ at $\Lambda = 0$ is imposed by the convexity property of the grand canonical potential.

The transition line between normal and symmetry-broken phases is shown in Fig. 16 for two choices of Λ_0. Compared to the corresponding mean-field result, the transition

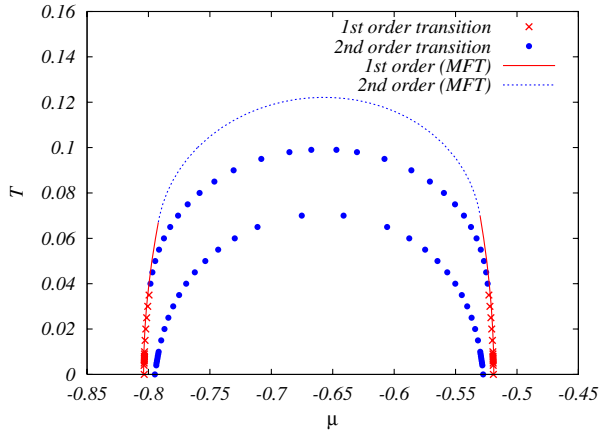

FIG. 16 (color online). Critical temperatures vs chemical potential for $\Lambda_0 = e^{-1}$ (larger dome with dots and crosses) and $\Lambda_0 = 1$ (smaller dome with dots). The mean-field transition line is also shown for comparison. From Jakubczyk, Metzner, and Yamase, 2009.

temperature is suppressed, with a larger reduction for larger Λ_0 (corresponding to a larger phase space for fluctuations). For $\Lambda_0 = 1$ the transition is continuous down to $T = 0$, leading to quantum critical points at the edges of the nematic dome. Increasing Λ_0 further (or reducing g), one may even eliminate the nematic phase completely from the phase diagram (Yamase, Jakubczyk, and Metzner, 2011).

C. Coupled flow of fermions and order parameter fluctuations

There are various systems where integrating out the electrons leads to an effective order parameter action with singular interactions which cannot be approximated by a local coupling (Belitz, Kirkpatrick, and Vojta, 2005; von Loehneysen *et al.*, 2007). In such cases it can be advantageous to keep the electrons in the action, treating the coupled system consisting of electrons and their order parameter fluctuations. Several coupled boson-fermion systems exhibiting quantum criticality have already been analyzed by various methods; see, e.g., Vojta, Zhang, and Sachdev (2000), Belitz *et al.* (2001a, 2001b), Abanov, Chubukov, and Schmalian (2003), Rech, Pepin, and Chubukov (2006), Huh and Sachdev (2008), Kaul and Sachdev (2008), and Metlitski and Sachdev (2010a, 2010b). The interplay of bosonic and fermionic infrared singularities at the quantum critical point poses an interesting problem.

The functional RG for coupled bosons and fermions described in Sec. II.G provides a suitable framework to study such problems. So far, it has not been applied to quantum phase transitions in metallic electron systems. However, encouraging works on relativistic field-theoretic models with gapless bosons and fermions have already appeared. For example, functional RG flow equations have been used to study the Gross-Neveu model (Rosa, Vitale, and Wetterich, 2001), quantum electrodynamics (Gies and Jaeckel, 2004), and supersymmetric Wess-Zumino models (Gies, Synatschke, and Wipf, 2009). In the context of condensed matter physics, a toy model for a semimetal-to-superfluid quantum phase transition has been studied by coupled flow equations for the electrons and the superfluid order parameter (Strack, Takei, and Metzner, 2010; Obert, Takei, and Metzner, 2011). In dimensions $d < 3$ the fermions and the order parameter fluctuations acquire anomalous scaling dimensions at the QCP of that model, leading to non-Fermi-liquid behavior and non-Gaussian criticality.

It will be interesting to devise suitable truncations of the coupled boson-fermion flow equations for magnetic and nematic quantum phase transitions in low-dimensional metallic systems, where many open questions need to be clarified.

VI. CORRELATION EFFECTS IN QUANTUM WIRES AND QUANTUM DOTS

As our last application of the functional RG to correlated fermion systems we discuss many-body effects in quantum wires and dots. The focus is on transport through such systems which are coupled to two or more semi-infinite leads. While in many of the above applications it was crucial to devise an approximation scheme in which the flow of the two-particle vertex (the effective two-particle interaction) was properly described, in the ones reviewed in this section the physics is dominated by the flow of the self-energy. We start out with a brief discussion of quantum transport through a region containing correlations in Sec. VI.A. To study transport beyond the linear response regime the functional RG was recently extended to Fermi systems out of equilibrium. In Sec. VI.B we review the main steps of this generalization. After discussing the most elementary example of linear transport through an inhomogeneous correlated quantum wire, a chain with a single local impurity, in Secs. VI.C.1–VI.C.4, we show how the functional RG can be used (i) to describe transport on all energy scales for more complex setups (Sec. VI.C.5), (ii) to identify unconventional low-energy fixed points of such systems (Sec. VI.C.6), and (iii) to study finite bias nonequilibrium transport (Sec. VI.C.7). As an example of the application of the functional RG to quantum dots, in Sec. VI.D.2 we consider an interacting chain of only three lattice sites corresponding to a dot.

A. Quantum transport

Experimental progress has made it possible to measure transport through mesoscopic regions such as one-dimensional (1D) quantum wires of up to micrometer length and "zero-dimensional" quantum dots. The experiments provide evidence for correlation effects (Hanson *et al.*, 2007; Deshpande *et al.*, 2010).[2] It is a theoretical challenge to describe transport when correlations in the mesoscopic system are important. Usually the leads to which this correlated region is connected are modeled as noninteracting. A general formal expression in terms of Keldysh Green functions for the current I through an *interacting* system coupled to two leads (indices L, R) in the stationary state was presented by Meir and Wingreen (1992). For either specific models or applying certain approximations to the two-particle interaction for each channel ζ it can be brought into a Landauer-Büttiker type form (Landauer, 1957; Büttiker, 1986)

$$I_\zeta = \frac{1}{2\pi} \int \mathcal{T}_\zeta(\epsilon, T, V_b)[f_L(\epsilon) - f_R(\epsilon)]d\epsilon, \tag{141}$$

where we set $e = 1 = \hbar$ such that the conductance quantum per channel is given by $1/(2\pi)$. Here $\mathcal{T}_\zeta$ is an effective transmission probability, $V_b = \mu_L - \mu_R$ is the bias voltage, and $f_{L/R}$ are Fermi functions with the chemical potentials of the left and right leads $\mu_{L/R}$. For the transport through a noninteracting system $\mathcal{T}_\zeta$ is the single-particle transmission probability. The goal is to compute $\mathcal{T}_\zeta$ in the presence of correlations. Here truncations of the functional RG flow equations which lead to *frequency-independent* self-energies are considered. In this case using Eq. (141), with $\mathcal{T}_\zeta$ being proportional to the "contact-to-contact" matrix element of the (retarded) one-particle Green function does not present an additional approximation as current vertex corrections vanish (Oguri, 2001; Enss, 2005). In this approximation the

[2]Correlation effects in effectively 1D electronic systems are also studied using photoemission. For a recent review, see Grioni, Pons, and Frantzeskakis (2009).

two-particle interaction affects the transport only via the renormalized self-energy which acts as an additional, T and V_b dependent scattering potential on noninteracting electrons (Langer and Ambegaokar, 1961; Oguri, 2001). For the linear conductance $g_\zeta(T)$ the transmission probability enters only at zero bias $V_b = 0$,

$$g_\zeta(T) = \frac{1}{2\pi} \int \mathcal{T}_\zeta(\epsilon, T, 0)\left(-\frac{\partial f}{\partial \epsilon}\right) d\epsilon, \tag{142}$$

i.e., $\mathcal{T}_\zeta(\epsilon, T, 0)$ is an equilibrium property. At zero temperature Eq. (142) simplifies further to $g_\zeta(0) = \mathcal{T}_\zeta(\mu, 0, 0)/(2\pi)$.

B. Functional RG in nonequilibrium

Recently, the functional RG approach was extended to study steady-state nonequilibrium transport through quantum wires and dots in the presence of a finite bias voltage given by the difference of the chemical potentials of the left and right leads $V_b = \mu_L - \mu_R$ (Jakobs, 2003, 2010; Gezzi, Pruschke, and Meden, 2007; Jakobs, Meden, and Schoeller, 2007; Jakobs, Pletyukhov, and Schoeller, 2010a; Karrasch, 2010; Karrasch, Pletyukhov *et al.*, 2010). The basic idea behind this extension is the use of real-time or real frequency Green functions on the Keldysh contour (Rammer and Smith, 1986) instead of Matsubara Green functions. As usual in diagrammatic approaches based on Keldysh Green functions one assumes that the initial statistical operator does not contain any correlations (Rammer and Smith, 1986). One can then use either a functional integral formulation (Kamenev, 2004) of the nonequilibrium many-body problem (Gezzi, Pruschke, and Meden, 2007) or a purely diagrammatic approach (Jakobs, 2003; Jakobs, Meden, and Schoeller, 2007) to derive the same flow equations for the self-energy and higher-order vertex functions. Although the method allows one to work with two-time Green functions and to study transient dynamics, in the current implementation of the functional RG in nonequilibrium for fermions the system is assumed to be in the steady state. For interacting bosons functional RG was also used to study dynamics (Gasenzer and Pawlowski, 2008; Kloss and Kopietz, 2011). On a technical level and compared to the equilibrium Matsubara functional RG in the steady state the Keldysh structure only leads to an additional index (the so-called Keldysh index $\pm$ referring to the upper and lower branches of the Keldysh contour) to be added to the set of quantum numbers.

One of the main challenges of the nonequilibrium functional RG is to devise cutoff schemes which do not violate causality and general Kubo-Martin-Schwinger (KMS) relations (Jakobs, 2010; Jakobs, Pletyukhov, and Schoeller, 2010b) after truncation of the infinite hierarchy of flow equations. For a general cutoff fulfilling the requirements discussed in Sec. II.D it is guaranteed only that causality and KMS relations hold up to the truncation order, e.g., first order for the level-1 truncation. In fact, an infrared (real) frequency cutoff similar to Eq. (143) violates causality in second order (Jakobs, 2003; Gezzi, Pruschke, and Meden, 2007). Its breaking constitutes a severe problem as relations connecting the Keldysh contour matrix elements of the Green function cannot be used. In particular, one cannot rotate from the $G^{a,b}$ Green function, with Keldysh indices $a, b = \pm$, to retarded, advanced, and Keldysh Green functions as it is usually done (Rammer and Smith, 1986). The momentum cutoff scheme used in other sections of this review avoids this problem but is not suitable for models with broken translational invariance. We return to this issue and discuss appropriate cutoff schemes when reviewing applications of nonequilibrium functional RG to transport through wires in Sec. VI.C.7 and dots in Sec. VI.D.2.

Besides its ability to be applied to nonequilibrium problems the real-time (or real frequency) Keldysh functional RG has a distinct advantage even in equilibrium: The analytic continuation from Matsubara to real frequencies can be avoided. In fact, computing the real frequency dependence of observables obtained by a numerical solution of the Matsubara RG flow equations truncated on a level which includes a flowing two-particle vertex and self-energy of initially unknown frequency structure presents a formidable task (Karrasch *et al.*, 2008; Karrasch, Meden, and Schönhammer, 2010) as it is known from other imaginary time quantum many-body methods such as the quantum Monte Carlo technique. This advantage was utilized in the real-time functional RG study of the single-impurity Anderson model (Jakobs, 2010; Jakobs, Pletyukhov, and Schoeller, 2010a) in which a frequency-dependent two-particle vertex and self-energy (complete level-2 truncation) were kept [for the imaginary time analog of this study, see Sec. VI.D.1, Hedden *et al.* (2004), and Karrasch *et al.* (2008)], and can be expected to be useful also in functional RG studies of other models.

C. Impurities in Luttinger liquids

The metallic state of correlated fermions in one dimension is a non-Fermi liquid. It falls into the Luttinger liquid (LL) class (Haldane, 1980). This state of matter is characterized by a power-law decay of space-time correlation functions with interaction dependent exponents (Luttinger, 1963; Mattis and Lieb, 1965; Luther and Peschel, 1974; Mattis, 1974; Giamarchi, 2004; Schönhammer, 2005) and spin-charge separation (Dzyaloshinskii and Larkin, 1974; Meden and Schönhammer, 1992; Voit, 1993). In particular, after Fourier transforming, the $2k_F$ component of the density-density response function shows a power-law divergence (Mattis, 1974; Apel and Rice, 1982) for repulsive interactions, instead of a logarithmic one for noninteracting electrons (Lindhard function in 1D). This indicates that any local inhomogeneity with a nonvanishing $2k_F$ component strongly affects the low-energy physics and thus the transport characteristics of a LL at low temperatures.

Perturbation theory is insufficient to describe the interaction effects as it fails to capture the RG flow of the inhomogeneity appearing even to first order in the interaction and higher-order diagrams diverge. As will become clear below the functional RG approach captures the impurity flow and does not require a simplified modeling of the inhomogeneity.

1. A single local impurity: The local sine-Gordon model

To understand the effect of a single impurity on the low-energy physics of a *spinless, infinite* LL (absence of

noninteracting leads), bosonization was used first [for a review of this method, see, e.g., von Delft and Schoeller (1998), Giamarchi (2004), and Schönhammer (2005)]. Within this approach the Fourier components of fermionic density operators are split into their chiral parts which obey Bose commutation relations in the low-energy subspace (Tomonaga, 1950). In this limit the kinetic energy and the two-particle interaction can be written as bilinears in these operators (Tomonaga, 1950), while a single-particle scattering impurity term generally takes a complicated form in the bosonic degrees of freedom. It simplifies if only the pure forward scattering $\tilde{V}(0)$ and backward scattering $\tilde{V}(2k_F)$ contributions are kept. Using bosonization to obtain results beyond this approximate modeling of the impurity is rather involved.

The forward scattering term is linear in the bosons and can easily be treated leading to a phase shift. This is irrelevant for the physics described in the following. The backward scattering term consists of the cosine of a local bosonic field and the resulting Hamiltonian is known from field theory as the local sine-Gordon (LSG) model. One can use either the exact Bethe ansatz solution (Fendley, Ludwig, and Saleur, 1995) of this model or a bosonic RG which is perturbative in $\tilde{V}(2k_F)$ (Kane and Fisher, 1992; Furusaki and Nagaosa, 1993a) to obtain analytical results. Alternatively numerical methods can be applied to the LSG model (Moon *et al.*, 1993; Egger and Grabert, 1995). This led to a complete picture of the RG scaling of $\tilde{V}(2k_F)$ which has direct consequences for the linear conductance. The RG flow connects two fixed points, the perfect chain fixed point with conductance $g = K/(2\pi)$ and the open chain fixed point with $g = 0$. In 1D spinless fermion systems only a single transport channel exists and we thus suppress the channel index ζ from now on. Here $K > 0$ denotes the so-called LL parameter which depends on the underlying model of the quantum wire and its parameters such as the strength and range of the two-particle interaction as well as the band filling. Independently of the model considered $K < 1$ for repulsive interactions and $K > 1$ for attractive ones, while the noninteracting case corresponds to $K = 1$. The corrections to the fixed-point conductances are power laws $s^{\gamma_{p/o}}$ with the infrared energy scale s (e.g., the temperature T or the energy cutoff Λ in a RG procedure). The exponents are *independent* of the bare impurity strength and given by $\gamma_p = 2(K - 1)$ and $\gamma_o = 2(1/K - 1)$, respectively. The sign of the scaling exponents implies that the open chain fixed point is stable for repulsive interactions and unstable for attractive ones. The opposite holds for the perfect chain fixed point. These insights confirmed earlier indications that impurities with a backscattering component strongly alter the low-energy physics of LLs with repulsive interactions (Mattis, 1974; Apel and Rice, 1982). The behavior can be summarized by saying that even a weak single impurity grows and eventually cuts the chain into two parts with open boundary conditions at the end points.

The exponent γ_o characterizing (for repulsive two-particle interactions) the suppression of g on small scales is twice the scaling exponent of the local single-particle spectral function of a LL close to an open boundary. This can be understood by viewing transport across the impurity as an end-to-end tunneling between two semi-infinite LLs [see, e.g., Kane and Fisher (1992)].

Bosonization was not only used for an infinite LL wire but also for the experimentally more relevant case in which an interacting wire containing a single impurity is contacted to two semi-infinite noninteracting leads. Contacts generically lead to single-particle backscattering and thus have an effect similar to the impurity. To disentangle the effect of the contacts and the impurity one often models the contacts such that they do not lead to any backscattering. In this case and in the absence of the impurity the conductance takes the maximal value $1/(2\pi)$ [instead of $K/(2\pi)$ for an infinite LL]. Using bosonization this can be achieved either within the so-called local Luttinger liquid picture (Maslov and Stone, 1995; Ponomarenko, 1995; Safi and Schulz, 1995; Janzen, Meden, and Schönhammer, 2006) or by appropriate boundary conditions for the bosonic fields (Egger and Grabert, 1997; Egger *et al.*, 2000). The fixed points and scaling exponents turned out to be the same as in the LSG model.

For weak two-particle interactions the problem of a single impurity in a LL was also studied using a fermionic RG (Matveev, Yue, and Glazman, 1993; Yue, Glazman, and Matveev, 1994). In this approach a flow equation for the transmission coefficient at k_F is derived using poor man's RG. An extension of this method to interactions of arbitrary strength was presented by Aristov and Wölfle (2008, 2009).

Remarkably, no intermediate fixed points appear within the LSG model and the crossover between the perfect and open chain is characterized by a one-parameter scaling function (Kane and Fisher, 1992; Moon *et al.*, 1993; Fendley, Ludwig, and Saleur, 1995; Egger *et al.*, 2000). In one spatial dimension a general impurity can be described by matrix elements $V_{k,k'}$ [only $V_{k_F,-k_F} = \tilde{V}(2k_F)$ is kept in the LSG model]. The RG analysis for such an impurity involves the coupling of all matrix elements $V_{k,k'}$ in the flow and one might wonder if this leads to an intermediate fixed point absent in the LSG model. To lowest order in the impurity strength the flow of $V_{k_F,-k_F}$ upon lowering the cutoff Λ is driven by $V_{k_F,-k_F}$ itself (see the next section). For repulsive two-particle interactions $V_{k_F,-k_F}$ increases and the perturbative RG breaks down. Now the other couplings, absent in the LSG model, might become relevant and eventually cut off the flow of $V_{k_F,-k_F}$ to large values, that is toward the open chain fixed point. That this does not happen can nicely be revealed within a functional RG approach. Before reviewing how this question was approached (see Sec. VI.C.4) we first present the most elementary functional RG flow equation to tackle inhomogeneous LLs and analytically show that it leads to the scaling behavior known from bosonization in the limit of weak impurities.

2. The functional RG approach to the single-impurity problem

As in the previous applications because of the necessary truncations the functional RG can be used only for small to intermediate two-particle interactions. For the application to inhomogeneous LLs it is crucial that it is nonperturbative in the single-particle inhomogeneity. Here the focus is on a description in which the RG flow and the interaction dependent exponents characterizing the physics close to fixed points are kept at least to leading order in the interaction. Following the discussion in the last paragraph of the

preceding section the feedback of the impurity into the flow of the self-energy dominates the physics to be studied. It is thus advantageous to use the one-particle irreducible functional RG scheme in which the full propagator including the self-energy appears on the right-hand side of the flow equations. For spinless fermions in a *homogeneous* wire the electron-electron interaction is renormalized only by a finite amount of order interaction squared (Sólyom, 1979). A single impurity does not alter this. To obtain the fixed-point value of the effective interaction to leading order one can therefore replace the flowing two-particle vertex by the antisymmetrized bare interaction corresponding to the level-1 truncation introduced in Sec. II.C.2. An improvement which includes the flow of the static two-particle vertex is reviewed in Sec. VI.C.4. After presenting the most elementary functional RG flow equation for the self-energy we show that it leads to the correct scaling properties for a weak impurity.

As one deals with systems in which translational invariance is broken it is advantageous to introduce the infrared cutoff Λ in *frequency* space. To set up the functional RG flow equations for the self-energy the propagator G_0 of the noninteracting Hamiltonian H_0 containing only the kinetic energy is replaced by $G_0^\Lambda(i\omega_n) = \Theta^\Lambda(\omega_n)G_0(i\omega_n)$ with a function Θ^Λ which is unity for $|\omega_n| \gg \Lambda$ and vanishes for $|\omega_n| \ll \Lambda$. More specifically,

$$\Theta^\Lambda(\omega_n) = \begin{cases} 0, & |\omega_n| \le \Lambda - \pi T, \\ \frac{1}{2} + \frac{|\omega_n|-\Lambda}{2\pi T}, & \Lambda - \pi T \le |\omega_n| \le \Lambda + \pi T, \\ 1, & |\omega_n| \ge \Lambda + \pi T, \end{cases} \tag{143}$$

was used (Enss *et al.*, 2005), where Λ starts at ∞ and goes down to 0.[3] For $T \to 0$, Θ^Λ becomes a sharp Θ function and Matsubara frequencies with $|\omega| < \Lambda$ are suppressed.

In this section a general continuum or lattice model of spinless fermions is considered with one-particle states $|\alpha\rangle$, which in the following will be either local states $|x\rangle$, where $x = j$ is the site index for the lattice model, with lattice constant $a = 1$, or momentum states $|k_n\rangle$ with $k_n = 2\pi n/L$. A general two-particle interaction Eq. (2) is assumed and an impurity term $V_{\rm imp} = \sum_{\alpha,\beta} V_{\alpha,\beta}\psi_\alpha^\dagger \psi_\beta$. The flow for the self-energy Eq. (50) in the level-1 truncation reads (Meden *et al.*, 2002)

$$\frac{d}{d\Lambda}\Sigma^\Lambda_{\alpha,\beta} = T\sum_{\omega_l} e^{i\omega_l 0^+} \sum_{\gamma,\delta} \Big\{ [1 - G_0^\Lambda(i\omega_l)\Sigma^\Lambda]^{-1} \times \frac{dG_0^\Lambda(i\omega_l)}{d\Lambda}[1 - \Sigma^\Lambda G_0^\Lambda(i\omega_l)]^{-1} \Big\}_{\delta,\gamma} U_{\alpha,\gamma,\beta,\delta}, \tag{144}$$

where G_0^Λ and Σ^Λ are matrices. The initial condition is given by $\Sigma^{\Lambda=\infty}_{\alpha,\beta} = V_{\alpha,\beta}$ and $U_{\alpha,\beta,\gamma,\delta}$ denotes the antisymmetrized bare two-particle vertex.

[3]A significant speedup of the numerical solution of the differential flow equations can be achieved using the alternative cutoff scheme discussed in the appendix of Andergassen *et al.* (2006).

At temperature $T = 0$ and applying Eq. (60) to products of Θ and δ functions, Eq. (144) simplifies to

$$\frac{d}{d\Lambda}\Sigma^\Lambda_{\alpha,\beta} = -\frac{1}{2\pi}\sum_{\omega=\pm\Lambda}\sum_{\gamma,\delta} U_{\alpha,\gamma,\beta,\delta}\tilde{G}^\Lambda_{\delta,\gamma}(i\omega)e^{i\omega 0^+}, \tag{145}$$

where

$$\tilde{G}^\Lambda(i\omega) = [Q_0(i\omega) - \Sigma^\Lambda]^{-1} \tag{146}$$

is the full propagator for the cutoff dependent self-energy and $Q_0 = (G_0)^{-1}$. The convergence factor $e^{i\omega 0^+}$ in Eq. (145) is relevant only for determining the flow from $\Lambda = \infty$ down to some arbitrarily large Λ_0. For Λ_0 much larger than the bandwidth this high energy part of the flow can be computed analytically leading to the initial condition $\Sigma^{\Lambda_0}_{\alpha,\beta} = V_{\alpha,\beta} + \sum_\gamma U_{\alpha,\gamma,\beta,\gamma}/2$.

Within the present scheme $\Sigma^\Lambda_{\alpha,\beta}$ is frequency independent and can be considered as a flowing effective impurity potential. To obtain an approximation for the Green function of the original cutoff free problem for arbitrary impurity parameters one has to determine the self-energy $\Sigma^\Lambda_{\alpha,\beta}$ at $\Lambda = 0$ by numerically solving the set of differential equations (144) or (145). To compute the right-hand side of the flow equations one has to invert the matrix Eq. (146), i.e., to solve the problem of a single particle moving in the effective scattering potential $\Sigma^\Lambda_{\alpha,\beta}$.

Because of the matrix inversion involved in calculating the right-hand side of Eq. (145) the flow equations can be solved analytically only in limiting cases, one being the situation of a weak impurity. One then works in momentum space and considers $\Sigma^\Lambda_{k,k'}$ for $k \ne k'$. The term linear in Σ^Λ presents the leading approximation in the expansion of $\tilde{G}^\Lambda$ on the right-hand side of Eq. (145) and one obtains (Meden *et al.*, 2002)

$$\frac{d}{d\Lambda}\Sigma^\Lambda_{k,k'} = -\frac{1}{2\pi}\sum_{k_1,k_2} U_{k,k_1,k',k_2}\Big[\frac{1}{i\Lambda - \xi_{k_2}}\Sigma^\Lambda_{k_2,k_1}\frac{1}{i\Lambda - \xi_{k_1}} + (\Lambda \to -\Lambda)\Big], \tag{147}$$

where $\xi_k = \epsilon_k - \mu$ with the one-particle dispersion ϵ_k. The antisymmetrized two-body matrix element U_{k,k_1,k',k_2} contains a momentum conserving Kronecker delta, where $k + k_1 = k' + k_2$ modulo the reciprocal lattice vector $2\pi n$ for the lattice model with $n = 0, \pm 1$, when the four momenta are in the first Brillouin zone. The umklapp processes $n = \pm 1$ involve low-energy excitations only for special fillings: half filling for the nearest-neighbor hopping model discussed later.

First models are considered for which umklapp processes are absent. To determine the backscattering properties of the self-energy one can put $k = k_F$ and $k' = -k_F - q$ with $|q| \ll k_F$. In order to read off the dominant behavior for small Λ the remaining summation variable is shifted $k_1 = -k_F + \tilde{k}_1$

$$\frac{d}{d\Lambda}\Sigma^{\Lambda}_{k_F,-k_F-q} = -\frac{1}{2\pi}\sum_{\tilde{k}_1} U_{k_F,-k_F+\tilde{k}_1,-k_F-q,k_F+q+\tilde{k}_1} \times\left[\frac{1}{i\Lambda-\xi_{k_F+q+\tilde{k}_1}}\Sigma^{\Lambda}_{k_F+q+\tilde{k}_1,-k_F+\tilde{k}_1}\frac{1}{i\Lambda-\xi_{-k_F+\tilde{k}_1}} + (\Lambda\rightarrow-\Lambda)\right]. \quad (148)$$

For $|\tilde{k}_1| \ll k_F$ one can linearize the dispersion $\xi_{-k_F+\tilde{k}_1} \approx -v_F\tilde{k}_1$ and $\xi_{k_F+q+\tilde{k}_1} \approx v_F(\tilde{k}_1+q)$, where v_F denotes the Fermi velocity. In the thermodynamic limit the two G_0 factors for $q=0$ and $\Lambda\rightarrow 0$ are proportional to $\delta(\tilde{k}_1)$. If only the singular contributions are kept, the differential equation for $\Sigma^{\Lambda}_{k_F,-k_F}$ reads

$$\frac{d}{d\Lambda}\Sigma^{\Lambda}_{k_F,-k_F} = -\frac{\hat{U}_{k_F,-k_F,k_F,-k_F}}{2\pi v_F}\frac{1}{\Lambda}\Sigma^{\Lambda}_{k_F,-k_F}, \quad (149)$$

where $\hat{U}_{k_F,-k_F,k_F,-k_F} = LU_{k_F,-k_F,k_F,-k_F}$ is independent of the system size. For the continuum model $\hat{U}_{k_F,-k_F,k_F,-k_F} = \tilde{U}(0)-\tilde{U}(2k_F)$, where $\tilde{U}(k)$ is the Fourier transform of the two-particle potential $U(x-x')$. This leads to the scaling relation

$$\Sigma^{\Lambda}_{k_F,-k_F} \sim \left(\frac{1}{\Lambda}\right)^{\hat{U}_{k_F,-k_F,k_F,-k_F}/(2\pi v_F)}. \quad (150)$$

As Eq. (149) was derived by expanding the Green function G^{Λ} in powers of the self-energy, the scaling behavior Eq. (150) can be trusted only as long as Σ^{Λ} stays small. Thus a single-particle backscattering term is a relevant perturbation for repulsive interactions and an irrelevant one for attractive ones consistent with the bosonization result.

Equation (149) holds even in the half-filled band case for the nearest-neighbor hopping lattice model. The additional singular contribution due to umklapp scattering is proportional to $\hat{U}_{k_F,k_F,-k_F,-k_F}$ which vanishes because of the antisymmetry of the matrix element (Meden *et al.*, 2002).

Neglecting all interaction effects beyond the renormalization of the impurity potential and using the Born approximation the correction to the perfect chain conductance is given by the self-energy squared. The corresponding exponent $\hat{U}_{k_F,-k_F,k_F,-k_F}/\pi v_F$ agrees to leading order in the interaction (Schönhammer, 2005) with $\gamma_p = 2(K-1)$ obtained within bosonization.

The opposite limit of a weak link can be treated analytically as well leading to results consistent to those of the bosonization approach with an exponent characterizing the deviation from the open chain fixed-point conductance $g=0$ which agrees to leading order in the interaction with $\gamma_o = 2(1/K-1)$ (Meden *et al.*, 2002).

Next the numerical solution of the RG flow for a specific lattice model with arbitrary impurity strength is discussed. This allows us to address the question of additional fixed points.

3. Basic wire model

In the following the tight-binding model of spinless fermions with nearest-neighbor interaction supplemented by an impurity is considered. The Hamiltonian is given by $H = H_{\mathrm{kin}} + H_{\mathrm{int}} + H_{\mathrm{imp}}$ with kinetic energy

$$H_{\mathrm{kin}} = -\sum_{j=-\infty}^{\infty}(c^{\dagger}_{j+1}c_j + c^{\dagger}_j c_{j+1}), \quad (151)$$

where $c^{\dagger}_j$ and c_j are the creation and annihilation operators on site j, respectively. The corresponding noninteracting dispersion is $\epsilon_k = -2\cos k$. The interaction is restricted to electrons on N neighboring sites (Enss *et al.*, 2005)

$$H_{\mathrm{int}} = \sum_{j=1}^{N-1} U_{j,j+1}[n_j-\nu(n,U)][n_{j+1}-\nu(n,U)], \quad (152)$$

with the local density operator $n_j = c^{\dagger}_j c_j$. The two regions of the lattice with $j<1$ and $j>N$ constitute the semi-infinite noninteracting leads. To model contacts which do not lead to single-particle backscattering the interaction $U_{j,j+1}$ between electrons on sites j and $j+1$ is allowed to depend on the position. A conductance $g = 1/(2\pi)$ in the absence of single-particle impurities is only achieved if $U_{j,j+1}$ is taken as a smoothly increasing function of j starting form zero at the bond (1, 2) and approaching a constant bulk value U over a sufficiently large number of bonds. Equally, the $U_{j,j+1}$ are switched off close to the bond $(N-1,N)$. The results are independent of the shape of the envelope function as long as it is sufficiently smooth. An abrupt two-particle inhomogeneity acts similarly to a single-particle impurity. A detailed discussion on the effect of the spatial variation of the two-particle interaction was presented by Meden and Schollwöck (2003a) and Janzen, Meden, and Schönhammer (2006).

In Eq. (152) the density n_j is shifted by a parameter $\nu(n,U)$, which depends on the filling factor n and the bulk interaction U. This is equivalent to introducing an additional one-particle potential which can compensate the Hartree potential in the bulk of the interacting wire. In the half-filled band case $\nu(1/2,U) = 1/2$ Enss *et al.*, 2005.

The general form of the impurity part of the Hamiltonian is

$$H_{\mathrm{imp}} = \sum_{j,j'} V_{j,j'}c^{\dagger}_j c_{j'}, \quad (153)$$

where $V_{j,j'}$ is a static potential. Site impurities are given by $V_{j,j'} = V_j\delta_{j,j'}$. For a single site impurity $V_j = V\delta_{j,j_0}$, j_0 is chosen to be far away from both leads. Impurities close to the contacts were discussed by Furusaki and Nagaosa (1996) and Enss *et al.* (2005). Resonant tunneling can be studied considering two site impurities of strengths V_l and V_r on the sites $\tilde{j}_l = j_l - 1$ and $\tilde{j}_r = j_r + 1$. The N_D sites between j_l and j_r define a quantum dot. The effect of a gate voltage restricted to the dot region is described by a constant V_g on sites j_l to j_r. This situation is sketched in Fig. 17. Hopping impurities are achieved setting $V_{j,j'} = V_{j',j} = -t_{j,j+1}\delta_{j',j+1}$. For the special case of a single hopping impurity, $t_{j,j+1} = (t'-1)\delta_{j,j_0}$, the unit hopping amplitude is replaced by t' on the bond linking

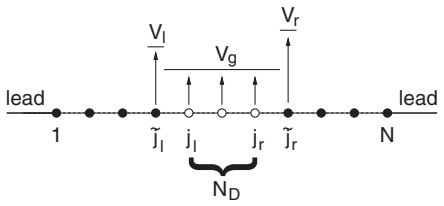

FIG. 17. Schematic plot of the quantum dot situation, where the barriers are modeled by two site impurities. From Enss *et al.*, 2005.

the sites j_0 and j_0+1. In the double-barrier problem a hopping t_l across the bond $(\tilde{j}_l, j_l)$ and t_r across $(j_r, \tilde{j}_r)$ is considered.

The homogeneous model $H = H_{\rm kin} + H_{\rm int}$ with a constant interaction U across *all bonds*, not only the ones within $[1, N]$, can be solved exactly by the Bethe ansatz and K is determined by a system of coupled integral equations (Haldane, 1980). In the half-filled case they can be solved analytically leading to

$$K = \left[\frac{2}{\pi}\arccos\left(-\frac{U}{2}\right)\right]^{-1} \tag{154}$$

for $|U| \le 2$. At other fillings the integral equations can be solved numerically. The model shows LL behavior for all particle densities n and any interaction strength except at half filling for $|U| > 2$ where either phase separation sets in (for $U < -2$) or the system orders into a charge-density-wave state (for $U > 2$).

Because of the presence of the semi-infinite leads the direct calculation of the noninteracting propagator related to $H_{\rm kin} + H_{\rm imp}$ requires the inversion of an infinite matrix. Using a standard projection technique (Taylor, 2000) it can be reduced to the inversion of an $N \times N$ matrix. The leads then provide an additional ω_n-dependent diagonal one-particle potential on sites 1 and N (Enss *et al.*, 2005):

$$V^{\rm lead}_{j,j'}(i\omega_n) = \frac{i\omega_n+\mu}{2}\left(1-\sqrt{1-\frac{4}{(i\omega_n+\mu)^2}}\right) \times \delta_{j,j'}(\delta_{1,j}+\delta_{N,j}). \tag{155}$$

Since the interaction is only nonvanishing on the bonds between sites 1 and N, the problem including the semi-infinite leads is this way reduced to the problem of an N-site chain. In the functional RG it is then advantageous to replace the *projected* noninteracting propagator G_0 including the impurity by a cutoff dependent one (Enss *et al.*, 2005).

4. Numerical solution of improved flow equations

With a minor increase in the numerical effort one can go beyond Eq. (144) for the flow of the self-energy and include a Λ-dependent static interaction U^Λ (Andergassen *et al.*, 2004). Its flow equation is derived from the general one for the two-particle vertex Eq. (52) applying the following approximations: (i) The three-particle vertex is set to zero. (ii) All frequencies are set to zero. (iii) The feedback of the inhomogeneity on the flow of the interaction is neglected. (iv) The interaction is assumed to remain of nearest-neighbor form. Then U^Λ obeys a simple differential equation (Andergassen *et al.*, 2004),

$$\frac{d}{d\Lambda}U^\Lambda = h(\Lambda)(U^\Lambda)^2, \tag{156}$$

where the function $h(\Lambda)$ depends only on the cutoff Λ and the Fermi momentum k_F. The solution of the flow equation is lengthy for arbitrary fillings (Andergassen *et al.*, 2004) but has a simple form for half filling

$$U^\Lambda = \frac{U}{1+[\Lambda-(2+\Lambda^2)/\sqrt{4+\Lambda^2}]U/(2\pi)}. \tag{157}$$

These approximations are sufficient to correctly describe the RG flow of the two-particle vertex on the Fermi surface of the homogeneous system (Andergassen *et al.*, 2004) to second order, as it is usually done in the so-called g-ology method (Sólyom, 1979). For the inhomogeneous LLs the flow of the effective interaction leads to improved results for the scaling exponents.

Within these approximations and using the projection of the leads, the self-energy at $T \ge 0$ is a frequency-independent tridiagonal matrix in real space determined by the flow equation ($j, j\pm1 \in [1, N]$)

$$\begin{aligned}
\frac{\partial}{\partial\Lambda}\Sigma^\Lambda_{j,j} &= -\frac{1}{2\pi}\sum_{|\omega_n|\approx\Lambda}\sum_{r=\pm1} U^\Lambda_{j,j+r} \\
&\quad\times\left[\frac{1}{Q_0(i\omega_n)-\Theta^\Lambda(\omega_n)\Sigma^\Lambda}Q_0(i\omega_n)\right. \\
&\quad\left.\times\frac{1}{Q_0(i\omega_n)-\Theta^\Lambda(\omega_n)\Sigma^\Lambda}\right]_{j+r,j+r}, \\
\frac{\partial}{\partial\Lambda}\Sigma^\Lambda_{j,j\pm1} &= \frac{1}{2\pi}\sum_{|\omega_n|\approx\Lambda} U^\Lambda_{j,j\pm1} \\
&\quad\times\left[\frac{1}{Q_0(i\omega_n)-\Theta^\Lambda(\omega_n)\Sigma^\Lambda}Q_0(i\omega_n)\right. \\
&\quad\left.\times\frac{1}{Q_0(i\omega_n)-\Theta^\Lambda(\omega_n)\Sigma^\Lambda}\right]_{j,j\pm1},
\end{aligned} \tag{158}$$

where the matrix $Q_0 = (G_0)^{-1}$ is the inverse of the projected noninteracting propagator with impurity. The symbol $|\omega_n| \approx \Lambda$ stands for taking the positive as well as negative frequency with absolute value closest to Λ.[4] The initial conditions for Σ at $\Lambda = \Lambda_0 \to \infty$ are independent of the precise realization of the inhomogeneity and read $\Sigma^{\Lambda_0}_{j,j} = [1/2 - \nu(n,U)]\times(U_{j-1,j}+U_{j,j+1})$ and $\Sigma^{\Lambda_0}_{j,j\pm1} = 0$. The frequency dependence of the self-energy which appears in the exact solution in order U^2 is not captured by this scheme. Thus only the leading order is completely kept in the flow of Σ.

The coupled flow equations can be solved numerically by an algorithm which approximately scales as N (Andergassen *et al.*, 2004). Typically systems of 10^4 lattice sites were considered, roughly corresponding to the length of quantum wires accessible to transport experiments. For the interacting wire of finite length the energy scale $\delta_N = v_F/N$ forms a cutoff for any RG flow. The flowing self-energy Eq. (158) depends on the three scales T, δ_N, and Λ. Saturation of Σ^Λ

[4]To achieve this result the cutoff scheme discussed in the appendix of Andergassen *et al.* (2006) was used.

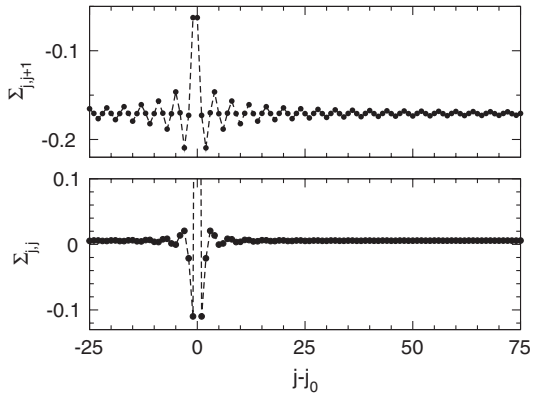

FIG. 18. Self-energy near a site impurity of strength $V = 1.5$ filling $n = 1/4$, and interaction $U = 1$; the impurity is located at $j_0 = 513$ with $N = 1025$ sites. From Andergassen *et al.*, 2004.

for $\Lambda \lesssim T$ or $\Lambda \lesssim \delta_N$ sets in "automatically" in contrast to more intuitive RG schemes in which the flowing couplings depend on Λ only and the flow is stopped "by hand" by replacing $\Lambda \to T$ or $\Lambda \to \delta_N$, respectively (Kane and Fisher, 1992; Yue, Glazman, and Matveev, 1994).

Figure 18 shows the self-energy Σ at the end of the RG flow, for $T = 0$ in the vicinity of a site impurity of intermediate strength. Both the on-site energy $\Sigma_{j,j}$ as well as the hopping $\Sigma_{j,j+1}$ become oscillatory functions with wave number $2k_F$ and a decaying amplitude. The asymptotic value of $\Sigma_{j,j+1}$ away from the impurity leads to a broadening of the band due to the interaction. A more detailed analysis of the oscillatory part $|\Delta\Sigma_{j,j+1}| = |\Sigma_{j,j+1} - \bar{\Sigma}_{\text{off}}|$, with the spatial average $\bar{\Sigma}_{\text{off}}$, for different $T > 0$ is presented in Fig. 19. The left panel shows that for $|j - j_0| \gtrsim 10$ it decays as $1/|j - j_0|$ up to a thermal length scale $\sim 1/T$ (provided $T > \delta_N$) beyond which the decay becomes exponential; see the right panel. For $U > 0$ this is the generic behavior for large bare impurities or on asymptotical large length scales. It is the scattering off such a long-ranged oscillatory potential, so-called Wigner–von Neumann potential (Reed and Simon, 1975), which leads to the power-law suppression of the conductance and the local

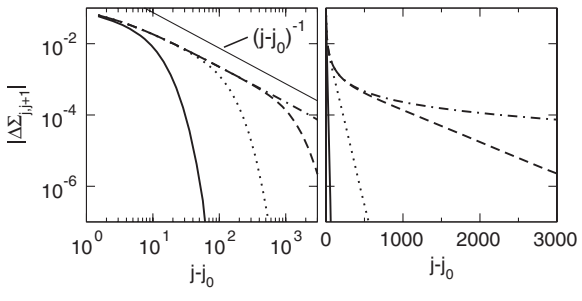

FIG. 19. Decay of the oscillatory part of the off-diagonal matrix element of the self-energy away from a single hopping impurity at bond j_0, $j_0 + 1$. Results for $t' = 0.1$, $j_0 = 5000$, $N = 10^4$, $U = 1$, $n = 1/2$, and different temperatures $T = 10^{-1}$ (solid line), $T = 10^{-2}$ (dotted line), $T = 10^{-3}$ (dashed line), and $T = 10^{-4}$ (dash-dotted line) are presented. The left panel shows the data on a log-log scale, and the right panel on a linear-log scale. For comparison the left panel contains a power law $(j - j_0)^{-1}$ (thin solid line). From Enss *et al.*, 2005.

spectral weight. One can analytically show that the amplitude of the asymptotic $1/|j - j_0|$ decay determines the exponent (Barnabé-Thériault *et al.*, 2005a). By virtue of the RG flow this amplitude, and thus the exponent, becomes independent of the impurity strength. For this reason first order perturbation theory fails. It also leads to an oscillatory self-energy which decays as $1/|j - j_0|$ but with an amplitude which depends on the bare impurity strength (Meden *et al.*, 2002) incorrectly leading to a power law with an impurity dependent exponent. The idea of an oscillatory decaying potential is similarly inherent to a poor man's fermionic RG approach (Yue, Glazman, and Matveev, 1994). Often these oscillations of the effective renormalized potential are referred to as Friedel oscillations. This is misleading as this term is reserved to the spatial oscillations of the *electron density*. In particular, in an inhomogeneous LL the effective potential decays as $|j - j_0|^{-1}$, while the density oscillations asymptotically decay as $|j - j_0|^{-K}$ (Egger and Grabert, 1995). The latter can also be shown within the functional RG formalism presented here (Andergassen *et al.*, 2004). The application of the self-consistent Hartree-Fock approximation leads to an oscillatory self-energy with a constant amplitude and thus to a charge-density-wave state (Meden *et al.*, 2002). This is an unphysical artifact of the approximation.

Using scattering theory (Enss *et al.*, 2005) one can show that the effective transmission $\mathcal{T}(\epsilon, T)$ is given by the $(1, N)$ matrix element of the single-particle Green function $\mathcal{T}(\epsilon_k, T) = 4\sin^2 k |\langle N|G(\epsilon_k + i0)|1\rangle|^2$. Via the T-dependent self-energy (see Fig. 19) G and thus $\mathcal{T}$ carries a temperature dependence. A typical example for the T dependence of the linear conductance $g(T)$ for a strong local impurity is shown as the solid line in Fig. 21. It clearly follows the expected power-law behavior for $\delta_N \lesssim T \ll B$ with the bandwidth $B = 4$. The T^{-1} scaling at larger T is a band effect. For $-0.5 \leq U \leq 1.5$ and fillings $n = 1/2$ as well as $1/4$, the exponent extracted (see lower panel of Fig. 21) agrees well with the one of the LSG model $\gamma_o = 2(1/K - 1)$, with K taken from the Bethe ansatz. Even for $U = 1.5$ the relative error is less than 5% [see Fig. 5 of Enss *et al.* (2005)]. Higher-order corrections in U present in the numerical solution of the flow equations (157) and (158) clearly improve the result over the one of the perturbative (in the impurity strength) analytical solution of Sec. VI.C.2 which yields a purely linear exponent. We emphasize that this improvement is not systematic as second- and higher-order terms are only partly kept in the RG. A similar agreement can be found for γ_p (Enss *et al.*, 2005).

Within the LSG model no intermediate fixed points appear which is reflected by one-parameter scaling $g = \tilde{g}_K(x)/2\pi$ with $x = (T/T_0)^{K-1}$ and a nonuniversal scale T_0 (Kane and Fisher, 1992; Moon *et al.*, 1993; Fendley, Ludwig, and Saleur, 1995; Egger *et al.*, 2000). For appropriately chosen T_0 data for different T and $\tilde{V}(2k_F)$ but fixed K can be collapsed onto the K-dependent scaling function $\tilde{g}_K(x)$. It has the limiting behavior $\tilde{g}_K(x) \propto 1 - x^2$ for $x \to 0$ and $\tilde{g}_K(x) \propto x^{-2/K}$ for $x \to \infty$. One can perform a similar scaling with data from the numerical solution of the flow equations for the microscopic lattice model considering different V and T as well as two sets of (U, n) leading to the same LL parameter (Enss *et al.*, 2005). The perfect collapse of the

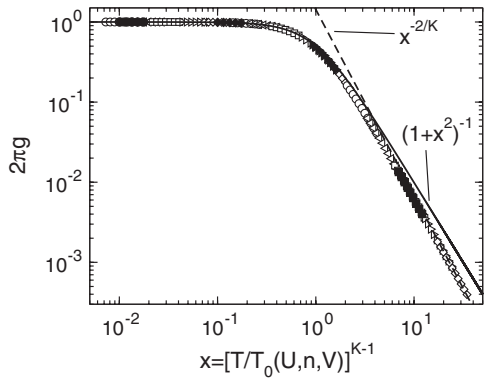

FIG. 20. One-parameter scaling plot of the conductance. Open symbols represent results obtained for $U = 0.5$, $n = 1/2$, and different T and V, while filled symbols were calculated for $U = 0.851$ and $n = 1/4$. Both pairs of U and n lead to the same $K = 0.85$ (within the present approximation). The solid line indicates the noninteracting scaling function $(1 + x^2)^{-1}$ and the dashed one the LSG model power-law decay with exponent $-2/K$. From Enss *et al.*, 2005.

data of Fig. 20 shows that the improved description of the impurity flow beyond the single amplitude approximation inherent to the LSG model does not lead to additional fixed points. The functional RG scaling function shows a sensible K dependence. The exponent of the large x power-law decay is smaller than the noninteracting one -2 (solid line at large x) and close to the LSG model exponent $-2/K$ shown as the dashed line in Fig. 20. This has to be contrasted to the K independent (noninteracting) scaling function $\tilde{g} = (1 + x^2)^{-1}$ resulting from the poor man's fermionic RG (Yue, Glazman, and Matveev, 1994), shown as the solid line in Fig. 20.

The functional RG results for a single local impurity in a LL show that the LSG model describes the physics (two fixed points, exponents, one-parameter scaling) of a broader class of models. The same approach was also used to study the persistent current through a LL ring with a local impurity pierced by a magnetic flux (Meden and Schollwöck, 2003a, 2003b; Gendiar, Krcmar, and Weyrauch, 2009). Aspects resulting from the *spin* degree of freedom of electrons were discussed by Andergassen, Enss, and Meden (2006) and Andergassen *et al.* (2006).

5. Resonant tunneling

We next review the results on resonant transport through a double barrier, defining an interacting quantum dot embedded in a LL (Enss *et al.*, 2005; Meden *et al.*, 2005). The setup is sketched in Fig. 17. The linear conductance g is characterized by a hierarchy of energy scales. The functional RG is a unique tool to access this problem as it provides reliable results on all scales. For a fixed dot size N_D and fixed barriers $V_{l/r}$ (or $t_{l/r}$) the dot can be tuned to resonance varying V_g. Only for symmetric dots with $V_l = V_r$ (or $t_l = t_r$) the peak conductance becomes "perfect" $g_p = 1/(2\pi)$. For asymmetric barriers a backscattering component of the single-particle inhomogeneity remains, leading to a reduced g_p. Because of the interaction backscattering grows during a RG procedure and on asymptotic scales the conductance vanishes with scaling exponent γ_o. The same holds away from resonance regardless of the ratio V_l/V_r (or t_l/t_r). Thus the noninteracting resonance of finite width either disappears (asymmetric barriers) or turns into a resonance of *zero width* (symmetric barriers). A rich T dependence is found on resonance and for symmetric barriers on which we now focus. Without loss of generality only site impurities are considered as barriers.

The functional RG procedure can directly be applied to the double-barrier problem. The dot parameters enter only via the noninteracting propagator. Figure 21 shows the peak conductance $g_p(T)$ for a dot with high barriers and two different dot sizes. The relevant energy scales B, $\delta_{N_D} = v_F/N_D$, $T^*_{N_D}$ (see below), and δ_N are indicated by the arrows. For $\delta_{N_D} \lesssim T$ the two barriers behave as independent impurities. Using scattering theory one can show that in this case g_p is obtained by adding the resistances of the two barriers (Enss *et al.*, 2005; Jakobs *et al.*, 2007). This explains why for $N_D = 100$, for which this temperature regime is clearly developed, $g_p(T)$ agrees to the solid line obtained by taking $g(T)/2$ of a single site impurity of equal height as used for the double barrier. Note that it is a nontrivial fact that in this temperature regime the individual resistances can be added to give the total resistance. In the presence of *inelastic processes* one would, of course, expect this result (resistors in series) but they are absent in the mesoscopic setup, the ones resulting from the electron-electron interaction are suppressed by the approximations. In fact, the case of three barriers constitutes an example for which adding resistances no longer holds (Jakobs *et al.*, 2007). For $T \lesssim \delta_{N_D}$ the width of $-\partial f/\partial \epsilon$ is smaller than δ_{N_D} and only the resonance peak around $\epsilon = 0$ of $\mathcal{T}(\epsilon, T)$ contributes to the integral in Eq. (142). The width w of this peak vanishes as $T^{\gamma_o/2}/N_D$ (Enss *et al.*, 2005) leading to $g_p(T) \propto T^{\gamma_o/2-1}$. The lower bound of this scaling regime, first discussed using bosonization (Furusaki and

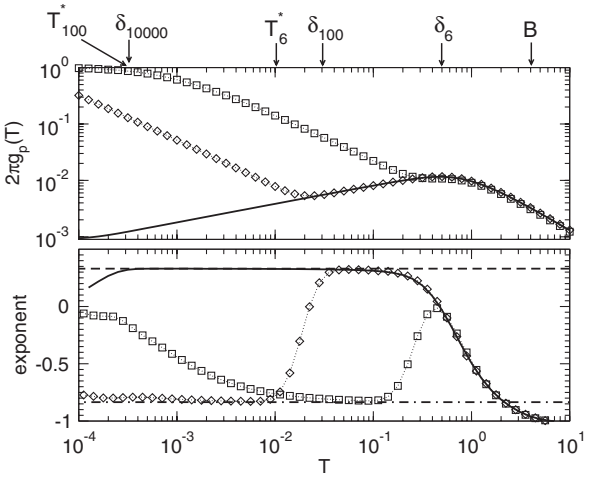

FIG. 21. Upper panel: $g_p(T)$ for $U = 0.5$, $N = 10^4$, $V_{l/r} = 10$, $n = 1/2$, and $N = 6$ (squares), 100 (diamonds). The arrows indicate the relevant energy scales B, δ_{N_D}, $T^*_{N_D}$, and δ_N. The solid curve shows $g(T)/2$ for a single barrier with $V = 10$ and $U = 0.5$, $N = 10^4$. Lower panel: Logarithmic derivative of the conductance. Dashed line: γ_o; dash-dotted line: $\gamma_o/2 - 1$. From Enss *et al.*, 2005.

Nagaosa, 1993b; Furusaki, 1998), is reached when $T = w$, i.e., at $T^*_{N_D} \propto N_D^{-1/(1-\gamma_o/2)}$. For $T < T^*_{N_D}$, $2\pi g_p$ approaches 1. For T reaching δ_N any power-law scaling in T with an interaction dependent exponent is cut off by the finite size of the interacting part of the quantum wire. In addition to identifying the different temperature regimes the functional RG approach allows one to (i) quantify the size of the crossover regime, typically half an order of magnitude, and to (ii) obtain results for "nonuniversal" regimes as, e.g., realized for $N_D = 6$ and $\delta_{N_D} < T \ll B$. For dots with weak barriers and sufficiently large N_D only the regime with scaling exponent $\gamma_o/2 - 1$ is realized and for weak barriers and small N_D none of the above power-law regimes emerges (Enss *et al.*, 2005; Meden *et al.*, 2005). Resonant transport in LLs was also studied by bosonization (Furusaki and Nagaosa, 1993b; Furusaki, 1998), poor man's fermionic RG (Nazarov and Glazman, 2003; Polyakov and Gornyi, 2003), and numerically (Hügle and Egger, 2004).

The temperature dependence of the peak conductance of resonant tunneling nicely exemplifies the fact that the functional RG approach provides sensible results on *all energy scales* even for problems with a hierarchy of scales. Other examples from this class are situations in which the wire-lead contacts are not modeled as being perfect (Jakobs *et al.*, 2007) and models in which the leads and contacts are described in a more realistic way (Wächter, Meden, and Schönhammer, 2009).

6. Y junctions

The power of the functional RG approach to uncover unconventional fixed points and the related interesting physics was exemplified by discussing a specific junction of three 1D wires, a so-called Y junction. The three LL wires (index $\nu = 1$, 2, and 3) each of length N and coupled to a noninteracting semi-infinite lead via a perfect contact are described by the basic model discussed in Sec. VI.C.3. The symmetric junction pierced by a magnetic flux ϕ is sketched in Fig. 22 and given by

$$H_Y = -t_Y \sum_{\nu=1}^{3} (c^\dagger_{1,\nu} c_{0,\nu} + \text{H.c.}) + V \sum_{\nu=1}^{3} n_{0,\nu} - t_\Delta \sum_{\nu=1}^{3} (e^{i\phi/3} c^\dagger_{0,\nu} c_{0,\nu+1} + \text{H.c.}), \tag{159}$$

where the wire indices 4 and 1 are identified. The junction is characterized by the three parameters t_Y, V, and t_Δ. Using scattering theory (Barnabé-Thériault *et al.*, 2005a, 2005b; Enss *et al.*, 2005), the $U = 0$ conductance from wire ν to wire ν' can be written as

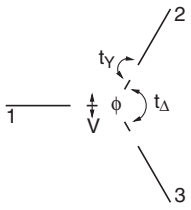

FIG. 22. Sketch of the symmetric Y-junction of three quantum wires Barnabé-Thériault *et al.*, 2005b.

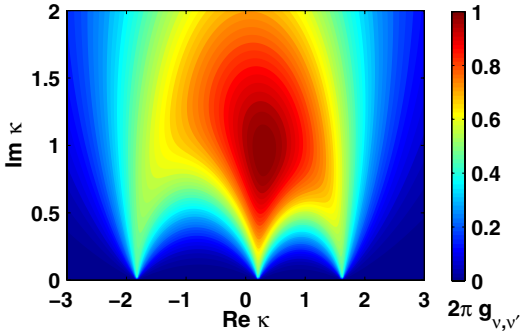

FIG. 23 (color online). The noninteracting conductance $2\pi g_{\nu,\nu'}$ (cyclic indices) as a function of the complex parameter κ which in turn is a function of the junction parameters t_Y, V, and t_Δ. The flux is $\phi = 0.4\pi$.

$$2\pi g_{\nu,\nu'} = \frac{4(\text{Im}\kappa)^2 |e^{-i\phi} - \kappa|^2}{|\kappa^3 - 3\kappa + 2\cos\phi|^2}, \tag{160}$$

with a single complex parameter $\kappa = (-V - t_Y^2 \hat{G}^0_{1,1})/|t_\Delta|$. The Green function $\hat{G}^0$ is obtained for one of the equivalent disconnected ($t_Y = 0$) wires and $\hat{G}^0_{1,1} \in \mathbb{C}$ denotes its diagonal matrix element taken at the first site $j = 1$. It is evaluated at energy $\epsilon + i0$ with $\epsilon \to 0$. Equation (160) holds if ν and ν' are in cyclic order and is independent of the wire pair considered; $g_{\nu',\nu}$ follows by replacing $\phi \to -\phi$. If ϕ does not correspond to an integer multiple of π and for generic junction parameters, the conductance from ν to ν' differs from the one with reversed indices indicating the breaking of time-reversal symmetry. This constitutes the most interesting situation and we focus on such fluxes. In Fig. 23 the conductance from wire ν to ν' (cyclic) for $\phi = 0.4\pi$ is shown for the upper half of the complex κ plane. For restored time-reversal symmetry the largest conductance allowed by the unitarity of the scattering matrix is $2\pi g_{\nu,\nu'} = 4/9$ (denoted the perfect junction value in the following); even for optimized parameters a reflection of $1/9$ is unavoidable.

For $U \neq 0$ the Y junction can straightforwardly be treated within the functional RG based approximation scheme (Barnabé-Thériault *et al.*, 2005b). Here we focus on $T = 0$. To compute the conductance from Eq. (160), $\hat{G}^0$ must be replaced by the auxiliary Green function $\hat{G}$ obtained by considering Σ (at the end of the RG flow for the full system) as an effective potential for a single disconnected wire setting $t_Y = 0$ (Barnabé-Thériault *et al.*, 2005b). Via the RG flow of Σ, $\hat{G}$ develops a dependence on (t_Y, t_Δ, and V) U and $\delta_N = v_F/N$. The latter energy scale is a natural infrared cutoff, in contrast to the flow parameter Λ which is artificial and sent to 0. A comprehensive picture of the low-energy physics is obtained from the dependence of κ on δ_N. In Fig. 24 each line is for a fixed set of junction parameters and δ_N as a variable. The flux is chosen as $\phi = 0.4\pi$ and the arrows indicate the direction of decreasing δ_N. As Imκ has the opposite sign of $\text{Im}\hat{G}_{1,1} < 0$ it is restricted to positive values.

Equation (160) allows for four distinguished conductance situations (see Fig. 23): (i) on the line Im$\kappa = 0$, $g_{\nu,\nu'} = g_{\nu',\nu} = 0$ for almost all Reκ; (ii) it is interrupted by three points having flux-dependent positions with the conductance

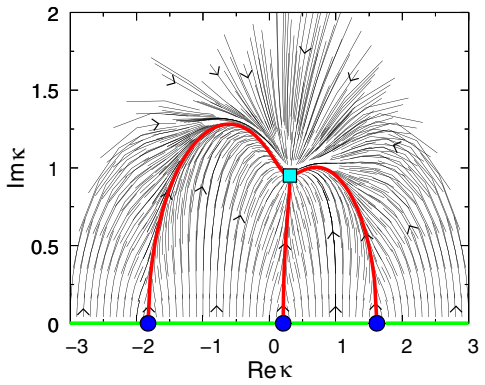

FIG. 24 (color online). Flow of κ for $U=-1$, $n=1/2$, and $\phi=0.4\pi$. Arrows indicate the direction for $U<0$. For $U>0$ it is reversed. For details, see text. From Barnabé-Thériault *et al.*, 2005b.

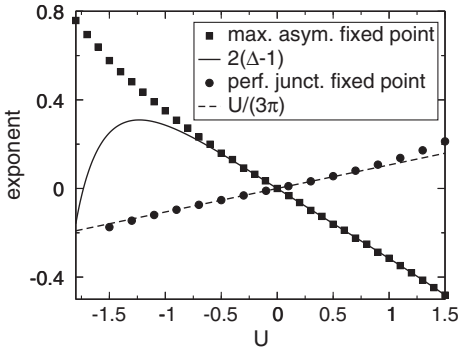

FIG. 25. Scaling exponents of the Y junction close to the fixed points. From Barnabé-Thériault *et al.*, 2005b.

$2\pi g_{\nu,\nu'}=2\pi g_{\nu',\nu}=4/9$; (iii) for a specific flux-dependent κ one finds $2\pi g_{\nu,\nu'}=1$ and $2\pi g_{\nu',\nu}=0$; and (iv) $g_{\nu,\nu'}=g_{\nu',\nu}=0$ is also reached for $|\kappa|\to\infty$. These are the fixed points of the RG flow as evident from Fig. 24. Situation (i) is an interrupted line of decoupled chain fixed points with vanishing conductances which is stable for $U>0$ and unstable in the opposite case. Analyzing the dependence of $g_{\nu,\nu'}$ on δ_N in its vicinity for different U one finds that the scaling exponent is independent of ϕ given by γ_o as obtained for the single impurity. Situation (ii) constitutes three perfect junction fixed points (circles in Fig. 24). For $U>0$ each of the three fixed points has a basin of attraction given by one of the three parts of the curve $\mathcal{C}(\phi)$ (thick curved line in Fig. 24 interrupted by the square) on which the reflection $1-2\pi g_{\nu,\nu'}-2\pi g_{\nu',\nu}$ takes a local minimum. The U dependence of the scaling exponent when approaching one of the fixed points along its corresponding line is shown in Fig. 25 (circles). It is independent of ϕ and for small $|U|$ it can be fitted by $U/3\pi$. These fixed points have not been found by any method which is based on bosonization and the exact dependence of their scaling exponent on K is presently unknown. Because of the factor $\frac{1}{3}$ in the leading order it must be different from the K dependence of any of the exponents discussed so far. (iii) The basins of attraction are separated by the maximal asymmetry fixed point (maximal breaking of time-reversal symmetry; square in Fig. 24). For $\phi=\pi/2$ this fixed point was identified by a bosonization based approach (Chamon, Oshikawa, and Affleck, 2003), and it was conjectured that the behavior found holds for all fluxes different from integer multiples of π. The functional RG results indeed confirm this, at least for small to intermediate $|U|$, as one finds this fixed point for all such ϕ and obtains a flux-independent scaling exponent which to leading order agrees with the bosonization result $\gamma_Y=2(\Delta-1)$ with $\Delta=4K/(3+K^2)$ (see Fig. 25). The bosonization exponent shows a nonmonotonic dependence on K and thus U, which the approximate functional RG approach does not capture. This implies that the maximal asymmetry fixed point is unstable for repulsive interactions, and stable for sufficiently small attractive ones but turns unstable again for larger attractive interactions. (iv) In the mapping of the complex plane onto the Riemann sphere the $g=\infty$ fixed point (north pole) is part of the projected line of decoupled chain fixed points and shows the same stability properties and scaling dimension.

The most interesting physics is associated with the perfect junction fixed points which for $U>0$ each have one stable direction. If the junction parameters of a noninteracting system at fixed $\phi\neq m\pi$, $m\in\mathbb{N}_0$ are chosen such that the resulting κ lies on $\mathcal{C}(\phi)$, but not on one of the three special points (ii), $g_{\nu,\nu'}\neq g_{\nu',\nu}$ and the conductance indicates the breaking of time-reversal symmetry as expected. Turning on an interaction $U>0$ the "fine-tuned" system flows to one of the perfect chain fixed points with equal perfect conductances $2\pi g_{\nu,\nu'}=4/9$ and $2\pi g_{\nu',\nu}=4/9$. Therefore, at small energy scales the junction conductance no longer indicates the explicit breaking of time-reversal symmetry. For generic junction parameters away from $\mathcal{C}(\phi)$ one finds related behavior. Close to the line of decoupled chain fixed points the relative difference $|g_{\nu,\nu'}-g_{\nu',\nu}|/(g_{\nu,\nu'}+g_{\nu',\nu})$ scales as a power law in δ_N with an exponent given by $\gamma_o/2$ and thus vanishes if $U>0$. This implies that $g_{\nu,\nu'}$ and $g_{\nu',\nu}$ become equal faster than they go to zero. In that sense for $U>0$ and up to the unstable maximal asymmetry fixed point, on small scales the conductance does not show the breaking of time-reversal symmetry, time-reversal symmetry is "restored" by the interaction.

Other types of junctions of an arbitrary number of LL wires were studied using functional RG (Barnabé-Thériault *et al.*, 2005a) as well as by the poor man's fermionic RG (Lal, Rao, and Sen, 2002; Aristov *et al.*, 2010) and bosonization based approaches (Nayak *et al.*, 1999; Chen, Trauzettel, and Egger, 2002).

7. Nonequilibrium transport through a contacted wire

Nonequilibrium functional RG was used to study a finite bias transport geometry with an impurity-free N site interacting wire contacted to two noninteracting semi-infinite leads by tunnel barriers modeled by reduced hopping matrix elements as introduced in Sec. VI.C.3: $t_{0,1}=(t_L-1)$ and $t_{N,N+1}=(t_R-1)$ (Jakobs, Meden, and Schoeller, 2007). In equilibrium this model features a local single-particle spectral function $\rho_j(\omega)$ which close to the chemical potential, in the vicinity of the contacts, and for repulsive interactions is suppressed: $\rho_j(\omega)\sim\omega^{\gamma_o}$ (Enss *et al.*, 2005). The linear conductance behaves as $g(T)\sim T^{\gamma_o}$ which can be understood from viewing transport as an end-to-end tunneling between a

LL and a Fermi-liquid lead and using the sum of two resistances as discussed in Sec. VI.C.5.

A cutoff scheme which conserves causality to any truncation order (Jakobs, 2010) is given by an imaginary frequency cutoff. The Fermi function of the two leads which can be written as a Matsubara sum

$$f_{L/R}(\omega) = [e^{\beta(\omega-\mu_{L/R})}+1]^{-1} = \beta^{-1}\sum_{\omega_n}\frac{e^{i\omega_n 0^+}}{i\omega_n-\omega+\mu_{L/R}} \tag{161}$$

is replaced by

$$f^{\Lambda}_{L/R}(\omega) = \beta^{-1}\sum_{\omega_n}\frac{\Theta(|\omega_n|-\Lambda)e^{i\omega_n 0^+}}{i\omega_n-\omega+\mu_{L/R}}. \tag{162}$$

Details of this procedure including a discussion of the initial conditions and its relation to the temperature flow scheme (Honerkamp and Salmhofer, 2001a) are presented by Jakobs (2010). Within the lowest-order truncation and after taking the equilibrium limit this cutoff implemented for Keldysh Green functions yields the same flow equations as the Matsubara functional RG with the frequency cutoff Eq. (143) (Jakobs, Meden, and Schoeller, 2007; Jakobs, 2010; Jakobs, Pletyukhov, and Schoeller, 2010b).

In the presence of a finite bias voltage the level-1 truncation scheme (bare two-particle vertex) with the cutoff procedure (162) was applied. As discussed in Sec. VI.C.2, in equilibrium this is sufficient to obtain scaling exponents correctly to leading order in U. For weak tunneling $\Gamma_{L/R} = \pi t^2_{L/R}\rho_0 \ll 1$, with ρ_0 the density of states of the disconnected, noninteracting leads taken at the last lattice site, the flow of the retarded nonequilibrium self-energy matrix $\Sigma^{\mathrm{ret},\Lambda}$ is given by a weighted sum of two equilibrium flows

$$\frac{d}{d\Lambda}\Sigma^{\mathrm{ret},\Lambda} = \sum_{\lambda=L,R}\frac{\Gamma_\lambda}{\Gamma_L+\Gamma_R}\left[\frac{d}{d\Lambda}\Sigma^{\mathrm{eq},\Lambda}\right]_{\mu=\mu_\lambda}, \tag{163}$$

where the terms inside the brackets on the right-hand side are given by Eq. (158) with the chemical potential set to μ_L or μ_R, respectively (and $U^\Lambda \to U$). As discussed in Sec. VI.C.4 each such term leads to an oscillatory slowly decaying self-energy originating at the inhomogeneity, the tunnel barriers in the present case, and extending into the interacting part of the wire. The two chemical potentials $\mu_{L/R}$ imply two different wave numbers $2k_F^{(L/R)}$. Because of the weighting factor $\Gamma_\lambda/(\Gamma_L+\Gamma_R)$ the amplitudes of the two superimposed decaying oscillations are generically different and depend on the strength of the bare inhomogeneity. The resulting nonequilibrium effect of two different and Γ_λ-dependent exponents characterizing the scaling of the spectral function close to μ_L and μ_R goes beyond the naive expectation that the bias voltage plays the role of an infrared cutoff scale only [see, e.g., Schoeller (2009)]. In Fig. 26 the local spectral function near the left contact and for a restricted energy range around $\mu_{L/R}$ is shown. Because of the finite temperature ($T = 10^{-4}$) and the finite size of the interacting wire ($N = 2\times 10^4$) the suppression at $\mu_{L/R}$ is incomplete (cut off by $\max\{T, \delta_N\}$), but the difference in the exponent is still apparent. A detailed analysis shows that the exponents at $\mu_{L/R}$ are given by

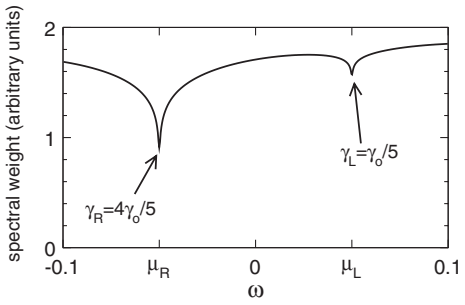

FIG. 26. Suppression of the local one-particle spectral weight as a function of energy near the left contact (at site 5) of an interacting wire driven out of equilibrium by a finite bias current. The parameters are $T = 10^{-4}$, $N = 2^4$, $U = 0.5$, $t_L = 0.075$, $t_R = 0.15$, and $\mu_{L/R} = \pm 0.05$. From Jakobs, Meden, and Schoeller, 2007.

$\gamma_{L/R} = \Gamma_{L/R}\gamma_o(\mu_{L/R})/(\Gamma_L+\Gamma_R)$, where the argument in the open boundary exponent γ_o indicates that it depends on the band filling and thus the chemical potential. After adding a third probe lead these nonuniversal exponents can be measured in a transport experiment (Jakobs, Meden, and Schoeller, 2007; Jakobs, 2010).

D. Quantum dots

A spatially confined system featuring a few energy levels is called a quantum dot. In a transport geometry the dot is coupled to at least two leads. Quantum dots show interesting physics if all relevant energy scales (e.g., level-lead couplings and T) are smaller than the level spacing of the isolated system. Because of the strong confinement the two-particle interaction on the dot cannot be neglected and leads to phenomena such as Coulomb blockade and the Kondo effect.

1. Spin fluctuations

In the Kondo regime the physics is dominated by *spin fluctuations*. The virtues and limitations of the functional RG approach to describe aspects of Kondo physics in and out of equilibrium were extensively studied within the single-impurity Anderson model and more complex variants of the latter (Hedden *et al.*, 2004; Andergassen, Enss, and Meden, 2006; Karrasch, Enss, and Meden, 2006; Meden and Marquardt, 2006; Gezzi, Pruschke, and Meden, 2007; Karrasch, Hecht, Weichselbaum, von Delft, *et al.*, 2007; Karrasch, Hecht, Weichselbaum, Oreg, *et al.*, 2007; Karrasch, Oguri, and Meden, 2008; Karrasch *et al.*, 2008; Weyrauch and Sibold, 2008; Xu, Gao, and Xiong, 2008, 2010; Bartosch *et al.*, 2009; Eichler *et al.*, 2009; Goldstein *et al.*, 2009; Karrasch and Meden, 2009; Kashcheyevs *et al.*, 2009; Isidori *et al.*, 2010; Jakobs, 2010; Jakobs, Pletyukhov, and Schoeller, 2010a; Karrasch, 2010; Schmidt and Wölfle, 2010). As the number of correlated degrees of freedom in quantum dots is small the static truncation used for LLs was extended to contain all second-order processes including a frequency-dependent two-particle vertex and self-energy, capturing the full real space as well as spin structure (Hedden *et al.*, 2004; Karrasch *et al.*, 2008; Jakobs, 2010; Jakobs, Pletyukhov, and Schoeller, 2010a; Karrasch, 2010; Karrasch, Pletyukhov *et al.*, 2010). In fact, the studies of the

single-impurity Anderson model constitute one of the rare examples of the functional RG approach to correlated Fermi systems using a complete level-2 truncation (even supplemented by parts of the six-point vertex through the replacement discussed in the second part of Sec. II.C.2). Including the frequency dependence clearly improves the results beyond bare perturbation theory of the same (that is second) order but it is presently not possible to reach the strong coupling regime in a controlled way. A discussion of the problems yet to be solved was presented by Karrasch *et al.* (2008), Karrasch, Pletyukhov *et al.* (2010), Karrasch (2010), Jakobs, Pletyukhov, and Schoeller (2010a), and Jakobs (2010). An alternative way to include the full frequency dependence was recently introduced for another impurity model by Schmidt and Enss (2011). In the following a simple quantum dot model dominated by charge fluctuations is discussed.

2. Charge fluctuations in nonequilibrium

The quantum dot model belongs to the class of spinless models introduced in Sec. VI.C.3. For a three site interacting chain ($N = 3$) with $U_{1,2} = U_L$ and $U_{2,3} = U_R$ two hopping impurities are located at bonds (1, 2) and (2, 3): $t_{1,2} = t_L - 1$, and $t_{2,3} = t_R - 1$. Lattice site 2 constitutes a single-level dot which can be adjusted in energy by a gate voltage V_g (see Fig. 17). An electron on this site interacts with lead electrons via a nearest-neighbor coupling $U_{L/R}$ which are otherwise noninteracting. Choosing $\nu = 1/2$ in Eq. (152), $V_g = 0$ corresponds to the particle-hole symmetric point with dot occupation $\langle n_2 \rangle = 1/2$. This model is a lattice realization of the interacting resonant level model (IRLM). The use of a variety of analytical as well as numerical methods led to a rather complete understanding of the physics of this model in equilibrium [see, e.g., Borda, Vladár, and Zawadowski (2007), and references therein]. In addition, the current under a finite bias voltage $\mu_L = V_b/2$ and $\mu_R = -V_b/2$ was investigated (Borda, Vladár, and Zawadowski, 2007; Doyon, 2007; Boulat, Saleur, and Schmitteckert, 2008). Field theoretical methods were applied in the *scaling limit* in which all energy scales are much smaller than the bandwidth B. In the following the focus is on this limit. Functional RG results for the equilibrium and nonequilibrium properties beyond the scaling limit including a favorable comparison with recent numerical time-dependent density-matrix renormalization group data (Boulat, Saleur, and Schmitteckert, 2008) are presented by Karrasch (2010), Karrasch, Pletyukhov *et al.* (2010), and Karrasch *et al.* (2010).

First order perturbation theory in $U_{L/R}$ leads to logarithmic terms in the self-energy of the form $U_{L/R} \ln(t_{L/R}/B)$ which in the scaling limit become large. They indicate the appearance of power laws in $t_{L/R}$ with $U_{L/R}$ dependent exponents. To uncover them requires a treatment which goes beyond perturbation theory. In the limit of weak to intermediate two-particle interactions a Keldysh functional RG approach to the IRLM in the level-1 truncation leads to a comprehensive picture of the physics in and out of equilibrium. In particular, it allows one to identify the relevant energy scales.

For the present model instead of Eq. (162) another cutoff scheme suitable for nonequilibrium (Jakobs, 2010; Jakobs, Pletyukhov, and Schoeller, 2010a) was implemented and tested (Karrasch, 2010; Karrasch, Pletyukhov *et al.*, 2010). In this approach each of the three interacting sites is coupled to its own auxiliary lead, in addition to the coupling of sites 1 and 3 to the physical leads. The local density of states at the contact points of the auxiliary leads is assumed to be energy independent (wide band limit) such that the hybridization is energy independent and forms an additional on-site "energy" $i\Lambda$ on each of the three sites. The auxiliary couplings are then considered as the cutoff and flow from $\Lambda = \infty$, at which regularization is achieved, down to $\Lambda = 0$, at which the auxiliary leads are decoupled and the original problem is restored. One can show that in the lowest-order truncation and in the equilibrium limit the Keldysh contour flow equations become equal to the equilibrium ones obtained using the Matsubara formalism with the (at $T = 0$) sharp energy cutoff Eq. (143). Similarly to the imaginary frequency cutoff of Sec. VI.C.7 it conserves causality even after truncation of the functional RG flow-equation hierarchy. In addition, in the equilibrium limit this so-called *reservoir cutoff* scheme obeys the KMS relation in any truncation order (Jakobs, 2010; Jakobs, Pletyukhov, and Schoeller, 2010a, 2010b).

In the scaling limit and to lowest order in U only flow equations for the hydridizations Γ_λ^Λ with initial values $\Gamma_\lambda^{\mathrm{ini}} = \pi\rho_0 t_\lambda^2$ appear ($\lambda = L/R$); the flow of the level energies of sites 1 to 3 is of order U^2. The renormalized hybridizations set the width of the resonance at $V_g = 0$. For Λ being smaller than the bandwidth the flow equations for the rates read ($\Gamma^\Lambda = \Gamma_L^\Lambda + \Gamma_R^\Lambda$)

$$\frac{d\Gamma_\lambda^\Lambda}{d\Lambda} = -2\rho_0 U_\lambda \Gamma_\lambda^\Lambda \frac{\Lambda + \Gamma^\Lambda}{(\mu_\lambda - V_g)^2 + (\Lambda + \Gamma^\Lambda)^2}. \tag{164}$$

They have the approximate solutions

$$\Gamma_\lambda \approx \Gamma_\lambda^{\mathrm{ini}} \left(\frac{\Lambda_0}{\max\{|\mu_\lambda - V_g|, \Gamma/2\}} \right)^{2\rho_0 U_\lambda}. \tag{165}$$

The scale Λ_0 is of the order of the bandwidth. Within the static approximation the current takes the form of the noninteracting expression with the bare hybridizations $\Gamma_\lambda^{\mathrm{ini}}$ replaced by the renormalized ones

$$I = \frac{1}{\pi} \frac{\Gamma_L \Gamma_R}{\Gamma} \left[\arctan \frac{V_b/2 - V_g}{\Gamma} + \arctan \frac{V_b/2 + V_g}{\Gamma} \right]. \tag{166}$$

It turns out to be useful (Karrasch *et al.*, 2010; Andergassen *et al.*, 2011) to introduce the two scales $T_u^\lambda = \Gamma_\lambda^{\mathrm{ini}} \Lambda_0 / T_u$, with $T_u = T_u^L + T_u^R$, and the asymmetry parameter $c^2 = T_u^L / T_u^R$. The same flow equation can be derived using the so-called real-time RG in frequency space (Schoeller, 2009; Karrasch *et al.*, 2010; Andergassen *et al.*, 2011). Within this approach also the relaxation into the steady state was analyzed in detail (Karrasch *et al.*, 2010; Andergassen *et al.*, 2011).

We first review the results obtained for the left-right symmetric model with $t_L = t_R = t'$ and $U_L = U_R = U$ as well as particle-hole symmetry $V_g = 0$ (Karrasch, 2010; Karrasch *et al.*, 2010; Andergassen *et al.*, 2011). From Eq. (165) it follows that in this case the maximum of either $|\mu_\lambda| = |V_b|/2$ or Γ itself cuts off the RG flow. The charge susceptibility $\chi = -d\langle n_2 \rangle / dV_g|_{V_g = 0}$ is directly given by the

renormalized width $\chi^{-1} = \pi\Gamma$, which at $V_b = 0$ and to leading order in U [$\Gamma_\lambda \to \Gamma_\lambda^{\rm ini}$ on the right-hand side of Eq. (165)] gives the scaling relation

$$\chi \sim (\Gamma^{\rm ini})^{\alpha_\chi - 1}, \qquad \alpha_\chi = 2\rho_0 U + \mathcal{O}(U^2). \tag{167}$$

In the noninteracting case $\chi \sim (\Gamma^{\rm ini})^{-1}$ as expected. From Eq. (166) it follows that the current for $T_u^\lambda = \Gamma_\lambda \ll V_b \ll B$ is given by

$$I \sim \Gamma \sim V_b^{-\alpha_I}, \qquad \alpha_I = 2\rho_0 U + \mathcal{O}(U^2). \tag{168}$$

Equations (167) and (168) were also obtained using other approaches (Borda, Vladár, and Zawadowski, 2007; Doyon, 2007; Boulat, Saleur, and Schmitteckert, 2008) and suggest that the bias voltage merely plays the role of an additional infrared cutoff, besides, e.g., Γ or temperature (Borda and Zawadowski, 2010). That this is in general not the case is nicely shown by a functional RG treatment *away* from particle-hole and/or left-right symmetry (Karrasch, 2010; Karrasch *et al.*, 2010; Andergassen *et al.*, 2011).

The differential conductance $g = dI/dV_b$ has a maximum when V_g crosses the chemical potential at $V_g = \pm V_b/2$ (Karrasch *et al.*, 2010; Andergassen *et al.*, 2011). In the on-resonance case the current for $V \gg \Gamma$ reads

$$I(V_b) \approx \frac{\Gamma_L \Gamma_R}{2\Gamma} = T_u \frac{(T_u/\Gamma)^{2\rho_0 U_L}(T_u/V_b)^{2\rho_0 U_R}}{c(T_u/\Gamma)^{2\rho_0 U_L} + \frac{1}{c}(T_u/V_b)^{2\rho_0 U_R}} \frac{c}{1+c^2}. \tag{169}$$

The bias voltage dependence is clearly more involved than in Eq. (168). In particular, simple power-law scaling with exponent $-2\rho_0 U_R$ is recovered only in the extreme limits of either $V_b \ggg T_u$ or $c \gg 1$ (Andergassen *et al.*, 2011) as the exponent of the second term in the denominator $2\rho_0 U_R$ is small. Off resonance (e.g., at $V_g = 0$) and for $V_b \gg \Gamma$ the current is given by

$$I(V_b) \approx T_u \frac{(T_u/|V_b/2 - V_g|)^{2\rho_0 U_L}(T_b/|V_b/2 + V_g|)^{2\rho_0 U_R}}{c(T_u/|V_b/2 - V_g|)^{2\rho_0 U_L} + (1/c)(T_u/|V_b/2 + V_g|)^{2\rho_0 U_R}} \frac{2c}{1+c^2}. \tag{170}$$

The more involved role of V_b is again apparent. A power law is obtained in the above studied left-right symmetric case or for strong left-right asymmtery ($c \ll 1$ or $c \gg 1$) (Andergassen *et al.*, 2011).

This concludes the analysis of the IRLM which shows that the functional RG can be a tool to obtain a comprehensive picture of the equilibrium and steady-state nonequilibrium physics of a dot model dominated by charge fluctuations. The approach allows for an unbiased analysis of the nonequilibrium rates and cutoff scales.

VII. CONCLUSION

A. Summary

The functional RG has proven to be a valuable source of new approximation schemes for interacting fermion systems. The heart of the method is an exact flow equation, which describes the flow of the effective action as a function of a suitable flow parameter. The flow provides a smooth evolution from the bare action to the final effective action from which all properties of the systems can be obtained. Approximations are obtained by truncating the effective action. In many cases, rather simple truncations turned out to capture rather complex many-body phenomena. Compared to the traditional resummations of perturbation theory these approximations have the advantage that infrared singularities are treated properly due to the built-in RG structure. Approximations derived in the functional RG framework can be applied directly to microscopic models, not only to renormalizable effective field theories. Remarkably, the functional RG reviewed here as a computational tool is similar to RG approaches used by mathematicians to derive general rigorous results for interacting fermion systems.

We dedicated a large portion of this review to general features of the functional RG method for interacting Fermi systems (see Sec. II). After defining the relevant generating functionals, we presented a self-contained derivation of the exact functional flow equation and its expansion leading to an exact hierarchy of flow equations for vertex functions. We reviewed the different choices of flow parameters used so far, along with their advantages and disadvantages. Truncations and their justification by power counting have been discussed in detail for translation-invariant bulk systems, with links to the closely related mathematical literature.

In Secs. III, IV, V, and VI we reviewed applications of the functional RG to specific systems. Most of the approximations used in these sections are based on relatively simple truncations involving only the flow of the two-particle vertex and/or the self-energy. Nevertheless a rich variety of phenomena associated with low-energy singularities and instabilities is captured. Instead of summarizing the content of each section, we merely highlight some distinctive features. Section III reviews functional RG work on the stability analysis of two-dimensional electron systems with competing instabilities. The main advantage of the functional RG based one-loop computation of the two-particle vertex, compared to other weak-coupling approximations, is that particle-particle and particle-hole channels are treated on equal footing, such that there is no artificial bias due to a selection or a different treatment of channels. In the conventional many-body framework a summation of all parquet diagrams would be required to achieve this, but a solution of the parquet equations is extremely difficult. Spontaneous symmetry breaking, the topic of Sec. IV, can be treated either by a purely fermionic flow or by coupled flow equations for the fermions and a Hubbard-Stratonovich field for the order parameter. It seems that a comprehensive treatment of all relevant fluctuation effects related to symmetry breaking can be achieved.

Applications of the functional RG to quantum criticality, reviewed in Sec. V, have begun only recently. Approximations beyond the Hertz-Millis theory can be obtained from nonperturbative truncations of the effective order parameter action, or by treating fermions and order parameter fluctuations in a coupled flow instead of integrating the fermionic degrees of freedom at once. While the applications reviewed in Secs. III, IV, and V address translation-invariant bulk systems, the purpose of Sec. VI is to show how the functional RG can be fruitfully applied to inhomogeneous systems such as quantum wires and quantum dots, in thermal equilibrium and also in a nonequilibrium steady state. A strikingly simple truncation of the flow-equation hierarchy turned out to describe a wealth of nontrivial quantum transport properties characterized by low-energy power laws and complex crossover phenomena.

B. Future directions

The number of functional RG based works on interacting Fermi systems has increased steadily over the last decade, but the possibilities opened by this approach are far from being exhausted. There are many opportunities and challenges concerning both fundamental developments of the method and the extension to a broader range of systems.

On the methodological side there are a number of open issues. In systems with an instability of the normal metallic state, the flow of the effective interactions is not yet fully understood, even on the level of truncations involving only the two-particle vertex and the self-energy, since a faithful parametrization of singular momentum and frequency dependences of the vertex is not easy.

The most outstanding challenge is probably to identify accurate and computable truncations of the exact flow equation for strongly interacting systems such as systems close to a Mott metal-insulator transition. It is clear that three-particle and higher-order vertices cannot be discarded in a strongly interacting system. However, they will usually not lead to qualitative changes such as new singularities. Hence, there is hope that the contribution from many-body vertices can be absorbed in the structure appearing already on the two-particle level. After all, many strong coupling phenomena, including the Mott transition, consist essentially in the formation of two-particle bound states. To capture effects related to strong local correlations, such as the Mott transition, one may also try to treat higher-order vertices in a local approximation. This would make a link to the dynamical mean-field theory (DMFT), where all vertices, including the self-energy, are approximated by local functions (Georges *et al.*, 1996).

For systems with strongly interacting order parameter fluctuations there are already a number of nonperturbative approximations for bosonic actions on the market. The local potential approximation presented in Sec. V is only the simplest one. It can be extended by taking nonlocal contributions into account, either in a derivative expansion (Berges, Tetradis, and Wetterich, 2002) or by including the full momentum or frequency dependence up to a certain level in the hierarchy (Blaizot, Mendez-Galain, and Wschebor, 2006). Such approximations may be useful for studying incommensurate density wave instabilities in cases where the modulation vector of the density wave can be determined only after taking fluctuations into account.

Recently, the functional RG was extended to a real-time (or real frequency) Keldysh functional RG which can be used for studying correlated Fermi systems in nonequilibrium (Jakobs, 2003, 2010; Gezzi, Pruschke, and Meden, 2007; Karrasch, 2010). First applications, partly reviewed in Sec. VI, indicate that also for these type of problems the functional RG constitutes a useful tool of outstanding flexibility. So far only nonequilibrium steady states were studied. To investigate a time evolution is technically straightforward but requires a significantly increased computational effort or additional approximations.

With few exceptions, applications of the functional RG to interacting Fermi systems have so far been limited to purely fermionic one-band systems. There are many extensions of this restricted class of systems, where the flexibility of the functional RG can be fruitfully used in the future. Multiband models have been studied already for the pnictide superconductors, but there are many more and qualitatively different models for transition metal oxides with orbital degrees of freedom. One may include phonons and analyze the electron-phonon interaction effects beyond the Eliashberg theory. Allowing for disorder one may study the complex interplay of interaction and disorder effects. It is not hard to generalize the exact flow equations for the extensions listed above. The interesting task is then to devise suitable truncations.

Last but not least, the functional RG is an ideal many-body tool to be combined with *ab initio* band structure calculations. A lot of work in the last 15 years has been dedicated to the *ab initio* calculation of correlated electron materials with the DMFT (Kotliar *et al.*, 2006; Anisimov and Izyumov, 2010). As in the DMFT, an arbitrary band structure can be used as input for a functional RG calculation. Furthermore, one can easily implement nonlocal potentials and nonlocal two-particle interactions.

ACKNOWLEDGMENTS

We are grateful for fruitful collaborations and/or discussions with S. Andergassen, J. Bauer, D. Baeriswyl, C. Castellani, A. Chubukov, C. Di Castro, J. von Delft, A. Eberlein, T. Enss, J. Feldman, R. Gersch, H. Gies, W. Hanke, C. Husemann, S. Jakobs, P. Jakubczyk, C. Karrasch, A. Katanin, H. Knörrer, P. Kopietz, D.-H. Lee, B. Obert, J. Pawlowski, C. Platt, M. Pletyukhov, M. Rice, D. Rohe, A. Rosch, H. Schoeller, P. Strack, S. Takei, R. Thomale, E. Trubowitz, C. Wetterich, P. Wölfle, and H. Yamase. All of us benefitted from the DFG research group Functional renormalization group in correlated fermion systems (FOR 723).

APPENDIX A: WICK-ORDERED FLOW EQUATIONS

In this Appendix we present a derivation of Wick-ordered flow equations for fermions, which have been used for calculations of instabilities and symmetry breaking in the two-dimensional Hubbard model.

Wick-ordered m-particle functions W_m^Λ are generated from the Wick-ordered effective interaction (Salmhofer, 1999)

$$\mathcal{W}^\Lambda[\chi,\bar\chi] = e^{\Delta_{\bar G_0^\Lambda}}\mathcal{V}^\Lambda[\chi,\bar\chi]. \tag{A1}$$

The exponent in the Wick-ordering factor is the functional Laplacian $\Delta_{\bar G_0^\Lambda} = (\partial_\chi, \bar G_0^\Lambda \partial_{\bar\chi})$ with $\bar G_0^\Lambda = G_0 - G_0^\Lambda$. The Wick-ordered interaction converges to $\mathcal{V}$ for $\Lambda \to 0$, since $\bar G_0^\Lambda$ vanishes in that limit. However, the flow equations for $\mathcal{W}^\Lambda$ and the corresponding m-particle functions differ from those for $\mathcal{V}^\Lambda$. The flow equation for the generating functional $\mathcal{W}^\Lambda$ reads (Salmhofer, 1999)

$$\frac{d}{d\Lambda}\mathcal{W}^\Lambda = \frac{1}{2} e^{\Delta^{\rm diff}_{\bar G_0^\Lambda}} \Delta^{\rm diff}_{\dot{\bar G}_0^\Lambda} \mathcal{W}^\Lambda \mathcal{W}^\Lambda, \tag{A2}$$

where the superscript "diff" indicates that the Laplacian takes one derivate on the first, and the other on the second factor $\mathcal{W}^\Lambda$ on the right-hand side. This equation is obtained as follows. Using the definition of $\mathcal{W}^\Lambda$ and the flow equation for $\mathcal{V}^\Lambda$, one can write

$$\begin{aligned}\frac{d}{d\Lambda}\mathcal{W}^\Lambda &= \frac{d}{d\Lambda}(e^{\Delta_{\bar G_0^\Lambda}}\mathcal{V}^\Lambda)\\ &= \Delta_{\dot{\bar G}_0^\Lambda} e^{\Delta_{\bar G_0^\Lambda}}\mathcal{V}^\Lambda \\ &\quad + e^{\Delta_{\bar G_0^\Lambda}}\left(-\Delta_{\dot{\bar G}_0^\Lambda}\mathcal{V}^\Lambda + \frac{1}{2}\Delta^{\rm diff}_{\dot{\bar G}_0^\Lambda}\mathcal{V}^\Lambda\mathcal{V}^\Lambda\right)\\ &= \frac{1}{2} e^{\Delta_{\bar G_0^\Lambda}} \Delta^{\rm diff}_{\dot{\bar G}_0^\Lambda}\mathcal{V}^\Lambda\mathcal{V}^\Lambda.\end{aligned}$$

Using the decomposition $\Delta_{\bar G_0^\Lambda} = \Delta^{\rm factor1}_{\bar G_0^\Lambda} + \Delta^{\rm factor2}_{\bar G_0^\Lambda} + \Delta^{\rm diff}_{\bar G_0^\Lambda}$ (when acting on a product) yields

$$\frac{d}{d\Lambda}\mathcal{W}^\Lambda = e^{\Delta^{\rm diff}_{\bar G_0^\Lambda}} \tfrac{1}{2}\Delta^{\rm diff}_{\dot{\bar G}_0^\Lambda}(e^{\Delta_{\bar G_0^\Lambda}}\mathcal{V}^\Lambda)(e^{\Delta_{\bar G_0^\Lambda}}\mathcal{V}^\Lambda)$$

and thus Eq. (A2).

Expanding in powers of Grassmann fields and comparing coefficients, one obtains a hierarchy of flow equations for the m-particle functions $W^{(2m)\Lambda}$, which is illustrated in Fig. 27. The line with the dash is due to contractions generated by $\Delta^{\rm diff}_{\dot{\bar G}_0^\Lambda}$ in Eq. (A2); the other lines are generated by the exponential of $\Delta^{\rm diff}_{\bar G_0^\Lambda}$. Note that the right-hand side of the Wick-ordered flow equations is bilinear in the effective interactions, and no tadpole terms appear. Note also that the propagators connecting the vertices have support for energies at and below the cutoff scale Λ, such that the integration region shrinks as Λ decreases. One might worry that the low-energy propagators lead to infrared divergences even for $\Lambda > 0$. This is not the case, as can be seen from the general infrared power-counting analysis presented by Salmhofer (1999).

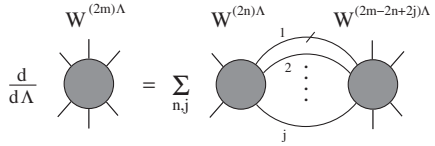

FIG. 27. Diagrammatic representation of the flow equations for the effective m-particle interactions $W^{(2m)\Lambda}$ in the Wick-ordered version of the functional RG; the internal line with a dash corresponds to $\partial_\Lambda \bar G_0^\Lambda$, the others to $\bar G_0^\Lambda$; all possible pairings leaving m ingoing and m outgoing external legs have to be summed.

APPENDIX B: DETAILS OF POWER COUNTING

1. Propagator bounds

Here we show, using properties of the dispersion function and the Fermi surface, that

$$s_\Lambda \le a + b\log\frac{\Lambda_0}{\Lambda}, \quad \text{and} \quad \|G^\Lambda\| \le c\Lambda^{-1}, \tag{B1}$$

where a, b, and c are constants that do not depend on Λ. In the absence of van Hove singularities, $b = 0$. We first consider the case where the self-energy effects are not taken into account (they are discussed in Sec. II.E.4). Then one can simply take $\chi^\Lambda(k) = \chi_>((k_0^2 + \xi_{\mathbf{k}}^2)/\Lambda^2)$, where $\chi_>(\eta)$ is a fixed (i.e., Λ-independent) increasing function that vanishes at least linearly at $\eta = 0$, tends to 1 as $\eta \to \infty$, and satisfies $\chi_>'(\eta) \le \eta^{-2}$ for large η. We can then verify Eq. (B1) by scaling as follows. The full propagator is $G^\Lambda(k) = (ik_0 - \xi_{\mathbf{k}})^{-1}\chi^\Lambda(k)$, so $|G^\Lambda(k)| \le c/\Lambda$ where $c = \max\{\eta^{-1}\chi_>(\eta^2): \eta > 0\}$ is finite. The single-scale propagator is

$$S^\Lambda(k) = -\frac{2}{\Lambda^3}(ik_0 + \xi_{\mathbf{k}})\chi_>'\left(\frac{k_0^2 + \xi_{\mathbf{k}}^2}{\Lambda^2}\right). \tag{B2}$$

Using the fact that the Matsubara sum is a Riemann sum for the convergent integral of S^Λ over k_0 and introducing the density of states $N(E) = \int d^dk\,\delta(\xi_{\mathbf{k}} - E)$, we get

$$s_\Lambda \le \frac{4}{\Lambda^3}\int dk_0 \int dE N(E)\sqrt{k_0^2 + E^2}\,\chi_>'\left(\frac{k_0^2 + E^2}{\Lambda^2}\right), \tag{B3}$$

where the 4 instead of 2 gives a crude bound for the change from the Matsubara sum to the integral for large enough β. Changing variables to $\rho = (k_0^2 + E^2)^{1/2}$ and a polar angle φ, we obtain

$$s_\Lambda \le \frac{4}{\Lambda^3}\int_0^\infty \rho^2 d\rho\,\chi_>'\left(\frac{\rho^2}{\Lambda^2}\right)\int_0^{2\pi} d\varphi N(\rho\cos\varphi). \tag{B4}$$

If the density of states N is bounded, using $N(E) \le N_0$ and scaling out Λ implies $s_\Lambda \le a$, with $a = 8\pi N_0 \int \rho^2\chi_>'(\rho^2)d\rho < \infty$. In the presence of a van Hove point on the Fermi surface, N stays bounded in dimensions $d \ge 3$, but diverges logarithmically for $d = 2$. In this case, the φ integral contributes an additional factor $\log\Lambda$.

Thus Eq. (B1) holds. The hypotheses on $\chi_>$ are satisfied, in particular, for the standard strict cutoff functions that vanish identically near $\eta = 0$, and which are identically 1 for $\eta \ge 1$. For such cutoffs, the single-scale propagator is nonvanishing only in a "momentum shell" of thickness Λ around the Fermi surface, and the above bounds can also be obtained by estimating the $\mathbf{k}$-space volume of this shell (see also Appendix B.3).

2. Power counting

Here we prove Eq. (70) to all orders in the running coupling expansion. All terms on the right-hand side of the flow equation for $\Gamma_r^{(2m)\Lambda}$ are of the form

$$\frac{1}{2}\,\mathrm{tr}(\mathbf{S}^\Lambda \mathbf{P}^\Lambda)(\underline{k},\underline{\sigma}) = \frac{1}{2}\int đl \sum_{\alpha,\alpha'} S^\Lambda_{\alpha,\alpha'}(l)\hat{P}^\Lambda_{\alpha,\alpha'}(\underline{k},\underline{\sigma};l,-l), \tag{B5}$$

where $\hat{P}^\Lambda = \hat{\Gamma}^{(2m+2)\Lambda}_r$ in the first term of Eq. (67) and given by the other summands in Eq. (67) for the other terms, and

$$\int đl = \frac{1}{\beta}\sum_{l_0}\int \frac{d^d l}{(2\pi)^d}$$

contains both frequency and momentum summations. Taking the absolute values inside the sum and estimating the factor $\hat{P}^\Lambda$ by its maximum $\|P^\Lambda\|$, we obtain

$$\|\tfrac{1}{2}\mathrm{tr}(\mathbf{S}^\Lambda \mathbf{P}^\Lambda)\| \le s_\Lambda \|P^\Lambda\| \tag{B6}$$

with $s_\Lambda = \max_\alpha \sum_{\alpha'} \int đk |\hat{S}^\Lambda_{\alpha,\alpha'}(k)|$. The second simple inequality that we use is that $\|P_1 \cdots P_n\| \le \|P_1\| \cdots \|P_n\|$. It implies bounds for all $\mathcal{L}^\Lambda_p$ contributions in terms of $\|G^\Lambda\|$ and $\|\Gamma^{(2m_q)\Lambda}_{r_q}\|$, so that $\|(d/d\Lambda)\Gamma^{(2m)\Lambda}_r\|$ is bounded by

$$s_\Lambda\Big[\|\Gamma^{(2m+2)\Lambda}_r\| + \|V^\Lambda\|\,\|G^\Lambda\|\,\|\Gamma^{(2m)\Lambda}_{r-1}\| + \sum_{p\ge 2}\|G^\Lambda\|^{p-1}\sum{}'\|\Gamma^{(2m_1)\Lambda}_{r_1}\|\cdots\|\Gamma^{(2m_p)\Lambda}_{r_p}\|\Big]. \tag{B7}$$

The power counting is now determined by s_Λ and $\|G^\Lambda\|$. Given Eqs. (B1) and (B7), the proof of Eq. (70) is an effortless induction argument. The inductive scheme proceeds in the standard way of Polchinski (1984), namely, upward in $r \ge 1$ and at fixed r, downward in m, starting at $m = r$, where $\Gamma^{(2m+2)\Lambda}_r = 0$. The induction start $r = 1$ is trivial. Let $r \ge 2$ and assume Eq. (70) to hold for all (r', m') with $r' < r$ and for $r' = r$, $m' > m$. The right-hand side of Eq. (B7) contains only terms to which the inductive hypothesis Eq. (70) applies. Inserting it, using Eq. (B1), and collecting powers in the form $1 - p + \sum_q (2 - m_q) = 1 - m$ and $\sum_{q=1}^p (r_q - m_q + 1) = r - m$, we obtain

$$\left\|\frac{d}{d\Lambda}\Gamma^{(2m)\Lambda}_r\right\| \le \tilde{\gamma}^{(2m)}_r s^{r-m+1}_\Lambda f^r_\Lambda \Lambda^{1-m}, \tag{B8}$$

where the constant $\tilde{\gamma}^{(2m)}_r$ is a weighted sum of products of the $\gamma^{(2m_q)}_{r_q}$. We now use the initial condition $\Gamma^{(2m)\Lambda}_r = 0$ to write

$$\Gamma^{(2m)\Lambda}_r = -\int_\Lambda^{\Lambda_0} d\ell\,\frac{d}{d\ell}\Gamma^{(2m)\ell}_r,$$

take the norm of this equation, and use Eq. (B8). This gives

$$\|\Gamma^{(2m)\Lambda}_r\| \le \tilde{\gamma}^{(2m)}_r \int_\Lambda^{\Lambda_0} d\ell\, s^{r-m+1}_\ell f^r_\ell \ell^{1-m}. \tag{B9}$$

By definition, $f_\Lambda \ge f_{\Lambda'}$ if $\Lambda \le \Lambda'$, so $f_\ell \le f_\Lambda$ for all ℓ in the integration interval. Thus the last integral is bounded by $\tilde{\gamma}^{(2m)}_r f^r_\Lambda \int_\Lambda^{\Lambda_0} d\ell s^{r-m+1}_\ell \ell^{1-m}$. Because s_ℓ is at most logarithmic in ℓ, and $m \ge 3$, $\int_\Lambda^{\Lambda_0} d\ell s^\alpha_\ell \ell^{1-m} \le K\Lambda^{2-m} s^\alpha_\Lambda$ with a constant K that depends on α and m. This, together with an appropriate choice of $\gamma^{(2m)}_r$, completes the induction step.

For $m = 2$, doing the last integral increases the power of the logarithm by 1. This case is discussed in more detail in Appendix B.3.

For $m = 1$, the self-energy term, the same simple bound gives $\|(d/d\Lambda)\Sigma^\Lambda\| \le s_\Lambda f_\Lambda$, so the integral gives a contribution of order f_Λ. When a counterterm is used to keep the Fermi surface fixed, the initial condition for Σ^Λ at $\Lambda = \Lambda_0$ is given by the counterterm, which needs to be adjusted such that at low scales Λ, $\Sigma^\Lambda(0,\mathbf{k}) = O(\Lambda)$ whenever $\xi_\mathbf{k} = 0$. This leads to the self-consistency relation mentioned in Sec. II.E.4.

A similar proof can be given in the Wick-ordered scheme (Salmhofer, 1998b); it is even simpler because the double induction used here is replaced by single induction on r.

A crucial point in obtaining Eq. (B8) is that all the dependence on p and on the m_q drops out when the power of Λ is collected. It is this property that makes many-fermion models with short-range interactions *renormalizable* in the strict quantum-field-theoretical sense. The classification in relevant, marginal, and irrelevant terms now also becomes apparent because for $m \ge 3$, the $\Gamma^{(2m)\Lambda}_r$ grow as Λ decreases: Suppose we add an additional $(2m \ge 6)$-point interaction vertex $\tilde{V}^{(2m)\Lambda_0}$ of order 1 to the initial interaction at Λ_0. Its insertion at a lower scale Λ is a factor $(\Lambda/\Lambda_0)^{m-2}$ smaller than that of the effective $2m$-point vertex created by the two-particle interaction. Thus the influence of $\tilde{V}^{(2m)\Lambda_0}$ wanes at low scales; it is irrelevant. A simple adaptation of the above inductive argument indeed shows that the inclusion of such additional terms with $m \ge 3$ in the interaction at Λ_0 changes only prefactors in the power-counting bounds. For $m = 2$, this suppressing factor is absent, so that these terms are marginal (the more detailed analysis of Appendix B.3 shows how to separate the marginally relevant from the marginally irrelevant terms). Moreover, it is clear that this power counting breaks down when $\Gamma^{(4)\Lambda}$ develops singularities as a function of $\mathbf{k}$ and ω, because then $f_\Lambda = \infty$. Finally, for $m = 1$, the scale derivative of the self-energy obtained by the above argument is of order Λ^{1-m}, as in Eq. (B8), but since $m = 1$, this integrates to $O(1)$ instead of $O(\Lambda^{2-m})$, and this term is relevant. To get its size back to $O(\Lambda^{2-m})$ in the momentum shell where $|\xi(\mathbf{k})| \sim \Lambda$, one needs a cancellation by a counterterm, as described in Sec. II.E.4. In the Taylor expansion required to do the cancellation, the derivative of the self-energy appears. By the above power counting, this is a marginal term. In the Luttinger model, it is really marginal and causes the anomalous exponents. For curved Fermi surfaces in $d \ge 2$ dimensions, it is seen to be irrelevant by the arguments discussed in Appendix B.3.b.

There is a hard problem hidden in the recursion of the constants $\gamma^{(2m)}_r$. In the recursion described above, the number of terms that gets added corresponds to the number of Feynman graphs with r vertices, which grows factorially in r, so that the bound obtained in this way for $\gamma^{(2m)}_r$ and $c^{(2m)}_r$ is of order $r!$. If saturated, it would lead to a convergence problem. However, due to the fermionic antisymmetry, sign cancellations in the sum over Feynman diagrams prevent this factorial from arising. For proofs, we refer interested readers to the literature [see Feldman *et al.* (1992), Feldman, Knörrer, and Trubowitz (1998), Disertori and Rivasseau (2000), Salmhofer and Wieczerkowski (2000), Feldman, Knörrer, and Trubowitz (2002), and Pedra and Salmhofer (2008), and references therein]. In their application to propagators with Fermi surfaces, these proofs also provide a

rigorous basis for the use of Fermi surface patches [first used by Feldman *et al.* (1992) and there called "sectors"]. Patching the Fermi surface has become an essential tool also in applications; see Sec. III.

In a typical lattice model, the kinetic energy per particle is bounded, so that the flow is usually started at the highest value (the bandwidth) of the kinetic energy Λ_0. The χ^Λ we used here also cuts off large frequencies. Thus the starting interaction is in this case one where the degrees of freedom with frequencies $|k_0|$ above Λ_0 have already been integrated over. This starting action can be obtained by convergent perturbation theory; see Pedra and Salmhofer (2008).

3. Improved power counting

This is a refinement of power counting, valid in a large class of bulk fermion systems in $d \geq 2$ (Feldman and Trubowitz, 1990; Shankar, 1994; Feldman, Salmhofer, and Trubowitz, 1996, 1998b, 1999, 2000). It is the deeper reason behind the emergence of Fermi-liquid behavior and of dominant Cooper pairing tendencies in weakly coupled standard fermion systems, and it provides a precise link between Fermi surface geometry and scaling properties of the effective m-particle vertices in general.

We discuss this in the absence of self-energy effects, to bring out the main effects as clearly as possible. (The self-energy changes the Fermi surface; if the interacting Fermi surface is regular, the following analysis remains essentially unchanged.) We also assume a strict cutoff function, i.e., $\chi_>(\eta) = 0$ for $\eta \leq (1-\delta)^2$, where $0 < \delta < 1/2$ is fixed, and $\chi_>(\eta) = 1$ for $\eta \geq 1$. Again, this choice is not essential; it just simplifies the discussion.

a. Effects of curvature on power counting

The integral $I_\Lambda(k) = \int dp_0 d^d p |S^\Lambda(p)||G^\Lambda(\pm p + k)|$ arises from the trace on the right-hand side of the RG equation when all effective vertices and all but one of the propagators G^Λ have been estimated by their maximal values. It thus determines the maximal possible value of a term on the right-hand side of the RG equation, where the dependence on one external momentum is kept. In particular, I_Λ is directly relevant for the one-loop contributions to the flowing four-point vertex. The power counting done above corresponds to the estimate $I_\Lambda(k) \leq \|G^\Lambda\| s_\Lambda \leq \Lambda^{-1} s_\Lambda$, so that $\int_\Lambda I_\lambda d\lambda$ grows logarithmically in Λ for small Λ.

Since $\Sigma^\lambda = 0$, $S^\Lambda(k) = (ik_0 - \xi_{\mathbf{k}})^{-1} \partial_\Lambda \chi^\Lambda(k)$, and

$$G^\Lambda(k) = \frac{\chi^\Lambda(k)}{ik_0 - \xi_{\mathbf{k}}} = G^{\Lambda_0}(k) - \int_\Lambda^{\Lambda_0} d\lambda S^\lambda(k). \tag{B10}$$

The term G^{Λ_0} is nonvanishing at large frequencies, but not important. [$\|G^{\Lambda_0}\| \leq \Lambda_0^{-1}$, hence a factor Λ/Λ_0 smaller than $\|G^\Lambda\|$ when Λ gets small. Thus $\int dp_0 d^d p |S^\Lambda(p)||G^{\Lambda_0}(p+k)| \leq s_\Lambda \Lambda_0^{-1}$, hence its integral over Λ is bounded by a constant.] The derivative of the strict cutoff function vanishes unless $\Lambda(1-\delta) \leq |ik_0 - \xi_{\mathbf{k}}| \leq \Lambda$, so $S^\Lambda(p)$ vanishes unless $|p_0| \leq \Lambda$ and $\mathbf{p}$ is in the momentum space shell $\mathcal{F}_\Lambda = \{\mathbf{k}: |\xi_{\mathbf{k}}| \leq \Lambda\}$, and there $|S^\Lambda(p)| \leq 1/\Lambda^2$. The p_0 sum in I_Λ gives at most 2Λ, and the $\mathbf{p}$ integral gives the d-dimensional volume of the intersection $\mathcal{F}_\Lambda \cap (\mathbf{k} \pm \mathcal{F}_\lambda)$ of two momentum space shells, where one is shifted by $\mathbf{k}$. It follows that

$$I_\Lambda(k) \leq O(\Lambda_0^{-1}) + \frac{2}{\Lambda} \int_\Lambda^{\Lambda_0} \frac{d\lambda}{\lambda^2} \mathrm{vol}_d[\mathcal{F}_\Lambda \cap (\mathbf{k} \pm \mathcal{F}_\lambda)]. \tag{B11}$$

This links the scaling behavior of terms in the RG equation to the geometric properties of the Fermi surface.

Obviously, the volume of the intersection is at most as large as the volume of $\mathcal{F}_\Lambda$ itself: $\mathrm{vol}_d[\mathcal{F}_\Lambda \cap (\mathbf{k} \pm \mathcal{F}_\lambda)] \leq \mathrm{vol}_d \mathcal{F}_\Lambda \leq \mathrm{const} \times \Lambda$. Using this in Eq. (B11) gives the general power-counting bound mentioned at the beginning of this section, $I_\Lambda(k) \leq \mathrm{const} \times \Lambda^{-1}$. Assuming that $\xi_{-\mathbf{k}} = \xi_{\mathbf{k}}$, this bound is always saturated for $\mathbf{k} = \mathbf{0}$, and also for those $\mathbf{k}$ for which the shift by $\mathbf{k}$ makes the two shells overlap over a significant region of the Fermi surface, that is, when $\mathbf{k}$ is a nesting vector of the Fermi surface.

For other values of $\mathbf{k}$, the intersection volume can be much smaller than that of $\mathcal{F}_\Lambda$. A general definition of non-nesting was given, and power-counting bounds were derived when it was satisfied, by Feldman, Salmhofer, and Trubowitz (1996), and extended to the case with van Hove singularities in Feldman and Salmhofer (2008a, 2008b). Here we cite only the result for the case of a strictly convex and positively curved Fermi surface without van Hove singularities, discussed also in the appendix of Salmhofer (1999). In that case, and for $\Lambda \leq \lambda \leq v_{F,\min}|\mathbf{k}|$, one can show that the volume ratio $\mathrm{vol}_d[\mathcal{F}_\Lambda \cap (\mathbf{k} \pm \mathcal{F}_\lambda)]/\mathrm{vol}_d \mathcal{F}_\Lambda$ is proportional to

$$\frac{\lambda}{|\mathbf{k}| v_{F,\min} \kappa}, \quad \text{if } \mathbf{k} \notin \mathcal{F}_\lambda^{(2)}, \tag{B12}$$

$$\left(\frac{\lambda}{\kappa}\right)^{(d-1)/2}, \quad \text{if } \mathbf{k} \in \mathcal{F}_\lambda^{(2)}. \tag{B13}$$

Here $v_{F,\min}$ is the smallest value of $|\nabla e|$ on the Fermi surface, $\mathcal{F}_\lambda^{(2)}$ is a $O(\lambda)$ neighborhood of the set $\{2\mathbf{k}: \xi_{\mathbf{k}} = 0\}$ (note that $2\mathbf{k}$ is taken modulo reciprocal lattice vectors), and κ denotes the minimal curvature on the Fermi surface. This is illustrated for $\lambda = \Lambda$ in Fig. 28. In the first case, the intersection is transversal, which decreases the intersection volume by the factor in Eq. (B12). The second case corresponds to a $2k_F$ intersection, where the curvature in a region of size $\sqrt{\lambda}$ determines the intersection volume, corresponding to Eq. (B13). In the third case, $|\mathbf{k}|$ is so small that the volume of the intersection is essentially equal to that of $\mathcal{F}_\Lambda$.

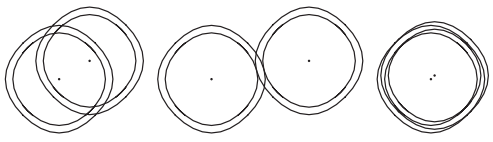

FIG. 28. Intersections of a momentum shell around the Fermi surface with its translate, as arising in loop integrals on the right-hand side of the RG equation. When the Fermi surface is curved, the intersection volume decreases strongly unless the translating momentum is small.

The scale in the flow where the improvements set in is determined by the curvature of the Fermi surface, because there is really only an improvement if the additional factors are smaller than 1. In cases where the curvature is small on large parts of the Fermi surface, as in the Hubbard model near to half filling and at small next-to-nearest hopping, one thus has an effective nesting at those scales and at those $\mathbf{k}$, where the quotients in Eqs. (B12) and (B13) are so large that they give a bound that is larger than the trivial bound 1 for the volume ratio.

Equations (B12) and (B13) imply that for small $|\mathbf{k}|$,

$$\int_0^{\Lambda_0} I_\Lambda(k) d\Lambda \leq \text{const} \times \log \frac{\Lambda_0}{|\mathbf{k}| v_{F,\min}} \tag{B14}$$

(where the constant depends on the curvature of the Fermi surface) and that the function remains bounded for $|\mathbf{k}|$ not close to zero [for details, see Feldman, Salmhofer, and Trubowitz (1996) and Salmhofer (1998a, 1999). Thus, for convex curved Fermi surfaces, the four-point function can diverge only at $\mathbf{k} = \mathbf{0}$ and there, only logarithmically (by a similar argument, one can see that it can diverge only at $k_0 = 0$). The particle-particle correction to the vertex function has exactly this behavior. In the particle-hole term, there is an additional sign cancellation that removes the logarithm. The same argument shows that in general, divergences can occur only at nesting vectors of the Fermi surface.

b. Uniform improvement from overlapping loops

An extension of these geometric estimates to two-loop integrals of the type $\int dp \int dq S^\Lambda(p) S^{\Lambda'}(q) S^{\Lambda''}(p \pm q \pm k)$ is useful for $d \geq 2$: Feldman, Salmhofer, and Trubowitz (1996) showed that in the absence of nesting and van Hove singularities, such integrals contain a scaling improvement independently of $\mathbf{k}$. Such two-loop integrals associated with graphs with overlapping loops arise when the RG equation gets iterated; the graph classification of Feldman, Salmhofer, and Trubowitz (1996, 1999) showed that in a precise sense, the overwhelming majority of graphs in the Feynman graph expansion contains one or even two such subintegrals, hence becoming subleading at low scales. As is explained in detail by Feldman, Salmhofer, and Trubowitz (1996), and Salmhofer (1998a), in the absence of nesting and van Hove singularities, this justifies the particle-particle-ladder approximation, it singles out the Hartree-Fock–type contributions to the self-energy by scaling arguments, and it allows one to show that the derivative of the self-energy is RG irrelevant instead of marginal.

REFERENCES

Abanov, A., and A. V. Chubukov, 2004, Phys. Rev. Lett. **93**, 255702.

Abanov, A., A. V. Chubukov, and J. Schmalian, 2003, Adv. Phys. **52**, 119.

Abdesselam, A., and V. Rivasseau, 1998, Lett. Math. Phys. **44**, 77.

Abrikosov, A., L. Gorkov, and I. Dzyaloshinski, 1963, *Methods of Quantum Field Theory in Statistical Physics* (Prentice-Hall, Englewood Cliffs, NJ).

Andergassen, S., T. Enss, and V. Meden, 2006, Phys. Rev. B **73**, 153308.

Andergassen, S., T. Enss, V. Meden, W. Metzner, U. Schollwöck, and K. Schönhammer, 2004, Phys. Rev. B **70**, 075102.

Andergassen, S., T. Enss, V. Meden, W. Metzner, U. Schollwöck, and K. Schönhammer, 2006, Phys. Rev. B **73**, 045125.

Andergassen, S., M. Pletyukhov, D. Schuricht, H. Schoeller, and L. Borda, 2011, Phys. Rev. B **83**, 205103.

Anders, F., and A. Schiller, 2005, Phys. Rev. Lett. **95**, 196801.

Anderson, P. W., 1997, *The Theory of High-Temperature Superconductivity* (Princeton University Press, Princeton, NJ).

Anisimov, V., and Y. Izyumov, 2010, *Electronic Structure of Strongly Correlated Materials* (Springer, Berlin).

Anisimov, V. I., D. M. Korotin, M. A. Korotin, A. V. Kozhevnikov, J. Kunes, A. O. Shorikov, S. L. Skornyakov, and S. V. Streltsov, 2009, J. Phys. Condens. Matter **21**, 075602.

Apel, W., and T. M. Rice, 1982, Phys. Rev. B **26**, 7063.

Aristov, D. N., A. P. Dmitriev, I. V. Gornyi, V. Y. Kachorovskii, D. G. Polyakov, and P. Wölfle, 2010, Phys. Rev. Lett. **105**, 266404.

Aristov, D. N., and P. Wölfle, 2008, Europhys. Lett. **82**, 27001.

Aristov, D. N., and P. Wölfle, 2009, Phys. Rev. B **80**, 045109.

Baier, T., E. Bick, and C. Wetterich, 2004, Phys. Rev. B **70**, 125111.

Bakrim, H., and C. Bourbonnais, 2010, Europhys. Lett. **90**, 27001.

Balaban, T., J. Feldman, H. Knörrer, and E. Trubowitz, 2010, Ann. Henri Poincaré **11**, 151.

Barnabé-Thériault, X., A. Sedeki, V. Meden, and K. Schönhammer, 2005a, Phys. Rev. B **71**, 205327.

Barnabé-Thériault, X., A. Sedeki, V. Meden, and K. Schönhammer, 2005b, Phys. Rev. Lett. **94**, 136405.

Bartosch, L., H. Freire, J. J. R. Cardenas, and P. Kopietz, 2009, J. Phys. Condens. Matter **21**, 305602.

Bartosch, L., P. Kopietz, and A. Ferraz, 2009, Phys. Rev. B **80**, 104514.

Bauer, J., P. Jakubczyk, and W. Metzner, 2011, Phys. Rev. B **84**, 075122.

Belitz, D., T. R. Kirkpatrick, M. T. Mercaldo, and S. L. Sessions, 2001a, Phys. Rev. B **63**, 174427.

Belitz, D., T. R. Kirkpatrick, M. T. Mercaldo, and S. L. Sessions, 2001b, Phys. Rev. B **63**, 174428.

Belitz, D., T. R. Kirkpatrick, and T. Vojta, 1997, Phys. Rev. B **55**, 9452.

Belitz, D., T. R. Kirkpatrick, and T. Vojta, 1999, Phys. Rev. Lett. **82**, 4707.

Belitz, D., T. R. Kirkpatrick, and T. Vojta, 2005, Rev. Mod. Phys. **77**, 579.

Benfatto, G., and G. Gallavotti, 1990a, Phys. Rev. B **42**, 9967.

Benfatto, G., and G. Gallavotti, 1990b, J. Stat. Phys. **59**, 541.

Benfatto, G., G. Gallavotti, A. Procacci, and B. Scoppola, 1994, Commun. Math. Phys. **160**, 93.

Benfatto, G., A. Giuliani, and V. Mastropietro, 2006, Ann. Henri Poincaré **7**, 809.

Berges, J., N. Tetradis, and C. Wetterich, 2002, Phys. Rep. **363**, 223.

Binz, B., D. Baeriswyl, and B. Doucot, 2003, Ann. Phys. (Leipzig) **12**, 704.

Binz, B., D. Baeriswyl, and B. Douçot, 2002, Eur. Phys. J. B **25**, 69.

Birse, M. C., B. Krippa, J. A. McGovern, and N. R. Walet, 2005, Phys. Lett. B **605**, 287.

Blaizot, J.-P., R. Mendez-Galain, and N. Wschebor, 2006, Phys. Lett. B **632**, 571.

Borda, L., K. Vladár, and A. Zawadowski, 2007, Phys. Rev. B **75**, 125107.

Borda, L., and A. Zawadowski, 2010, Phys. Rev. B **81**, 153303.

Boulat, E., H. Saleur, and P. Schmitteckert, 2008, Phys. Rev. Lett. **101**, 140601.

Brydges, D. C., and J. Wright, 1988, J. Stat. Phys. **51**, 435.

Büttiker, M., 1986, Phys. Rev. Lett. **57**, 1761.

Chakravarty, S., R. B. Laughlin, D. K. Morr, and C. Nayak, 2001, Phys. Rev. B **63**, 094503.
Chamon, C., M. Oshikawa, and I. Affleck, 2003, Phys. Rev. Lett. **91**, 206403.
Chen, S., B. Trauzettel, and R. Egger, 2002, Phys. Rev. Lett. **89**, 226404.
Chitov, G. Y., and D. Sénéchal, 1995, Phys. Rev. B **52**, 13487.
Chubukov, A. V., D. Efremov, and I. Eremin, 2008, Phys. Rev. B **78**, 134512.
Daghofer, M., A. Nicholson, A. Moreo, and E. Dagotto, 2010, Phys. Rev. B **81**, 014511.
Deshpande, V. V., M. Bockrath, L. I. Glazman, and A. Yacoby, 2010, Nature (London) **464**, 209.
Diehl, S., H. Gies, J. Pawlowski, and C. Wetterich, 2007, Phys. Rev. A **76**, 021602(R).
Disertori, M., and V. Rivasseau, 2000, Commun. Math. Phys. **215**, 291.
Doyon, B., 2007, Phys. Rev. Lett. **99**, 076806.
Dzyaloshinskii, I. E., 1987, Sov. Phys. JETP **66**, 848.
Dzyaloshinskii, I. E., and A. I. Larkin, 1974, Sov. Phys. JETP **38**, 202.
Eberlein, A., and W. Metzner, 2010, Prog. Theor. Phys. **124**, 471.
Egger, R., and H. Grabert, 1995, Phys. Rev. Lett. **75**, 3505.
Egger, R., and H. Grabert, 1997, Phys. Rev. Lett. **79**, 3463.
Egger, R., H. Grabert, A. Koutouza, H. Saleur, and F. Siano, 2000, Phys. Rev. Lett. **84**, 3682.
Eichler, A., R. Deblock, M. Weiss, C. Karrasch, V. Meden, C. Schönenberger, and H. Bouchiat, 2009, Phys. Rev. B **79**, 161407(R).
Ellwanger, U., and C. Wetterich, 1994, Nucl. Phys. **B423**, 137.
Enss, T., 2005, Ph.D. thesis (University Stuttgart).
Enss, T., V. Meden, S. Andergassen, X. Barnabé-Thériault, W. Metzner, and K. Schönhammer, 2005, Phys. Rev. B **71**, 155401.
Feldman, J., H. Knörrer, and E. Trubowitz, 1998a, Commun. Math. Phys. **195**, 465.
Feldman, J., H. Knörrer, and E. Trubowitz, 2002, *Fermionic Functional Integrals and the Renormalization Group* (American Mathematical Society, Providence, RI).
Feldman, J., H. Knörrer, and E. Trubowitz, 2003, Rev. Math. Phys. **15**, 949–1169.
Feldman, J., H. Knörrer, and E. Trubowitz, 2004, Commun. Math. Phys. **247**, 1–320.
Feldman, J., J. Magnen, V. Rivasseau, and R. Sénéor, 1986, Commun. Math. Phys. **103**, 67.
Feldman, J., J. Magnen, V. Rivasseau, and E. Trubowitz, 1992, Helv. Phys. Acta **65**, 679.
Feldman, J., and M. Salmhofer, 2008a, Rev. Math. Phys. **20**, 233.
Feldman, J., and M. Salmhofer, 2008b, Rev. Math. Phys. **20**, 275.
Feldman, J., M. Salmhofer, and E. Trubowitz, 1996, J. Stat. Phys. **84**, 1209.
Feldman, J., M. Salmhofer, and E. Trubowitz, 1998b, Commun. Pure Appl. Math. **51**, 1133.
Feldman, J., M. Salmhofer, and E. Trubowitz, 1999, Commun. Pure Appl. Math. **52**, 273.
Feldman, J., M. Salmhofer, and E. Trubowitz, 2000, Commun. Pure Appl. Math. **53**, 1350.
Feldman, J., and E. Trubowitz, 1990, Helv. Phys. Acta **63**, 157.
Feldman, J., and E. Trubowitz, 1991, Helv. Phys. Acta **64**, 213.
Fendley, P., A. W. W. Ludwig, and H. Saleur, 1995, Phys. Rev. Lett. **74**, 3005.
Floerchinger, S., M. Scherer, S. Diehl, and C. Wetterich, 2008, Phys. Rev. B **78**, 174528.
Floerchinger, S., and C. Wetterich, 2009, Phys. Lett. B **680**, 371.
Fradkin, E., 1991, *Field Theories of Condensed Matter Systems* (Addison-Wesley, Redwood City, CA).
Fradkin, E., S. A. Kivelson, M. J. Lawler, J. P. Eisenstein, and A. P. Mackenzie, 2010, Annu. Rev. Condens. Matter Phys. **1**, 153.
Friederich, S., H. C. Krahl, and C. Wetterich, 2010, Phys. Rev. B **81**, 235108.
Friederich, S., H. C. Krahl, and C. Wetterich, 2011, Phys. Rev. B **83**, 155125.
Fulde, P., 1991, *Electron Correlations in Molecules and Solids* (Springer, Heidelberg).
Furukawa, N., T. M. Rice, and M. Salmhofer, 1998, Phys. Rev. Lett. **81**, 3195.
Furusaki, A., 1998, Phys. Rev. B **57**, 7141.
Furusaki, A., and N. Nagaosa, 1993a, Phys. Rev. B **47**, 4631.
Furusaki, A., and N. Nagaosa, 1993b, Phys. Rev. B **47**, 3827.
Furusaki, A., and N. Nagaosa, 1996, Phys. Rev. B **54**, R5239.
Gasenzer, T., and J. M. Pawlowski, 2008, Phys. Lett. B **670**, 135.
Gawedzki, K., and A. Kupiainen, 1985, Commun. Math. Phys. **102**, 1.
Gendiar, A., R. Krcmar, and M. Weyrauch, 2009, Phys. Rev. B **79**, 205118.
Georges, A., G. Kotliar, W. Krauth, and M. J. Rozenberg, 1996, Rev. Mod. Phys. **68**, 13.
Gersch, R., C. Honerkamp, and W. Metzner, 2008, New J. Phys. **10**, 045003.
Gersch, R., C. Honerkamp, D. Rohe, and W. Metzner, 2005, Eur. Phys. J. B **48**, 349.
Gersch, R., J. Reiss, and C. Honerkamp, 2006, New J. Phys. **8**, 320.
Gezzi, R., T. Pruschke, and V. Meden, 2007, Phys. Rev. B **75**, 045324.
Giamarchi, T., 2004, *Quantum Physics in One Dimension* (Oxford University Press, Oxford, UK).
Gies, H., and J. Jaeckel, 2004, Phys. Rev. Lett. **93**, 110405.
Gies, H., F. Synatschke, and A. Wipf, 2009, Phys. Rev. D **80**, 101701.
Gies, H., and C. Wetterich, 2002, Phys. Rev. D **65**, 065001.
Gies, H., and C. Wetterich, 2004, Phys. Rev. D **69**, 025001.
Goldstein, M., R. Berkovits, Y. Gefen, and H. A. Weidenmüller, 2009, Phys. Rev. B **79**, 125307.
Gonzalez, J., F. Guinea, and M. A. H. Vozmediano, 1996, Europhys. Lett. **34**, 711.
Graser, S., T. A. Maier, P. J. Hirschfeld, and D. J. Scalapino, 2009, New J. Phys. **11**, 025016.
Grioni, M., S. Pons, and E. Frantzeskakis, 2009, J. Phys. Condens. Matter **21**, 023201.
Grote, I., E. Körding, and F. Wegner, 2002, J. Low Temp. Phys. **126**, 1385.
Haag, R., 1962, Nuovo Cimento **25**, 287.
Halboth, C. J., and W. Metzner, 2000a, Phys. Rev. B **61**, 7364.
Halboth, C. J., and W. Metzner, 2000b, Phys. Rev. Lett. **85**, 5162.
Haldane, F. D. M., 1980, Phys. Rev. Lett. **45**, 1358.
Hankyevych, V., B. Kyung, and A.-M. S. Termblay, 2003, Phys. Rev. B **68**, 214405.
Hanson, R., L. P. Kouwenhoven, J. R. Petta, S. Tarucha, and L. M. K. Vandersypen, 2007, Rev. Mod. Phys. **79**, 1217.
Hedden, R., V. Meden, T. Pruschke, and K. Schönhammer, 2004, J. Phys. Condens. Matter **16**, 5279.
Herbut, I. F., 2006, Phys. Rev. Lett. **97**, 146401.
Hertz, J. A., 1976, Phys. Rev. B **14**, 1165.
Hewson, A. C., 1994, Adv. Phys. **43**, 543.
Hirschfeld, P. J., and D. J. Scalapino, 2010, Physics **3**, 64.
Honerkamp, C., 2001, Eur. Phys. J. B **21**, 81.
Honerkamp, C., 2003, Phys. Rev. B **68**, 104510.
Honerkamp, C., 2005, Phys. Rev. B **72**, 115103.
Honerkamp, C., 2008, Phys. Rev. Lett. **100**, 146404.
Honerkamp, C., H. C. Fu, and D.-H. Lee, 2007, Phys. Rev. B **75**, 014503.

Honerkamp, C., and W. Hofstetter, 2004, Phys. Rev. Lett. **92**, 170403.
Honerkamp, C., D. Rohe, S. Andergassen, and T. Enss, 2004, Phys. Rev. B **70**, 235115.
Honerkamp, C., and M. Salmhofer, 2001a, Phys. Rev. B **64**, 184516.
Honerkamp, C., and M. Salmhofer, 2001b, Phys. Rev. Lett. **87**, 187004.
Honerkamp, C., and M. Salmhofer, 2003, Phys. Rev. B **67**, 174504.
Honerkamp, C., and M. Salmhofer, 2005, Prog. Theor. Phys. **113**, 1145.
Honerkamp, C., M. Salmhofer, N. Furukawa, and T. M. Rice, 2001, Phys. Rev. B **63**, 035109.
Honerkamp, C., M. Salmhofer, and T. M. Rice, 2002, Eur. Phys. J. B **27**, 127.
Hügle, S., and R. Egger, 2004, Europhys. Lett. **66**, 565.
Huh, Y., and S. Sachdev, 2008, Phys. Rev. B **78**, 064512.
Husemann, C., and M. Salmhofer, 2009, Phys. Rev. B **79**, 195125.
Ikeda, H., R. Arita, and J. Kunes, 2010, Phys. Rev. B **81**, 054502.
Ishida, K., Y. Nakai, and H. Hosono, 2009, J. Phys. Soc. Jpn. **78**, 062001.
Isidori, A., D. Rosen, L. Bartosch, W. Hofstetter, and P. Kopietz, 2010, Phys. Rev. B **81**, 235120.
Jakobs, S. G., 2003, Diploma thesis (RWTH Aachen University).
Jakobs, S. G., 2010, Ph.D. thesis (RWTH Aachen University).
Jakobs, S. G., V. Meden, and H. Schoeller, 2007, Phys. Rev. Lett. **99**, 150603.
Jakobs, S. G., V. Meden, H. Schoeller, and T. Enss, 2007, Phys. Rev. B **75**, 035126.
Jakobs, S. G., M. Pletyukhov, and H. Schoeller, 2010a, Phys. Rev. B **81**, 195109.
Jakobs, S. G., M. Pletyukhov, and H. Schoeller, 2010b, J. Phys. A **43**, 103001.
Jakubczyk, P., 2009, Phys. Rev. B **79**, 125115.
Jakubczyk, P., J. Bauer, and W. Metzner, 2010, Phys. Rev. B **82**, 045103.
Jakubczyk, P., W. Metzner, and H. Yamase, 2009, Phys. Rev. Lett. **103**, 220602.
Jakubczyk, P., P. Strack, A. A. Katanin, and W. Metzner, 2008, Phys. Rev. B **77**, 195120.
Janzen, K., V. Meden, and K. Schönhammer, 2006, Phys. Rev. B **74**, 085301.
Kamenev, A., 2004, *Les Houches, Volume Session LX*, edited by H. Bouchiat, Y. Gefen, S. Guéron, G. Montambaux, and J. Dalibard (Elsevier, North-Holland, Amsterdam).
Kane, C. L., and M. P. A. Fisher, 1992, Phys. Rev. B **46**, 15233.
Karrasch, C., 2010, Ph.D. thesis (RWTH Aachen University).
Karrasch, C., S. Andergassen, M. Pletyukhov, D. Schuricht, L. Borda, V. Meden, and H. Schoeller, 2010, Europhys. Lett. **90**, 30003.
Karrasch, C., T. Enss, and V. Meden, 2006, Phys. Rev. B **73**, 235337.
Karrasch, C., T. Hecht, A. Weichselbaum, Y. Oreg, J. von Delft, and V. Meden, 2007, Phys. Rev. Lett. **98**, 186802.
Karrasch, C., T. Hecht, A. Weichselbaum, J. von Delft, Y. Oreg, and V. Meden, 2007, New J. Phys. **9**, 123.
Karrasch, C., R. Hedden, R. Peters, T. Pruschke, K. Schönhammer, and V. Meden, 2008, J. Phys. Condens. Matter **20**, 345205.
Karrasch, C., and V. Meden, 2009, Phys. Rev. B **79**, 045110.
Karrasch, C., V. Meden, and K. Schönhammer, 2010, Phys. Rev. B **82**, 125114.
Karrasch, C., A. Oguri, and V. Meden, 2008, Phys. Rev. B **77**, 024517.
Karrasch, C., M. Pletyukhov, L. Borda, and V. Meden, 2010, Phys. Rev. B **81**, 125122.
Kashcheyevs, V., C. Karrasch, T. Hecht, A. Weichselbaum, V. Meden, and A. Schiller, 2009, Phys. Rev. Lett. **102**, 136805.
Katanin, A. A., 2004, Phys. Rev. B **70**, 115109.
Katanin, A. A., 2009, Phys. Rev. B **79**, 235119.
Katanin, A. A., and A. P. Kampf, 2003, Phys. Rev. B **68**, 195101.
Katanin, A. A., and A. P. Kampf, 2004, Phys. Rev. Lett. **93**, 106406.
Kaul, R. K., and S. Sachdev, 2008, Phys. Rev. B **77**, 155105.
Kee, H.-Y., E. H. Kim, and C.-H. Chung, 2003, Phys. Rev. B **68**, 245109.
Kehrein, S., 2006, *The Flow Equation Approach to Many-Particle Systems* (Springer, Berlin).
Khavkine, I., C.-H. Chung, V. Oganesyan, and H.-Y. Kee, 2004, Phys. Rev. B **70**, 155110.
Kino, H., and H. Fukuyama, 1996, J. Phys. Soc. Jpn. **65**, 2158.
Kirkpatrick, T. R., and D. Belitz, 1996, Phys. Rev. B **53**, 14364.
Klironomos, F. D., and S. W. Tsai, 2006, Phys. Rev. B **74**, 205109.
Klironomos, F. D., and S. W. Tsai, 2007, Phys. Rev. Lett. **99**, 100401.
Kloss, T., and P. Kopietz, 2011, Phys. Rev. B **83**, 205118.
Kopietz, P., L. Bartosch, and F. Schütz, 2010, *Introduction to the Functional Renormalization Group* (Springer, Berlin).
Kopietz, P., and T. Busche, 2001, Phys. Rev. B **64**, 155101.
Kotliar, G., S. Y. Savrasov, K. Haule, V. S. Oudovenko, O. Parcollet, and C. A. Marianetti, 2006, Rev. Mod. Phys. **78**, 865.
Krahl, H. C., S. Friederich, and C. Wetterich, 2009, Phys. Rev. B **80**, 014436.
Krahl, H. C., J. A. Müller, and C. Wetterich, 2009, Phys. Rev. B **79**, 094526.
Krippa, B., 2007, Eur. Phys. J. A **31**, 734.
Kuroki, K., S. Onari, R. Arita, H. Usui, Y. Tanaka, H. Kontani, and H. Aoki, 2008, Phys. Rev. Lett. **101**, 087004.
Lal, S., S. Rao, and D. Sen, 2002, Phys. Rev. B **66**, 165327.
Landauer, R., 1957, IBM J. Res. Dev. **1**, 223.
Langer, J. S., and V. Ambegaokar, 1961, Phys. Rev. **121**, 1090.
Läuchli, A., C. Honerkamp, and T. Rice, 2004, Phys. Rev. Lett. **92**, 037006.
Lederer, P., G. Montambaux, and D. Poilblanc, 1987, J. Phys. (Paris) **48**, 1613.
Ledowski, S., and P. Kopietz, 2003, J. Phys. Condens. Matter **15**, 4779.
Ledowski, S., and P. Kopietz, 2007a, Phys. Rev. B **75**, 045134.
Ledowski, S., and P. Kopietz, 2007b, Phys. Rev. B **76**, 121403(R).
Ledowski, S., P. Kopietz, and A. Ferraz, 2005, Phys. Rev. B **71**, 235106.
Lee, P. A., N. Nagaosa, and X. G. Wen, 2006, Rev. Mod. Phys. **78**, 17.
Lesniewski, A., 1987, Commun. Math. Phys. **108**, 437.
Litim, D., 2001, Phys. Rev. D **64**, 105007.
Lopez-Sancho, M. P., F. de Juan, and M. A. H. Vozmediano, 2009, Phys. Rev. B **79**, 075413.
Luther, A., and I. Peschel, 1974, Phys. Rev. B **9**, 2911.
Luttinger, J. M., 1963, J. Math. Phys. (N.Y.) **4**, 1154.
Maier, T. A., S. Graser, D. J. Scalapino, and P. J. Hirschfeld, 2009, Phys. Rev. B **79**, 224510.
Maslov, D. L., and M. Stone, 1995, Phys. Rev. B **52**, R5539.
Mathey, L., S. W. Tsai, and A. H. Castro Neto, 2006, Phys. Rev. Lett. **97**, 030601.
Mathey, L., S. W. Tsai, and A. H. Castro Neto, 2007, Phys. Rev. B **75**, 174516.
Mattis, D. C., 1974, J. Math. Phys. (N.Y.) **15**, 609.
Mattis, D. C., and E. H. Lieb, 1965, J. Math. Phys. (N.Y.) **6**, 304.
Matveev, K. A., D. Yue, and L. I. Glazman, 1993, Phys. Rev. Lett. **71**, 3351.

Mazin, I. I., D. J. Singh, M. D. Johannes, and M. H. Du, 2008, Phys. Rev. Lett. **101**, 057003.

McKenzie, R. H., 1997, Science **278**, 820.

Meden, V., T. Enss, S. Andergassen, W. Metzner, and K. Schönhammer, 2005, Phys. Rev. B **71**, 041302.

Meden, V., and F. Marquardt, 2006, Phys. Rev. Lett. **96**, 146801.

Meden, V., W. Metzner, U. Schollwöck, and K. Schönhammer, 2002, J. Low Temp. Phys. **126**, 1147.

Meden, V., and U. Schollwöck, 2003a, Phys. Rev. B **67**, 193303.

Meden, V., and U. Schollwöck, 2003b, Phys. Rev. B **67**, 035106.

Meden, V., and K. Schönhammer, 1992, Phys. Rev. B **46**, 15753.

Meir, Y., and N. S. Wingreen, 1992, Phys. Rev. Lett. **68**, 2512.

Meng, Z. Y., T. C. Lang, S. Wessel, F. F. Assaad, and A. Muramatsu, 2010, Nature (London) **464**, 847.

Metlitski, M., and S. Sachdev, 2010a, Phys. Rev. B **82**, 075128.

Metlitski, M., and S. Sachdev, 2010b, Phys. Rev. B **82**, 075127.

Metlitski, M. A., and S. Sachdev, 2010c, New J. Phys. **12**, 105007.

Metzner, W., C. Castellani, and C. Di Castro, 1998, Adv. Phys. **47**, 317.

Metzner, W., D. Rohe, and S. Andergassen, 2003, Phys. Rev. Lett. **91**, 066402.

Millis, A. J., 1993, Phys. Rev. B **48**, 7183.

Mitra, A., S. Takei, Y. Kim, and A. Millis, 2006, Phys. Rev. Lett. **97**, 236808.

Miyake, T., K. Nakamura, R. Arita, and M. Imada, 2010, J. Phys. Soc. Jpn. **79**, 044705.

Moon, K., H. Yi, C. L. Kane, S. M. Girvin, and M. P. A. Fisher, 1993, Phys. Rev. Lett. **71**, 4381.

Morita, H., S. Watanabe, and M. Imada, 2002, J. Phys. Soc. Jpn. **71**, 2109.

Morris, T. R., 1994, Int. J. Mod. Phys. A **9**, 2411.

Mühlschlegel, B., 1962, J. Math. Phys. (N.Y.) **3**, 522.

Nayak, C., M. P. A. Fisher, A. W. W. Ludwig, and H. H. Lin, 1999, Phys. Rev. B **59**, 15694.

Nazarov, Y. V., and L. I. Glazman, 2003, Phys. Rev. Lett. **91**, 126804.

Negele, J. W., and H. Orland, 1987, *Quantum Many-Particle Systems* (Addison-Wesley, Reading, MA).

Neumayr, A., and W. Metzner, 2003, Phys. Rev. B **67**, 035112.

Nickel, J. C., R. Duprat, C. Bourbonnais, and N. Dupuis, 2005, Phys. Rev. Lett. **95**, 247001.

Nickel, J. C., R. Duprat, C. Bourbonnais, and N. Dupuis, 2006, Phys. Rev. B **73**, 165126.

Norman, M. R., 2008, Physics **1**, 21.

Nozières, P., 1964, *Theory of Interacting Fermi Systems* (Benjamin, Amsterdam).

Obert, B., S. Takei, and W. Metzner, 2011, Ann. Phys. (Berlin) **523**, 621.

Oguri, A., 2001, J. Phys. Soc. Jpn. **70**, 2666.

Okamoto, S., D. Sénéchal, M. Civelli, and A. Tremblay, 2010, Phys. Rev. B **82**, 180511.

Ossadnik, M., C. Honerkamp, T. M. Rice, and M. Sigrist, 2008, Phys. Rev. Lett. **101**, 256405.

Pedra, W., and M. Salmhofer, 2008, Commun. Math. Phys. **282**, 797.

Pistolesi, F., C. Castellani, C. Di Castro, and G. C. Strinati, 2004, Phys. Rev. B **69**, 024513.

Platt, C., C. Honerkamp, and W. Hanke, 2009, New J. Phys. **11**, 055058.

Platt, C., R. Thomale, and W. Hanke, 2011a, Ann. Phys. (Berlin) **523**, 638.

Platt, C., R. Thomale, and W. Hanke, 2011b, Phys. Rev. B **84**, 235121.

Polchinski, J., 1984, Nucl. Phys. **B231**, 269.

Polchinski, J., 1993, *Proceedings of 1993 Theoretical Advanced Studies Institute in Elementary Particle Physics*, edited by J. Harvey, and J. Polchinski (World Scientific, Singapore).

Polyakov, D. G., and I. V. Gornyi, 2003, Phys. Rev. B **68**, 035421.

Pomeranchuk, I. J., 1959, Sov. Phys. JETP **8**, 361.

Ponomarenko, V. V., 1995, Phys. Rev. B **52**, R8666.

Popov, V. N., 1987, *Functional Integrals and Collective Excitations* (Cambridge University Press, Cambridge, UK).

Raghu, S., X.-L. Qi, C. Honerkamp, and S.-C. Zhang, 2008, Phys. Rev. Lett. **100**, 156401.

Rammer, J., and H. Smith, 1986, Rev. Mod. Phys. **58**, 323.

Rech, J., C. Pepin, and A. V. Chubukov, 2006, Phys. Rev. B **74**, 195126.

Reed, M., and B. Simon, 1975, *Methods of Modern Mathematical Physics* (Academic Press, New York), Vols. 3–4.

Reiss, J., D. Rohe, and W. Metzner, 2007, Phys. Rev. B **75**, 075110.

Reuther, J., and R. Thomale, 2011, Phys. Rev. B **83**, 024402.

Reuther, J., and P. Wölfle, 2010, Phys. Rev. B **81**, 144410.

Reuther, J., P. Wölfle, R. Darradi, W. Brenig, M. Arlego, and J. Richter, 2011, Phys. Rev. B **83**, 064416.

Rohe, D., and W. Metzner, 2005, Phys. Rev. B **71**, 115116.

Rosa, L., P. Vitale, and C. Wetterich, 2001, Phys. Rev. Lett. **86**, 958.

Rosch, A., J. Kroha, and P. Wölfle, 2001, Phys. Rev. Lett. **87**, 156802.

Sachdev, S., 1999, *Quantum Phase Transitions* (Cambridge University Press, Cambridge, UK).

Safi, I., and H. J. Schulz, 1995, Phys. Rev. B **52**, R17040.

Sahebsara, P., and D. Sénéchal, 2008, Phys. Rev. Lett. **100**, 136402.

Salmhofer, M., 1998a, Rev. Math. Phys. **10**, 553.

Salmhofer, M., 1998b, Commun. Math. Phys. **194**, 249.

Salmhofer, M., 1999, *Renormalization: An Introduction* (Springer, Heidelberg).

Salmhofer, M., 2007, Ann. Phys. (Leipzig) **16**, 171.

Salmhofer, M., and C. Honerkamp, 2001, Prog. Theor. Phys. **105**, 1.

Salmhofer, M., C. Honerkamp, W. Metzner, and O. Lauscher, 2004, Prog. Theor. Phys. **112**, 943.

Salmhofer, M., and C. Wieczerkowski, 2000, J. Stat. Phys. **99**, 557.

Schmidt, H., and P. Wölfle, 2010, Ann. Phys. (Leipzig) **19**, 60.

Schmidt, R., and T. Enss, 2011, Phys. Rev. A **83**, 063620.

Schoeller, H., 2000, *Low-Dimensional Systems: Interaction and Transport Properties*, edited by T. Brandes (Springer, Berlin).

Schoeller, H., 2009, Eur. Phys. J. Special Topics **168**, 179.

Schoeller, H., and J. König, 2000, Phys. Rev. Lett. **84**, 3686.

Schönhammer, K., 2005, *Interacting Electrons in Low Dimensions*, edited by D. Baeriswyl (Kluwer Academic Publishers, Dordrecht).

Schulz, H. J., 1987, Europhys. Lett. **4**, 609.

Schütz, F., L. Bartosch, and P. Kopietz, 2005, Phys. Rev. B **72**, 035107.

Schütz, F., and P. Kopietz, 2006, J. Phys. A **39**, 8205.

Shankar, R., 1991, Physica A (Amsterdam) **177**, 530.

Shankar, R., 1994, Rev. Mod. Phys. **66**, 129.

Sólyom, J., 1979, Adv. Phys. **28**, 201.

Strack, P., 2009, Ph.D. thesis (University Stuttgart).

Strack, P., R. Gersch, and W. Metzner, 2008, Phys. Rev. B **78**, 014522.

Strack, P., S. Takei, and W. Metzner, 2010, Phys. Rev. B **81**, 125103.

Tam, K. M., S. W. Tsai, and D. K. Campbell, 2006, Phys. Rev. Lett. **96**, 036408.

Tam, K.-M., S.-W. Tsai, D. K. Campbell, and A. H. Castro Neto, 2007a, Phys. Rev. B **75**, 161103(R).

Tam, K.-M., S.-W. Tsai, D. K. Campbell, and A. H. Castro Neto, 2007b, Phys. Rev. B **75**, 195119.

Taylor, J. R., 2000, *Scattering Theory* (Dover Publications, New York).

Tetradis, N., and C. Wetterich, 1994, Nucl. Phys. **B422**, 541.
Thomale, R., C. Platt, W. Hanke, and B. A. Bernevig, 2011a, Phys. Rev. Lett. **106**, 187003.
Thomale, R., C. Platt, W. Hanke, J. Hu, and B. A. Bernevig, 2011b, Phys. Rev. Lett. **107**, 117001.
Thomale, R., C. Platt, J. Hu, C. Honerkamp, and A. B. Bernevig, 2009, Phys. Rev. B **80**, 180505.
Tomonaga, S., 1950, Prog. Theor. Phys. **5**, 544.
Tsai, S. W., A. H. Castro Neto, R. Shankar, and D. K. Campbell, 2005, Phys. Rev. B **72**, 054531.
Tsai, S. W., and J. B. Marston, 2001, Can. J. Phys. **79**, 1463.
Voit, J., 1993, Phys. Rev. B **47**, 6740.
Vojta, M., 2003, Rep. Prog. Phys. **66**, 2069.
Vojta, M., Y. Zhang, and S. Sachdev, 2000, Phys. Rev. Lett. **85**, 4940.
von Delft, J., and H. Schoeller, 1998, Ann. Phys. (Leipzig) **7**, 225.
von Loehneysen, H., A. Rosch, M. Vojta, and P. Wölfle, 2007, Rev. Mod. Phys. **79**, 1015.
Wächter, P., V. Meden, and K. Schönhammer, 2009, J. Phys. Condens. Matter **21**, 215608.
Wang, F., H. Zhai, and D.-H. Lee, 2009, Europhys. Lett. **85**, 37005.
Wang, F., H. Zhai, and D.-H. Lee, 2010, Phys. Rev. B **81**, 184512.
Wang, F., H. Zhai, Y. Ran, A. Vishwanath, and D.-H. Lee, 2009, Phys. Rev. Lett. **102**, 047005.
Wegner, F., 1994, Ann. Phys. (Leipzig) **506**, 77.
Wegner, F. J., and A. Houghton, 1973, Phys. Rev. A **8**, 401.
Wetterich, C., 1993, Phys. Lett. B **301**, 90.
Weyrauch, M., and D. Sibold, 2008, Phys. Rev. B **77**, 125309.
Wieczerkowski, C., 1988, Commun. Math. Phys. **120**, 149.
Wilson, K. G., and J. B. Kogut, 1974, Phys. Rep. **12**, 75.
Xu, Q. Q., B. L. Gao, and S. J. Xiong, 2008, Physica B (Amsterdam) **403**, 2468.
Xu, Q. Q., B. L. Gao, and S. J. Xiong, 2010, Int. J. Mod. Phys. B **24**, 575.
Yamase, H., 2009, Phys. Rev. Lett. **102**, 116404.
Yamase, H., P. Jakubczyk, and W. Metzner, 2011, Phys. Rev. B **83**, 125121.
Yamase, H., and W. Metzner, 2006, Phys. Rev. B **73**, 214517.
Yamase, H., and W. Metzner, 2007, Phys. Rev. B **75**, 155117.
Yamase, H., V. Oganesyan, and W. Metzner, 2005, Phys. Rev. B **72**, 035114.
Yoshioka, T., A. Koga, and N. Kawakami, 2009, Phys. Rev. Lett. **103**, 036401.
Yue, D., L. I. Glazman, and K. A. Matveev, 1994, Phys. Rev. B **49**, 1966.
Zanchi, D., 2001, Europhys. Lett. **55**, 376.
Zanchi, D., and H. J. Schulz, 1997, Z. Phys. B **103**, 339.
Zanchi, D., and H. J. Schulz, 1998, Europhys. Lett. **44**, 235.
Zanchi, D., and H. J. Schulz, 2000, Phys. Rev. B **61**, 13609.